Politecnico di Torino

Doctoral Thesis

Fabrication and Characterization of a microfluidic device for 3D cells analysis

Author:
Simone Benetto

Supervisor:
Prof. Fabrizio Pirri
Co-Supervisor:
Prof. Matteo Cocuzza

A thesis submitted for the degree of
Doctor of Philosophy in Physics

XXVIII cycle: 2013-2016

"And the only way to do great work is to love what you do. If you haven't found it yet, keep looking. Don't settle. As with all matters of the heart, you'll know when you find it. And, like any great relationship, it just gets better and better as the years roll on. So keep looking until you find it. Don't settle. [...] Stay hungry. Stay foolish."

Steve Jobs

POLITECNICO DI TORINO

Abstract

Department of Applied Science and Technology

Doctor of Philosophy in Physics

Fabrication and Characterization of a microfluidic device for 3D cells analysis

by Simone Benetto

The study of cells chemotaxis and angiogenesis phenomena plays a significant role in a better understanding of cancer evolution. As a matter of fact, cells are influenced by the physiological environment, which contains all the substances that could influence their regular life. The importance of the study of the impact nutrients or toxic elements may have is generally accepted. In fact, in the last decade a large number of studies were carried on simple 2D devices. However, this type of platform did not allow a well-simulated physiological behavior, and they were soon replaced with the study of 3D platforms.

This thesis reports the fabrication, simulation and testing of a 3D microfluidic circuit to study cells chemotaxis in a platform where reagents concentration is controlled spatially and temporally. In the first part of the thesis all the technologies and processes used for the device manufacturing are listed and explained (Chapter 1). Then, an overview of the biological and physics phenomena that occur during the device usage is reported (Chapter 2). The main part of the work is focused on the experimental fabrication processes (Chapter 3) and simulations and tests for the correct device behavior (Chapter 4). In these sections, all the steps and alternatives in the fabrication process are explained, coming to the final correct device production with PDMS casting in situ process with a SU8 photoresist mold; afterward, all the simulations and tests are reported in order to analyze the device: the static and dynamic regimes are analyzed and tested, from the fluorescence method (in order to check if the gradient is correctly maintained) to some biological tests for the cells growth. Finally, conclusions and future perspectives are reported (Chapter 5).

Acknowledgements

Per il mio lavoro di dottorato vorrei ringraziare innanzitutto il prof. Pirri ed il mio tutor Cocuzza Matteo, per il supporto e la dedizione con cui mi hanno incoraggiato e seguito in questi anni. In secondo luogo vorrei ringraziare tutti i miei colleghi di lavoro presso il laboraorio *Chilab* di Chivasso: Denis Perrone, Beppe Mina, Alessio Tommasi, Simone Marasso, Domenico Mombello e Chiara Ottone.

Ma un buon impegno sul lavoro dipende anche da tutti coloro che ruotano attorno alla vita privata. Ecco quindi un primo enorme grazie a tutta la mia famiglia, 'capitanata' da Danilo, Marisa e Federica, senza i quali il supporto che ho avuto in questi anni sicuramente sarebbe venuto meno. Un grazie speciale anche alle nonne Armida ed Elvira, sempre presenti, ed ai nonni Franco ed Egidio che mi seguono da lassù. Un caloroso grazie anche agli zii Renzo&Rita e Ivano&Ornella.

Un paragrafo esclusivo va dedicato alla persona che da poco è entrata nella mia vita: Sara Borellini. In poco tempo hai saputo legarti a me in modo speciale ed unico, dandomi la forza e l'energia di cui avevo bisogno. Sei sempre propositiva e positiva, una vera combattente. Sono fiero di averti al mio fianco.

Un enorme grazie ai membri del club *'Poker d'Assi'*: Came, Carletto e Kcris. Vi conosco da meno tempo di molti altri, ma sono legato a voi come se fossimo amici da sempre. Le serate passate a darci foza a vicenda non sono mai sufficienti. Mi conoscete meglio di chiunque altro e siete come fratelli.
Un pensiero particolare anche alla neo-moglie di uno degli assi nonchè super amica: Paoletta. Degna sostenitrice in momenti bui e compagna di risate in quelli allegri.

Un grazie specialissimo a tutti i banditi a cui sono legato da anni, e specialmente a Roby, Silvietta, Virgi, Giu, MB, Terence, Lucy, Mary, Chri e tutti coloro che ho dimenticato. I momenti passati insieme sono caratterizzati dalla musica e dell'amicizia, un binomio che rende speciale qualunque situazione. Un grazie particolare ai miei colleghi di sezione, compagni di sventure musicali, in particolare a Simo e Fac.
Sempre in ambito musicale un grazie al mio maestro, Giorgio, che sa illuminare la via con consigli e dedizione.

Un grazie speciale anche a tutti coloro che sono entrati nella mia vita e che non ho nominato: tutti voi avete contribuito a farmi crescere per arrivare ad essere ciò che sono.

Contents

List of Figures

Abbreviations

BOE	**B**uffered **O**xide **E**tchant
CAD	**C**omputer-**A**ided **D**esign
CNC (machine)	**C**omputer **N**umerical **C**ontrol (machine)
COC	**C**yclic **O**lefin **C**opolymer
DI (water)	**D**e-**I**onized (water)
DMSO	**D**i**M**ethyl **S**ulf**O**xide
DRIE	**D**eep **R**eactive **I**on **E**tching
ES (cells)	**E**mbrionic **S**tem (cells)
FITC	**F**luorescein **I**so**T**hio**C**yanate
LIGA	**Li**thographie **G**alvanoformung **A**bformung (Lithography, Electroplating and Molding)
LOC (system)	**L**ab **O**n **C**hip (system)
PC	**P**oly **C**arbonate
PDMS	**P**oly **D**i **M**ethyl **S**iloxane
PEB	**P**ost **E**xposure **B**ake
PMMA	**P**oly **M**ethyl **M**eth**A**crilate
PVC	**P**oly**V**inyl **C**hloride
RIE	**R**eactive **I**on **E**tching

Dedicated to my family

Chapter 1

MEMS fabrication technologies and polymeric machining

In this chapter I will describe the micromachining techniques we mostly used in this thesis work for the devices fabrication shown in the next chapters, the laboratory environment and all the main characterization techniques for the produced devices.

1.1 Cleanroom environment

The micro and nano scale fabrication of devices requires a very controlled environment. This because the dimensions of dust and other particles are bigger than the device itself, and they may irreversibly damage it. In order to obtain this, it is necessary to work in a Cleanroom environment. Typically used in manufacturing or scientific research, a cleanroom is a controlled environment that has a very low level of pollutants such as dust, airborne microbes, aerosol particles, and chemical vapors. Moreover, temperature, humidity and pressure are controlled too.

Figure 1.1 shows an overview of a clean room working. Our cleanroom works in a "laminar flow" configuration. This means that the air is forced from the ceiling to the floor, ensuring that all the micro and nano particles are eliminated through the holes in the bottom part of the room (on the floor or on the walls). The air is continuously filtered by some filters positioned in the outside area of the cleanroom, called "grey room". Also temperature and humidity are controlled and fixed according to settings and necessities. As a function of the dimensions of the porosity in these filters, different air qualities are obtained: we have *Class 100* and *Class 1000* rooms. The numbers denote, according to FED-STD-209E, the maximum number of particles of size 0.5 μm

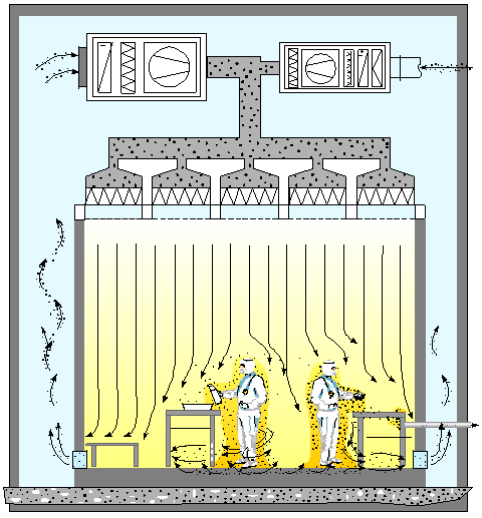

FIGURE 1.1: Air Flow principle for unidirectional (laminar) flow Cleanrooms

or larger permitted per cubic foot of air. Consequently, the first one contains a lower number of particles in the air. Also a difference in pressure is needed in order to avoid the blending when the different areas are in direct communication.

1.2 Photolithographic Process

Photolithography, also termed *optical lithography* or *UV lithography*, is a process used in microfabrication to pattern parts of a thin film or the bulk of a substrate. It uses light to transfer a geometric pattern from a photomask to a light-sensitive chemical "photoresist", or simply "resist," on the substrate. A series of chemical and physical treatments then either engraves the exposure pattern into, or enables deposition of a new material in the desired pattern upon, the material underneath the photo resist.

According to the polarity of the photoresist, we can obtain the original geometry, the reversal one or both the cases.

The Figure 1.2 shows the difference between a positive and negative photoresist. The first one allows to obtain the same geometries of the original pattern, while the second one allows to obtain exactly the negative pattern. The Figure 1.3 shows the capacity of image reversal resists to obtain the original or the dual pattern, depending on the process steps followed.

In the Figure 1.4 we can see an overview of a photolithographic process, whose steps are described in the following subsections.

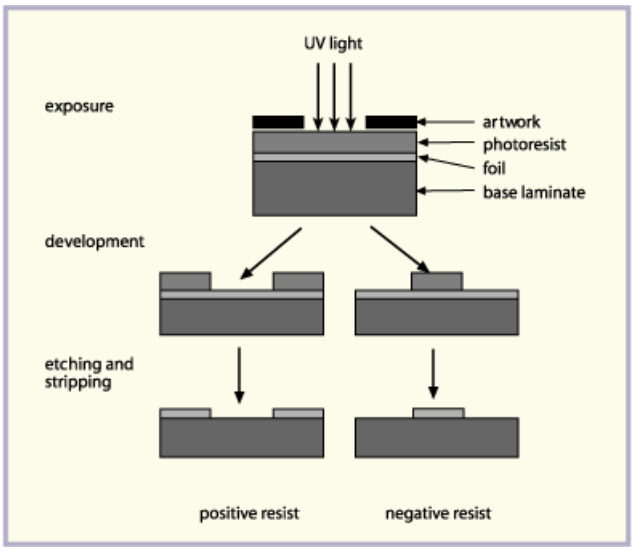

FIGURE 1.2: General photolithographic process

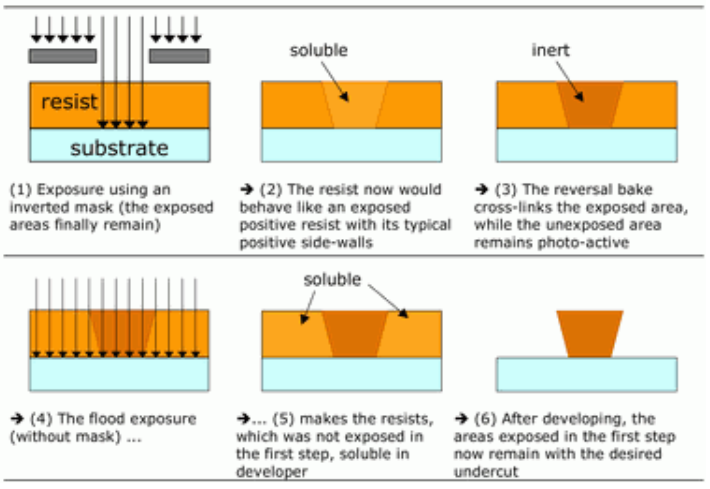

FIGURE 1.3: Image reversal photoresist

1.2.1 Preparation and cleaning

A preliminar step is required in order to have the perfectly clean substrate. There are different methods to clean the wafer:

- use of solvents: *isopropyl alcohol* and *acetone* are the two mainly used solvents; they allow an initial cleaning process and they restore the perfect wettability of the substrate;
- use of *piranha solution*: Piranha solution, also known as *piranha etch*, is a mixture of sulfuric acid (H_2SO_4) and hydrogen peroxide (H_2O_2), (3 : 1 vol), and it is used to clean organic residues off substrates. Because the mixture is a strong oxidizing

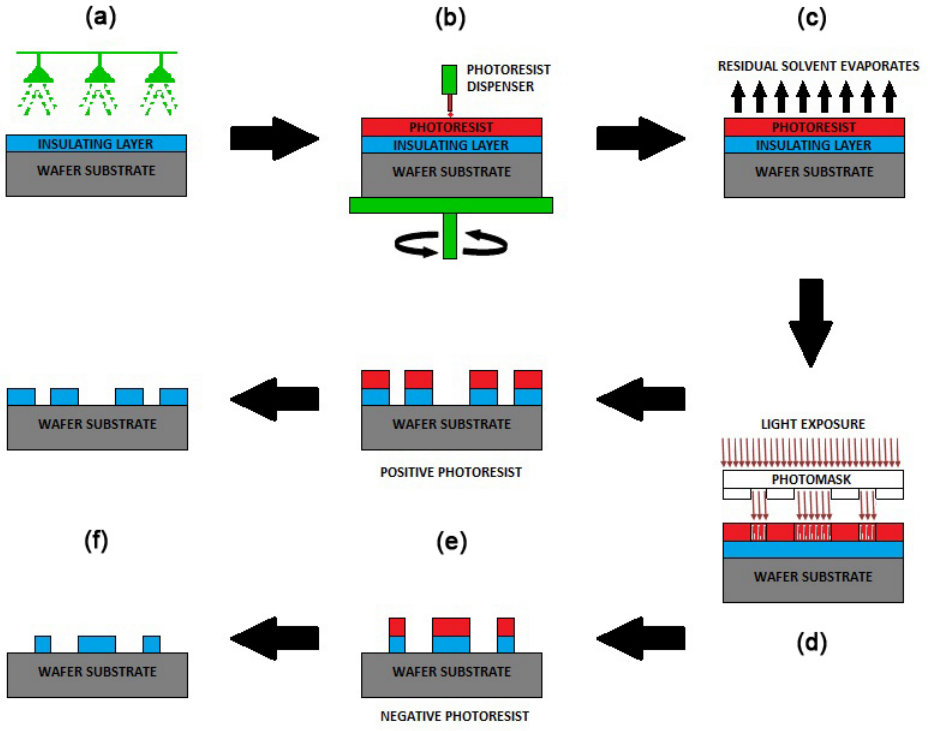

FIGURE 1.4: Overview of a photolithographic process. (a) Deposition of a insulating layer (optional). (b) Deposition of resist layer. (c) Bake of the resist. (d) Light exposure (with a mask if necessary). (e) Developing of the reisist. (f) Removal (strip) of residual resist

agent, it will remove most organic matter, and it will also hydroxylate most surfaces (add $-OH$ groups), making them highly hydrophilic (water-compatible). [1] - [2]. For these reasons, a following solvent-based rinsing is required in order to restore the original wettability of the surface.

1.2.2 Prebake (optional)

After the preparation of the substrate a warming step on a hot plate (Figure 1.5) could be necessary, if the substrate is self-oxidation safe. In our case, since the substrate is a Silicon wafer, this step could be done in order to eliminate all the possible water residual that remained after the previous steps.

However, there are some processes in which this step is crucial. For instance, in general almost all MEMS production projects require an initial baking ([3], [4], [5]).

FIGURE 1.5: Hotplate for baking

1.2.3 Spin coating

The Figure 1.6 shows the basic concepts of spin coating: firstly, a photoresist drop is poured on substrate hosted on the chuck of the spin coater (a). Secondly, applying a rotation, the resist covers all the area of the substrate (b); during this step, that is a transitory step, since we have an acceleration, the aim is to let the resist covering all the available area. In the final step a constant rotation is applied, in order to obtain a controlled thickness of the resist layer (c).

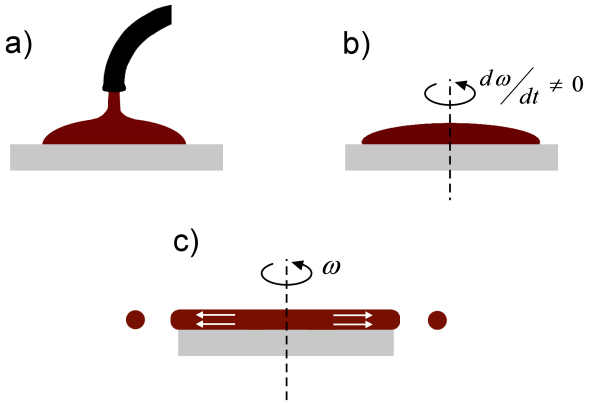

FIGURE 1.6: Spin coating

Since there are different resists with different viscosities, at the same velocity we can obtain different thicknesses according to the used the material. Therefore, a combination of viscosity and velocity set up is fundamental in order to obtain the requested thickness ([6], [7]).

1.2.4 Soft bake

After coating, the resist film contains a remaining solvent concentration depending on the resist, the solvent, the resist film thickness and the resist coating technique. The softbake reduces the remaining solvent content in order to:

- avoid mask contamination and/or sticking to the mask,
- prevent popping or foaming of the resist by N_2 evolved during exposure,
- improve resist adhesion to the substrate,
- minimize dark erosion during development,
- prevent dissolving one resist layer by a following multiple coating,
- prevent bubbling during subsequent thermal processes (coating, dry etching).

This is a crucial step in almost all the processes involving photoresist materials [8].

1.2.5 Alignment and exposure

In the following step the substrate with the resist is loaded in the exposure equipment, called *mask aligner*. In this way, with a controlled energy, the resist changes its chemical properties, so that irradiated and non-irradiated regions have different solubility in the specific solvent or developer.

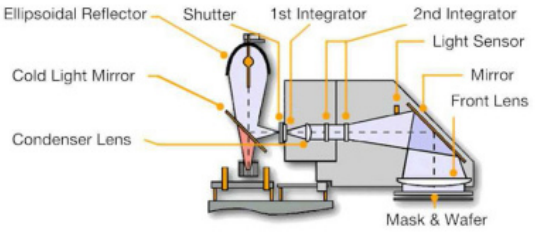

(A) Exposure/mask aligner/wafer system

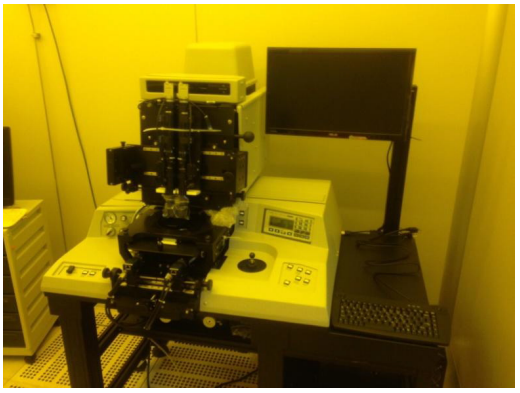

(B) Neutronix Quintel NXQ4006 double side mask aligner.

FIGURE 1.7: Mask aligner sketch (A) and equipment (B).

In the Figure 1.7 we can see on the left how the system works, and on the right our particular system that is installed in the cleanroom.

The exposure to light causes a chemical change that allows some parts of the photoresist to be removed by a special solution, called "developer". Positive photoresist, the most common type, becomes soluble in the developer when exposed; on the other hand, with negative photoresist, unexposed regions are soluble in the developer. In particular, exposing a positive resist chain splitting processes are induced in the long polymer chains so that the molecular weight of resists greatly decreases.

The pattern is reproduced on the resist using a mask that selectively allows the passage of the light through transparent regions. The mask is usually a transparent glass or quartz sheet, on which a thin Chromium layer in selectively deposited by evaporation or sputtering techniques in order to create the non-transparent areas. A thickness of Chromium of 100 nm is usually able to block completely all the light.

Another important aspect of photoresist exposure is the *scattering* effect. This phenomenon occurs when between the mask and the substrate a small gap occurs: the light begins to be reflected between these two layers, and this worsens the final resolution of the pattern on the resist, because the borders between masked and non-masked areas are not well defined.

1.2.6 Post exposure bake - PEB

A post-exposure bake (PEB) is performed before developing, typically to help minimizing standing waves caused by the destructive and constructive interference patterns between incident and reflected light.

1.2.7 Development

The development step allows the removal of the exposed parts (for the positive resist) or of the not exposed parts (for the negative resist) on the substrate. Development is undoubtedly one of the most critical steps in the photoresist process. The characteristics of the resist-developer interactions determine to a large extent the shape of the photoresist profile and, more importantly, the linewidth control.

FIGURE 1.8: Puddle development

One of the methods for the development is the so-called *puddle development*. In this method, the substrate with the resist is dipped into a stationary solution, for a time

that depends on the type of the resist, the thickness of the layer and the pattern that we want to obtain (as shown in Figure 1.8). This step is very crucial in order not to destroy the geometries that were replicated during the exposition step. The most common developers are basic solutions.

1.2.8 Hard bake (optional)

This step solidifies the remaining photoresist, to make a more durable protecting layer for future ion implantation, wet chemical etching, or plasma etching. During the hard bake all the physical characteristics of the resist are fixed, and the layer is made more resistant for the following processes.
The temperatures used are high if compared to previous steps (120°C - 150°C), and it is important to avoid resist flowing phenomena, that are related to the glass transition temperature and cause degradation of the image.

1.3 Pattern transfer

1.3.1 Etching

The etching process consists in the removal of a layer from the areas that have been left opened at the end of a photolithographic process, whereas the areas that are covered by the mask are not involved in this phenomenon. This is because the etching rate of the resist is several orders of magnitude lower than the etching rate of the same solution on the dedicated material.

The etching could be *isotropic* or *anisotropic*. The first one is the etching that occurs with the same velocity in all the directions, independently from the crystal lattice orientation. The second one, instead, is the etching with different etching rates depending on the considered direction. One example is shown in Figure 1.9.

According to the nature of etching phase, we may distinguish between *wet etching* and *dry etching*.

1.3.1.1 Wet etching

In the wet etching, the substrate is typically immersed in a solution that is able to remove a particular material. The etching rate depends on different factors: the type of material, the thickness of the sacrificial layer, the affinity between material that has to

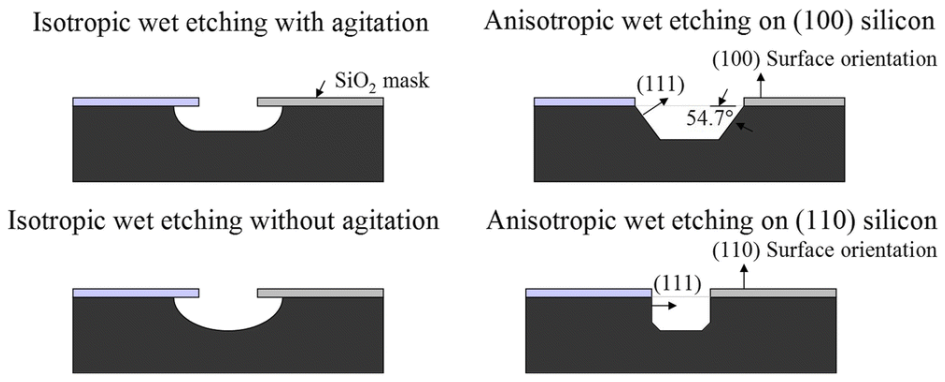

FIGURE 1.9: Isotropic and anisotropic etching

be removed and the etching solution, the temperature of the solution, the fact that the solution is in static or dynamic state. [9] - [10] - [11] - [12]

Every material has its own best fitting etching solution, as shown in Table 1.1.

TABLE 1.1: Wet etchants for different materials (mostly room temperature)

SiO_2	$NH_4F : HF$ (7:1) Called BOE, for buffered oxide etchant
Poly-Si	$HF : HNO_3 : H_2O$ (6:10:40)
Al, Cu	$H_3PO_4 : HNO_3 : H_2O$ (80:4:16) at 70°C
Mo	$H_3PO_4 : HNO_3 : H_2O$ (80:4:16)
W, TiW	$H_2O_2 : H_2O$ (1:1)
Cr	$Ce(NH_4)NO_3 : HNO_3 : H_2O$ (1:1:1)
Ni	$HNO_3 : CH_3COOH : H_2SO_4$ (5:5:2)
Ti	$HF : H_2O_2$ (1:1)
Au	$KI : I_2 : H_2O$
Pt, Au	$HNO_3 : HCl$ (1:3), "aqua regia," H_2O dilution may be used
Ag	$NH_3 : H_2O_2$ (1:1)
Si	KOH (different rates in weight)

1.3.1.2 Dry etching

The dry etching is carried on without a liquid solution. It refers to the removal of material by exposing the same to a ions bombardment (usually a plasma of reactive gases such as fluorocarbons, oxygen, chlorine, boron trichloride; sometimes with addition of nitrogen, argon, helium and other gases) that dislodge portions of the material from the exposed surface. Two common types of dry etching are **Reactive-Ion Etching (RIE)** and **Deep Reactive Ion Etching (DRIE)**.

The process is carried on by a plasma that is activated using a RF electro-magnetic field. This plasma removes the material on the surface that is not masked. In this way,

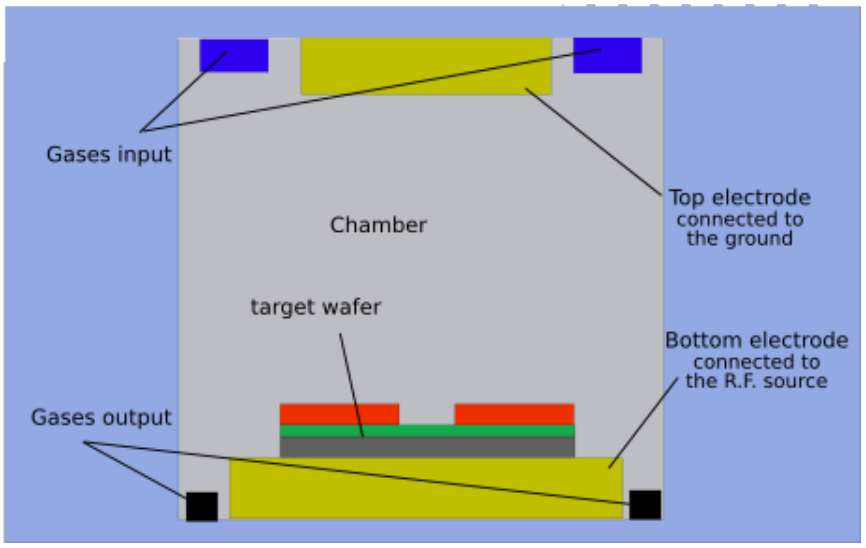

FIGURE 1.10: RIE chamber

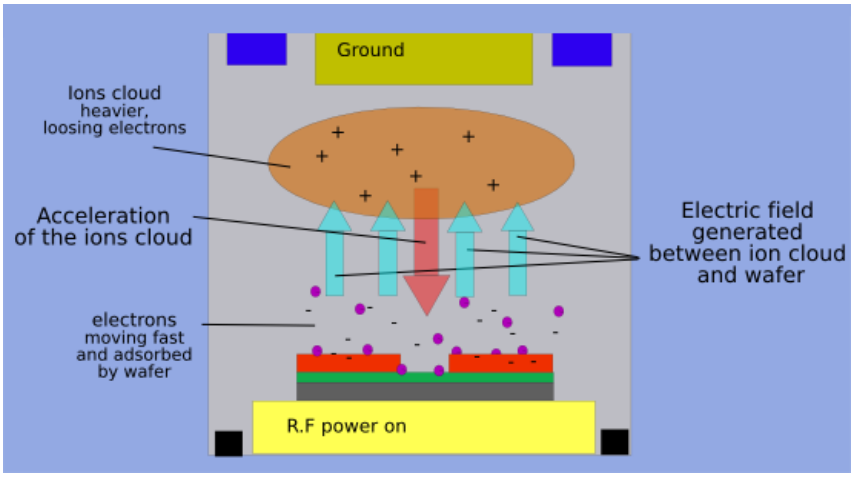

FIGURE 1.11: Reactions in a RIE chamber

the reaction that takes place can be done utilizing high kinetic energy of particle beams, chemical reaction or a combination of both.

In Figure 1.10 we can see the chamber of the RIE device. In Figure 1.11 the above described process is shown.

There are two main types of DRIE processes: Bosch and Cryogenic Process.

In ***Bosch process***, whose name derives from the German company that invented this procedure, there are two steps that are repeated alternatively in order to obtain vertical walls:

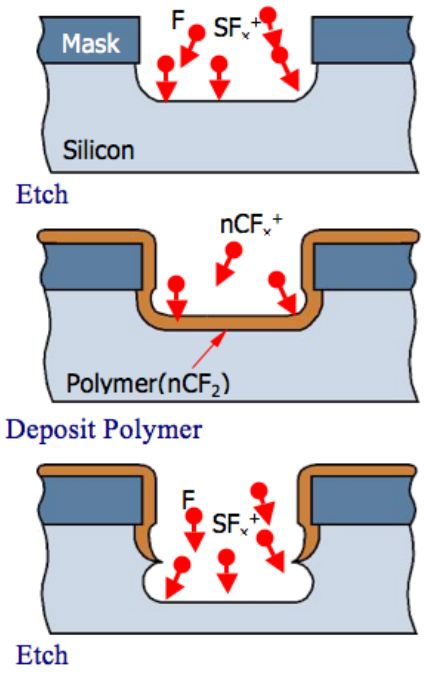

(A) Overview of Bosch process

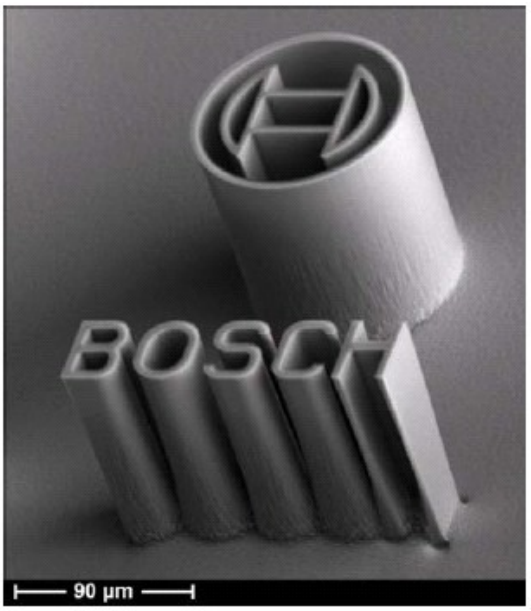

(B) SEM Image after a Bosch process

FIGURE 1.12: The Bosch process.

- an isotropic standard etching step, using for example SF_6 -based plasma for attacking Silicon substrate;
- a step in which a thin fluorocarbon layer is deposited on the walls just dug, using for example C_4F_8 (passivation step).

In this way, the lateral walls are protected by the fluorocarbon layer for the subsequent etching steps, while the bottom floor is every times etched again (because the horizontal layer is etched each time). The repetition of etching and passivation cycles results in almost vertical sidewalls [13].
The figure 1.12 shows the process described and an example of final patterning.

The disadvantage of the process is the final roughness of the sidewalls, due to the alternating etching and passivation steps (see figure 1.12). It can be solved by reducing the duration of this two steps or by post processing [14].

In ***Cryogenic process*** the etching and passivation steps are applied at the same time. A gryogenic temperature is reached (-120°C), and the plasma used is SF_6/O_2. At that temperature, the thickness of the passivation layer depends on the O_2 flux: a too high provision of O_2 creates a too thick passivation layer, while on the other hand a too low flux doesn't allow a formation of a useful passivation layer and the consequent etching step is then isotropic.

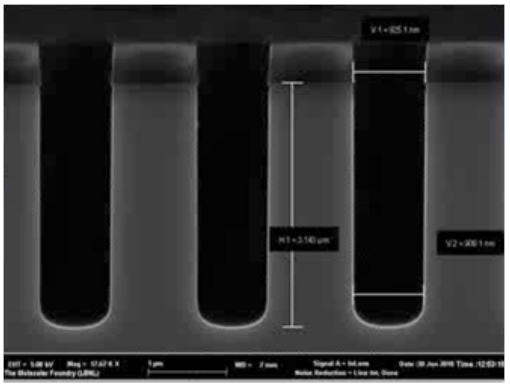

FIGURE 1.13: Structure obtained in Cryogenic process

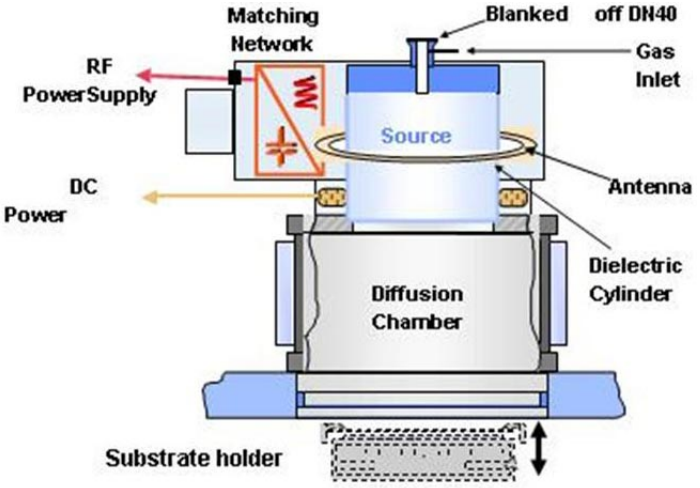

FIGURE 1.14: Setup for DRIE Cryogenic process

The final quality of sidewalls in Cryogenic process is higher than the one obtained in Bosch process, as shown in Figure 1.13.

In the Figure 1.14 the set up for the Cryogenic DRIE process is shown.

The Bosch process offers higher etch rates but at the cost of sidewall roughness. To limit this roughness the rates are usually in the range of 10-20 $\mu m/min$, which is still higher then the cryo process. Cryo processes have usually a better selectivity than Bosch processes, thanks to the fact that the ions have a lower energy. [15] - [16]

1.3.2 Lift-off

Lift-off is a patterning process in which a sacrificial resist layer is used. After a photolythographic process, a metal layer is deposited on the whole area of the substrate, both regions covered or not covered by the resist. The following step is the removal of the

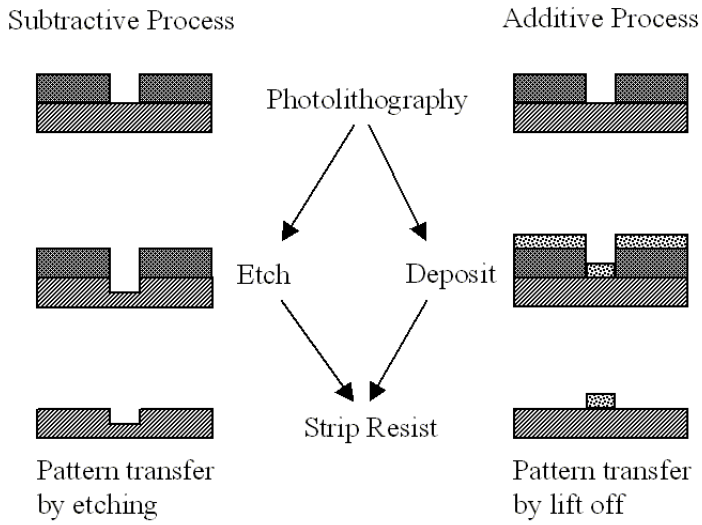

FIGURE 1.15: Differences between etching and lift-off

resist using solvents, for examples *acetone*, *dimethylsulfoxide* (DMSO) or *N-Methyl-2-pyrrolidone* (NMP). As a consequence, also the metal deposited on the resist is removed, and the film will remain only in the areas left open during photolithographic process.

The Figure 1.15 shows the differences between Lift-Off and Etching Processes.

NMP is a powerful lift-off medium due to its properties: NMP yields a low vapor pressure, strongly solves organic impurities as well as resists, keeps solved particles in solution, and can be heated up to 80°C due to its high boiling point. DMSO can be regarded as a non toxic alternative to NMP. [17]

The metal deposition process has photoresist-imposed limitations: it must take place under about 150°C because of resist poor thermal stability.
Moreover, also the polarity of the resist used is fundamental: the negative ones have a profile that allow a perfect separation between the areas that have to remain after all the process and the areas that have to be covered by the resist (negative slope sidewalls); this type of resist is more suitable for the lift-off process. On the other hand, positive resists have the opposite profile (positive slope sidewalls), and they can generate some problems during the removal of the resist. The Figure 1.16 shows this aspects of the process.

1.4 Polymeric machining

In this section some techniques for the manipulation of plastic materials are presented, and in particular some processes for the polymeric machining will be analyzed in details.

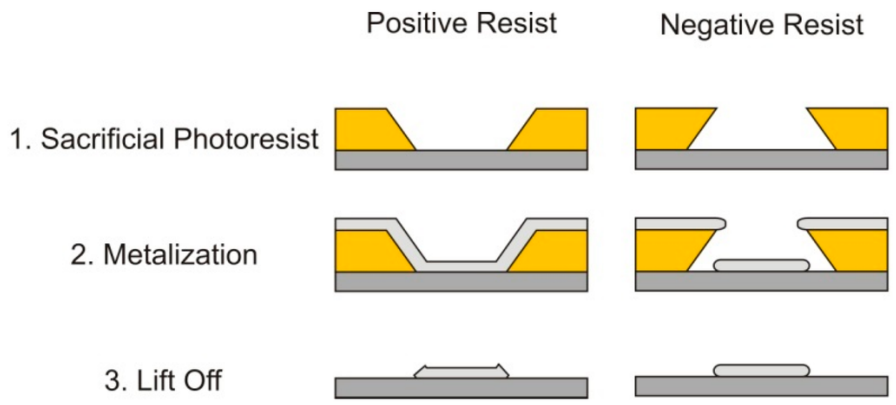

FIGURE 1.16: Polarity of resists in Lift-off processes

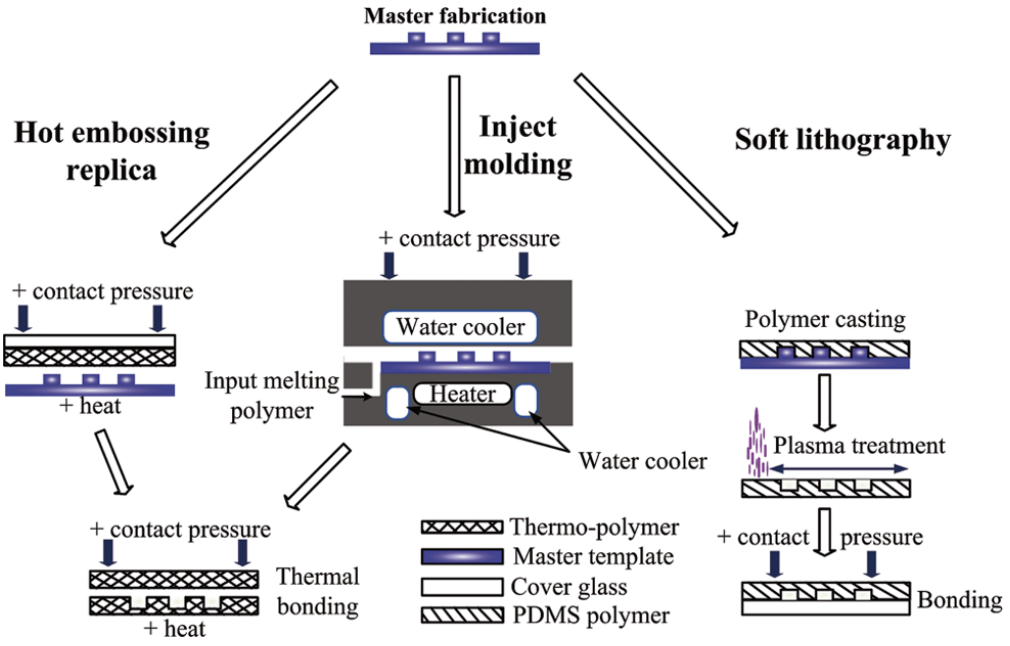

FIGURE 1.17: Three different processes in polymeric machining

In general, there are a lot of different techniques to work with plastic materials. Here we focus our attention on some processes that were used during this thesis work.

The Figure 1.17 shows three of the different types of techniques that are described in the following pages.

1.4.1 Elastomer casting in-situ

This technique allows to obtain a replica device from a master, using precursors and pre-polymers that assume the shape and volume of the master (see Figure 1.17). In this work we have used *PolyDiMethylSiloxane (PDMS)*.

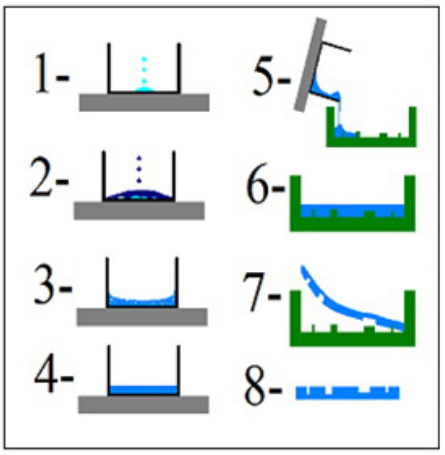

FIGURE 1.18: PDMS casting in-situ

PDMS belongs to a group of polymeric organosilicon compounds that are commonly referred to as silicones. PDMS is the most widely used silicon-based organic polymer, and it is particularly known for its unusual rheological (or flow) properties. PDMS is optically clear and, in general, inert, non-toxic, and non-flammable. The starting material is a fluid elastomer, to which a curing agent is added in a 10:1 weight ratio in order to start reticulation of monomers ad obtain the final elastic solid, similar to rubber.

The Figure 1.18 shows the process in detail:

1. firstly the curing agent is weighted, in a quantity that is a tenth in weight than the elastomer;
2. the second step is the addition of elastomer;
3. then a thourough mixing of the two is performed;
4. a fundamental step is the degassing of the mixture, in order to remove all the bubbles;
5. the degassed mixture is cast in the mold;
6. the following step is the cure; this passage is faster with increasingly temperature;
7. the demolding step allows the separation of the device from the mold (that can be re-used);
8. the final cut of the device gives the ultimate chip;
9. a rinse step in isopropyl alcohol (not shown in figure) is typically necessary mostly for microfluidic devices, in order to restore the normal wettability condition.

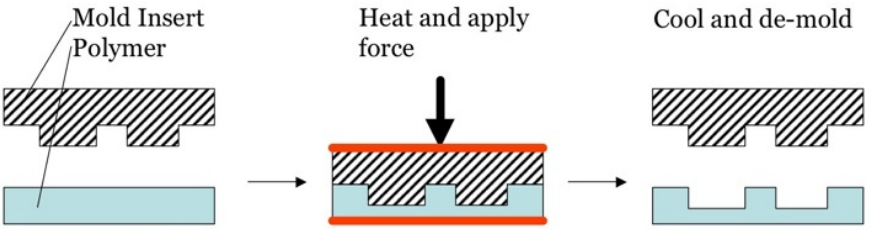

FIGURE 1.19: Scheme of hot embossing process

Our elastomeric product is *Sylgard®184* from *DowCorning®*.
The curing reaction could occur at room temperature, but it is possible to increase the curing speed by warming the mixture. In our case, we used an oven at 90°C; this allows to reduce the curing time from 48 hours to 30 minutes. After this process, the device is immediately ready to use. [18]

1.4.2 Hot embossing replica

Referring to the Figure 1.17, hot embossing is the process in which a pattern is replicated from a mold to a substrate through high pressures and high temperature. Since substrates used in this process are generally polymeric (and so not crystalline), the warming of the mold needs to reach the glass transition temperature of the substrate in order to allow the printing of the pattern. All the process occurs in a vacuum chamber, in order to avoid particulate insertion between mold and substrate; after a cooling time the tool is removed (de-molding step) [19]. The figure 1.19 shows schematically this process.

In the Figure 1.20 we can see the hot embossing machine utilized in our laboratory. It is a *HEX01* hot embossing from *JENOPTIK Mikrotechnik* designed for applications in the fields of micro-optics, microfluidics, smart materials and electronics subcomponents. It ensures highly precise moulding of any structures in polymers, especially microstructures with aggressive aspect ratio (up to 150:1).

1.4.3 Injection molding

According to the Figure 1.17, the third type of polymeric machining process is the *Injection Molding*. As the name suggests, it is a manufacturing process for producing parts by injecting material into a mold. The Figure 1.21 shows the schematic process.

The material is introduced into the injection molding machine via a hopper. The injection molding machine consists of a heated barrel equipped with a reciprocating screw

(A) Vacuum chamber (B) The complete equipment

FIGURE 1.20: Hot embossing machine

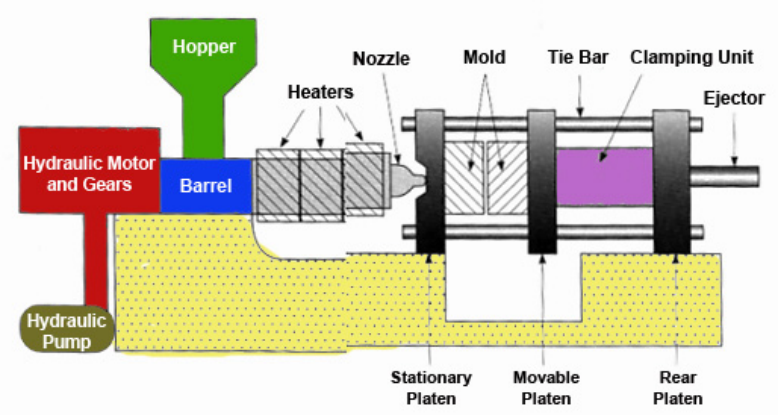

FIGURE 1.21: Scheme of injection molding process

(driven by a hydraulic or electric motor), which feeds the molten polymer into a temperature controlled split mold via a channel system of gates and runners. Then, the screw melts (plasticizes) the polymer. The screw action also provides additional heating by virtue of the shearing action on the polymer. The polymer is finally injected into a mold tool that defines the shape of the molded part. The injection pressure is high (up to one thousand atmospheres), dependent on the material being processed.

Our system is a *BabyPlast*. Thermoplastics, such as PMMA, PC, Polyvinyl Chloride (PVC), Cyclic Olefin Copolymer (COC), are common materials used in micro injection.

1.5 Electroplating

Electroplating is a process that uses electric current to reduce dissolved metal cations so that they form a coherent metal coating on an electrode. The figure 1.23 shows this

(A) Babyplast machine

(B) Detail of the mold

FIGURE 1.22: Micro Injection Molding Machine

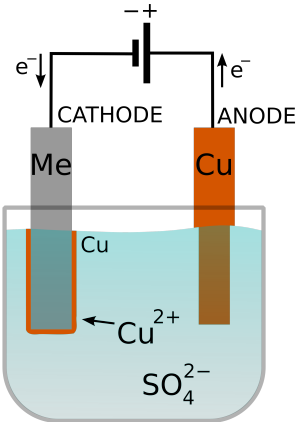

FIGURE 1.23: Scheme of electroplating process

phenomenon.

Electroplating is primarily used to change the surface properties of an object (e.g. abrasion and wear resistance, corrosion protection, lubricity, aesthetic qualities, etc.), but may also be used to build up thickness on undersized parts or to form objects by electroforming. In this way it is not only possible to cover a substrate with a thin layer of metals, but it is also possible to control metal growth in order to obtain areas that have a well determined thickness and geometry.

1.6 Rapid prototyping

One of the most common classification of rapid prototyping equipments is between additive and subtractive processes:

- ***additive manufacturing process***: in this type of process the model is produced adding some material layer by layer or drop by drop in order to obtain the final result;
- ***subtractive manufacturing process***: this type of process removes material from a larger piece of material through standard machining processes.

One example of additive equipment is *OBJET30*. The 3D prototype, independently from its geometrical shape and complexity, is built layer by layer, by superimposing successive layers of two commercial UV photocurable polymers (a structural polymer and a sacrificial one used for the implementation of undercuts and removable by water jet) which are ejected through a special system of ink-jet printer heads. In Figure 1.24 the equipment and an example of final product are shown.

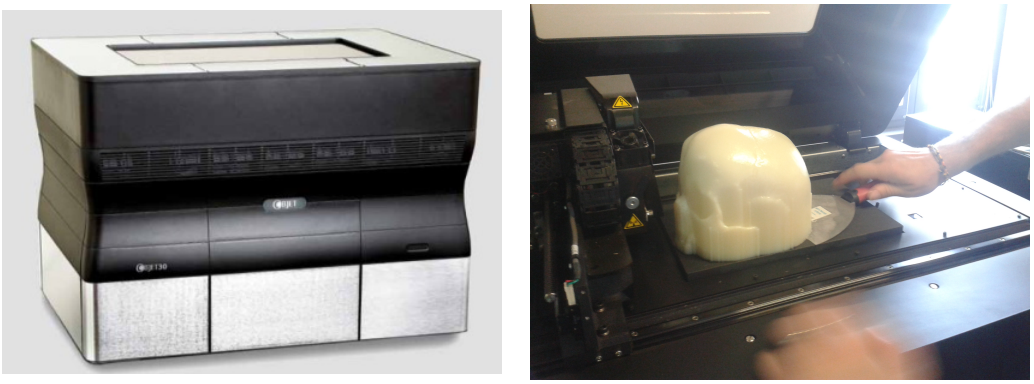

(A) OBJET machine (B) Example of final product

FIGURE 1.24: OBJET equipment

One example of subtractive equipment is the Computer Numerical Control (CNC) Milling: in our laboratory the *BENCHMAN VMC4000* is installed (shown in Figure 1.25).

With this machine it is possible to remove sequentially material from a metallic or polymeric substrate using a rotating tool. This tool follows a path defined by a CAD file, in order to obtain a master that has the negative pattern of the final device (if we need to do the casting-in-situ processes) or directly the final device with the right direct geometry.

1.7 Characterization of devices

In this section some techniques for the characterization of the various process steps are described.

FIGURE 1.25: CNC Milling machine

1.7.1 Profilometry

The ***profilometer*** is a computerized, highly sensitive equipment that measures roughness, waviness, step height, and other surface characteristics in a variety of applications. This is done by a tip that scan the surface of the sample and measures the variations of surface topography, through the measure of the force that is exchanged between the tip and the surface.

Our profilometer is a *Tencor PLA10* and it has the following characteristics:

- Vertical range = 160 μm and 1 Å vertical data resolution.
- Measurement 205 mm (8 in.) substrates.

In the Figure 1.26 the profiler hosted in our class 1000 and an example of image captured from a profilometer are shown; it is possible to see the profile of the surface of the device.

1.7.2 Fluorescence microscopy

A fluorescence microscope is an optical microscope that uses fluorescence and phosphorescence instead of, or in addition to, reflection and absorption to study properties of organic or inorganic substances. The specimen is illuminated with light of a specific wavelength (or wavelengths) which is absorbed by the fluorophores, causing them to emit light of longer wavelengths (i.e., of a different color than the absorbed light). The illumination light is separated from the much weaker emitted fluorescence through the

(A) Profilometer

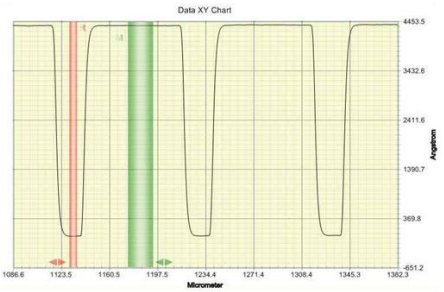

(B) An example of image of profilometry

FIGURE 1.26: Profilometry

use of a spectral emission filter. In the Figure 1.27 our *Carl Zeiss Axio Observer A1* fluorescence microscope is shown.

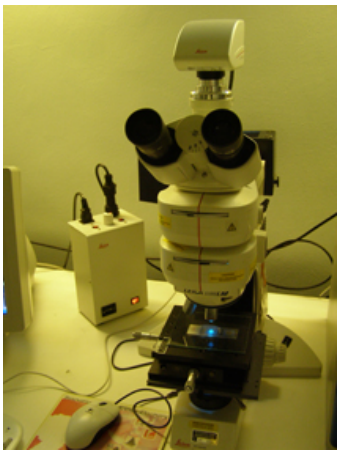

FIGURE 1.27: Fluorescence microscopy

The main limit of this technique is that fluorophores could lose their ability to fluoresce as they are illuminated in a process; this is called *photobleaching*. Photobleaching occurs as the fluorescent molecules accumulate chemical damage from the electrons excited during fluorescence. This problem can severely limit the time over which a sample can be observed by fluorescent microscopy. Several techniques exist to reduce photobleaching such as the use of more robust fluorophores or by minimizing illumination.

Chapter 2

Overview on physiological and physical processes and state of art

In this chapter I will briefly describe the phenomena of cells angiogenesis and chemotaxis that are involved in cancer evolution. Then, I will briefly describe some methods of cells culture and the microfluidic phenomena. Finally, I will show the state of the art in this field, focusing the attention on the developing and realization of microfluidic devices for this aim.

2.1 Angiogenesis of cells

Angiogenesis is the physiological process through which new blood vessels form from pre-existing vessels. This is distinct from vasculogenesis, which is the de novo formation of endothelial cells from mesoderm cell precursors.[20] The first vessels in the developing embryo form through vasculogenesis, after which angiogenesis is responsible for most, if not all, blood vessel growth during development and in disease. [21]

Angiogenesis is a normal and vital process in growth and development, as well as in wound healing and in the formation of granulation tissue. However, it is also a fundamental step in the transition of tumors from a benign state to a malignant one, leading to the use of angiogenesis inhibitors in the treatment of cancer. The essential role of angiogenesis in tumor growth was first proposed in 1971 by Judah Folkman, who described tumors as 'hot and bloody'. [22]

As we said, tumor angiogenesis refers to the ability of a tumor to stimulate new blood vessels formation. This critical step in development enables tumor expansion, local invasion, and dissemination through three passages: 1) Delivery of oxygen, nutrients, and

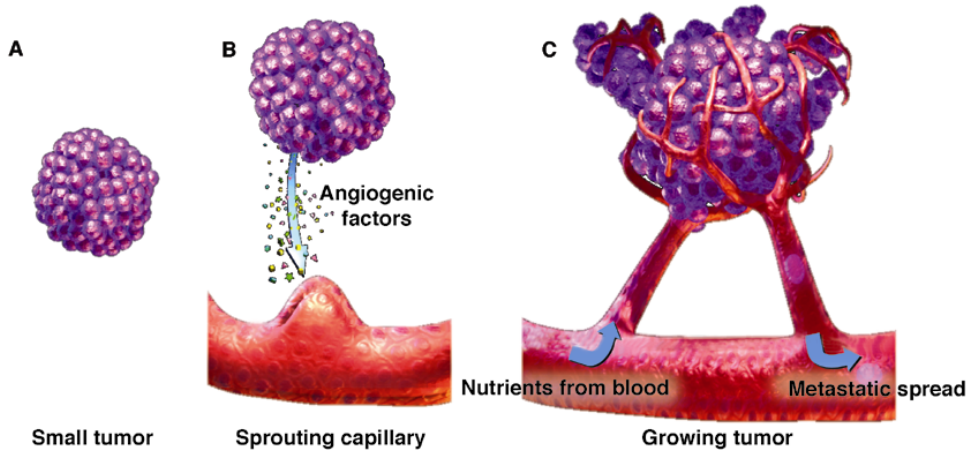

FIGURE 2.1: Angiogenesis phenomenon

survival factors; 2) Production of growth factors that benefit tumor cells; 3) Formation of a route for tumor cell egress. [23]-[24]-[25]

In the Figure 2.1 the basic scheme of the angiogenesis phenomenon is shown. It is possible to notice that the formation of new vessels is influenced by a preliminary agglomeration of tumor cells.

There are two mainly types of angiogenesis:

- in the **sprouting angiogenesis** new vessels form from a first original one, moving towards growing factors and creating more than one smaller vessels, like some branches in a tree;
- in the **intussusceptive angiogenesis** new vessels form in order to connect the old vessels that were already formed; in this way, a sort of net is created between pre-existing vessels.

These two different types of angiogenesis are shown in the Figure 2.2.

Chemical stimulation of angiogenesis is performed by various angiogenic proteins, including several growth factors. The study of these growing factors is crucial in order to try to understand the cancer phenomena and, consequently, in order to try to defeat this desease. Each single factor has been studied, but a lot of more useful information are not still discovered.

The role of angiogenesis in tumor growth has been studied continuously for over 45 years. We can cite the most recent works done all around the world.

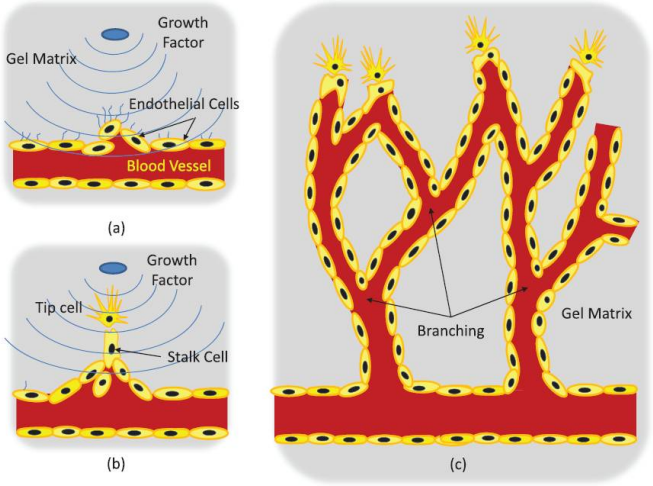

(A) Sprouting angiogenesis

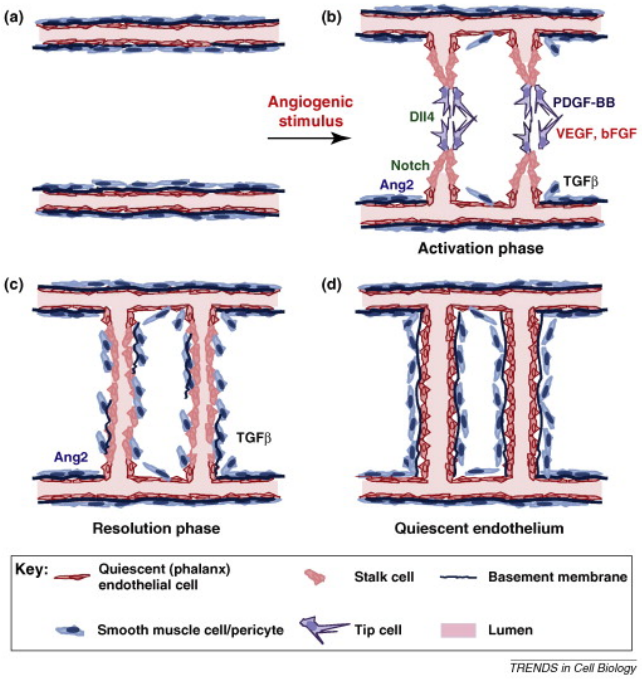

(B) Intussusceptive angiogenesis

FIGURE 2.2: The two main types of angiogenesis

The first example could be the work of Bielenberg et Al. [26], in which new important evidences are discovered regarding the correlation between cancer and angiogenesis phenomena. In particular they focus the attention on the role of angiogenesis as a necessity for the escape of tumor cells into the bloodstream and for the establishment of metastatic colonies in secondary sites.

Another example is the state of art regarding new Methods for Evaluation of Angiogenesis and Tissue Vascularization, written by Simons et Al. [27]. In this work, all the new models for the different phenomena of angiogenesis discovered until now are described. All these models require a 3-D environment for the growing of the tumor cells.

One more article is the therapeutic procedure for contrasting the developing of tumors by not allowing the fonding of proteins involved in angiogenesis phenomenon (K. Banerjee et Al. [28]).
Zongwei Wang et Al. wrote another articles regarding the target of angiogenesis in order to prevent the tumor developing of cells. [29].

Most of the articles in even the recent years are focused on the relationship between these two phenomena. [30]−[31]−[32]−[33]−[34]−[35]−[36]
So that means that the studies and the researches in these fields are crucial to better understand how this physiological process carries on and, consequentially, how to try to defeat this desease.

2.2 Chemotaxis of cells

Chemotaxis is the movement of an organism in response to a chemical stimulus. Somatic cells, bacteria, and other single-cell or multicellular organisms direct their movements according to certain chemicals in their environment. This is important for bacteria to find food (e.g., glucose) by swimming toward the highest concentration of food molecules, or to flee from poisons (e.g., phenol). In multicellular organisms, chemotaxis is critical to early development (e.g., movement of sperm towards the egg during fertilization) and subsequent phases of development (e.g., migration of neurons or lymphocytes) as well as in normal function.

There are two types of chemotaxis:

- *positive* chemotaxis occurs if the movement is toward a higher concentration of the chemical in question;
- *negative* chemotaxis if the movement is in the opposite direction.

Chemoattractants and chemorepellents are inorganic or organic substances possessing chemotaxis-inducer effect in motile cells. Effects of chemoattractants are elicited via described or hypothetic chemotaxis receptors, the chemoattractant moiety of a ligand is target cell specific and concentration dependent. Most frequently investigated chemoattractants are formyl peptides and chemokines. Responses to chemorepellents result in axial swimming and they are considered a basic motile phenomena in bacteria. The most frequently investigated chemorepellents are inorganic salts, amino acids, and some chemokines.

The Figure 2.3 shows the phenomenon described above.

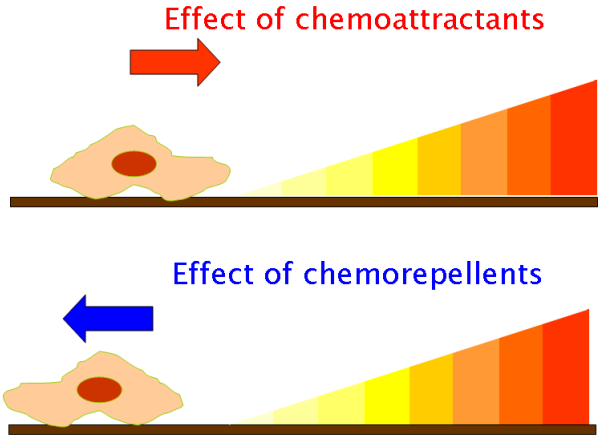

FIGURE 2.3: Chemotaxis phenomenon

Although chemotaxis is the most frequently studied form of migration there are several other forms of locomotion in the cellular level (shown in Figure 2.4):

- the first one is called *chemokinesis*: it is also induced by molecules of the liquid phase of the surrounding environment; however, the response elicited is a not vectorial, random taxis. Neither amplitude nor frequency of motion has characteristic, directional components, as this behaviour provides more scanning of the environment than migration between two distinct points;
- in *haptotaxis* the gradient of the chemoattractant is expressed or bound on a surface, in contrast to the classical model of chemotaxis, in which the gradient develops in a soluble fluid. The most common biologically active haptotactic surface is the *ExtraCellular Matrix (ECM)*; the presence of bound ligands is responsible for induction of transendothelial migration and angiogenesis;
- *necrotaxis* embodies a special type of chemotaxis when the chemoattractant molecules are released from necrotic or apoptotic cells. Depending on the chemical character of released substances, necrotaxis can accumulate or repel cells, which underlines the pathophysiological significance of this phenomenon.

In addition, it has been recognized that mechanisms that allow chemotaxis in animals can be subverted during cancer metastasis. Also in these cases, there are a lot of papers in literature regarding this link between these two phenomena.
For example, one research in the field of ovarian cancer, led out by Pranesh M Gunjal et Al., focuses the attention on the particular area limited to the ovarian cells. [37]

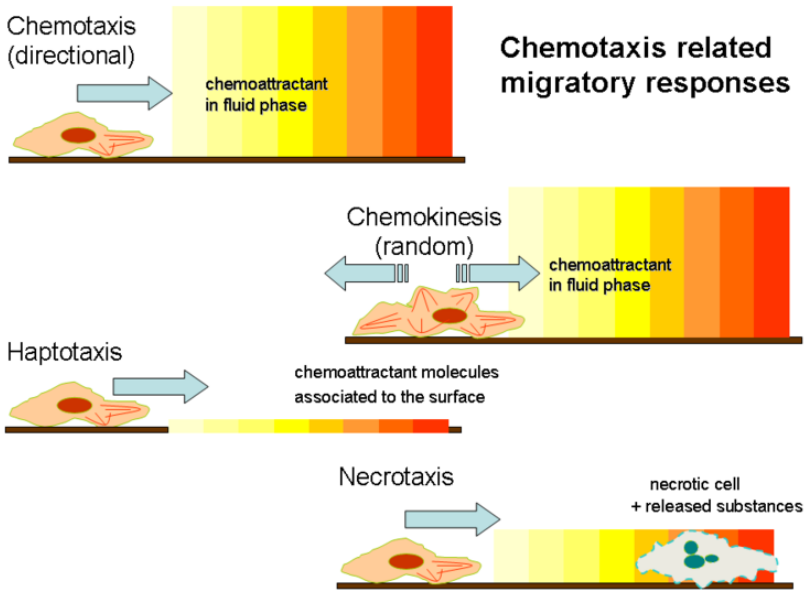

FIGURE 2.4: Some forms of locomotion of cells

Another work is related to the fiber cells and their connection to the cancer and chemotaxis phenomena (Nelson et Al.,[38]).
Another work, in a completely different field, is led by Broadway et Al., in which the same aim is carried out with the *salmonella enterica* [39].

All these examples show that the interest is very high on this phenomenon; moreover, a lot of different fields are involved in this research, and in each of them there are many aspects and processes that are still unknown.

2.3 Cells culturing

The cell migration mechanisms play a fundamental role in physiological adult cells processes as well in cancer metastasis as in embryogenesis. Cells move in a 3D environment where they are subjected to different kinds of stimuli. However, nowadays the ability to understand their formation, function, and related pathology has often depended on two-dimensional cell cultures. The exploitation of microfluidic platforms leads to a better mimic of a 3D environment. Moreover, microfluidic devices ensure a high throughput testing due to the possibility of their integration in a small area of substrate, allowing also an easier exploitation of parallelism in analysis. Moreover it permits a minimum loss in reagents, solutions and chemicals used to perform experiments.

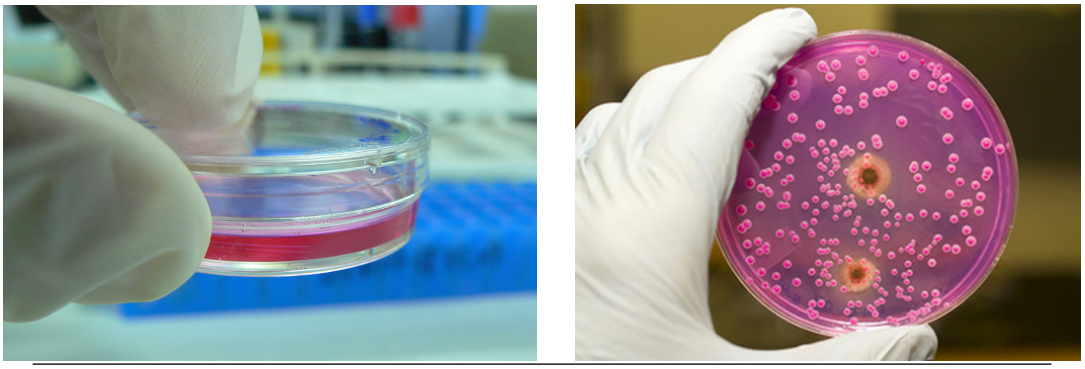

FIGURE 2.5: Two examples of cells culture in Petri dishes

Cell culturing is the process by which living cells are grown in similar controlled conditions outside their natural environment. Traditionally, researchers grow cells in glass or plastic Petri dishes in an attempt to replicate in vivo conditions. Cell growth is promoted by periodically replacing the cell culture nutrient media in which the cells reside. Traditional cell culturing occurs on the flat interior surface of a Petri dish, which can be considered as a 2D culture (Figure 2.5).

The main problems that arise with manual 2D cell culturing approaches are linked to the necessity having a natural growth environment, eliminating contamination, supporting multiple cultures simultaneously and maintaining consistency and quality. The first issue, unnatural growing conditions, arises from the fact that cells grown in the traditional 2D fashion do not resemble those that are observed in vivo. Cells do not achieve in vivo like phenotypes and activity when attached to and propagating on a glass or plastic surface. 3D cell culture systems use growth substrates that more closely resemble those in the body. These bio-mimetic surfaces are known to stimulate the growing cells to form organ-like attachments and behaviors. Suspending cells in the cell culture media is advantageous to facilitate feeding and harvesting the cell cultures.
One of probable solution could be growing cells on porous, hydrogel beads containing magnetic particles enables the cells to be maintained in suspension by rapid back and forth agitation of the growth vessel (Levitube^{TM}) using a stepper motor equipped device (Bio Wiggler^{TM}), as shown in Figure 2.6. The growth beads may be aspirated and dispensed by a liquid handling robot. Harvesting the growth beads is accomplished by using an externally applied magnetic field. This project focuses on developing subsystems that support these 3D cell culturing techniques [40] - [41] - [42].

Contamination is an issue in many veins of biological research. In most cases, contamination by foreign bacteria or viruses is easy to be detected due to cell death. There are however some hard problems to detect protozoan contaminants, single cell organisms such as amoeba, that do not kill cells through infection but cause abnormal behavior in tests. Because these protozoa are ubiquitous, the one effective method for eliminating

FIGURE 2.6: Levitube device

contamination risk is to maintain a closed, sterile environment with minimal human contact. To reduce or even eliminate this issue can be by providing a sterile enclosure in which a robot performs all the cell culturing functions a researcher would typically perform. [43]

Lab grown cell populations, called ***cell-lines***, require constant nourishment and monitoring. Limits on human capabilities prevent most researchers from growing more than four cell-lines without introducing significant human errors that results in unsatisfactory results or misidentified cell lines. It is estimated that over 8% of published cell lines are misidentified [44] [45]. This limits the amount of usable and consistent cell cultures. By developing automated subsystems that provide scheduled and consistent cultivation of cell lines it is possible to eliminate variance introduced by human error, allowing the system to be scaled up to maintain larger cell line populations due to the consistency of an automated system. Several 2D cell culture automation systems have been previously developed, but the application of automation to 3D cell culture is still in its infancy. Automation improves the consistency of cell cultures while also improving the quality of results and repeatability of experiments.

2.4 Overview on Physics and Properties of Microfluidics

Microfluidics is the science and technology of manipulating and controlling fluids, usually in the range of microliters, μl (10^{-6}), to picoliters, pl (10^{-12}), in networks of channels with lowest dimensions from tens to hundreds micrometers. In our case, the dimensions of the devices are large enough to contain single-cells (5-10 μm) and cluster formations (50-100 μm), but they are still in the microfluidic field (the minimum dimension of the device is 350 μm).

Typically, 'micro' means one of the following features: small volumes, small size, low energy consumption and micro domain effects. The behavior of fluids at the microscale can differ from 'macrofluidic' behavior in that factors such as surface tension, energy dissipation, and fluidic resistance that start to dominate the system. Microfluidics studies how these properties change, and how they can be worked around, or exploited for new uses. [46] - [47]

The most important phenomena involved in the microscale are the following:

- There is a predominance of viscous effects over the inertial ones. The formula that shows this behavior is the *Reynolds Number*:

$$Re = \frac{vd\rho}{\mu}$$

where v:velocity, d:dimension of the channel, ρ:density, μ:viscosity. If $Re < 2300$, the viscosity effect is bigger than the inertial one, and the flow is laminar; on the other hand, if $Re > 4000$, the flow is turbulent [48]. Therefore in the microscale the fluid is laminar (Fig. 2.7).

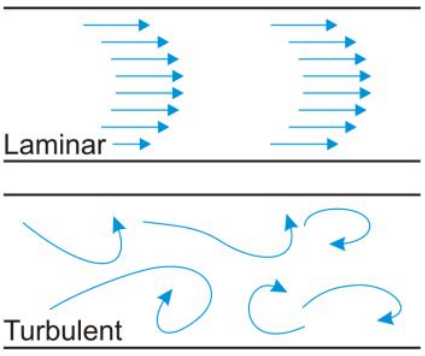

FIGURE 2.7: Difference between turbulent and laminar flow

- *Surface tension* of liquids plays a fundamental role at microscopic scale, allowing the exploitation of different phenomena (Fig. 2.8). Such microscopic scale physical phenomena were largely employed in this project in order to avoid the penetration of liquid in specific zones, despite some apertures were created. The project is mainly depending on surface tension force of liquids at the microscopic scale to prevent the passage of the fluids through the lateral channels from the main central channel. It was performed using pillars distanced by few tens of micrometers to prevent the fluids to enter according to their surface tensions.

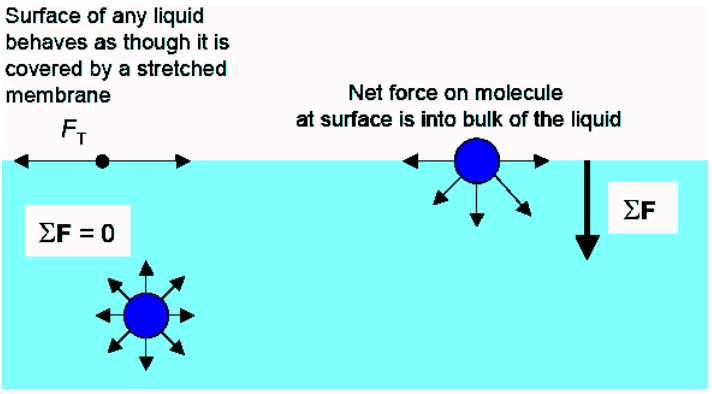

FIGURE 2.8: Explanation of surface tension

- *Capillarity effects*, as a consequence, also become much more relevant at small scale, leading to effects very different from the corresponding macro-scale.

Another important aspect in microfluidics is the formation of bubbles: this could be a very big problem for many reasons. First of all, micro-bubbles can damage the device itself (for instance pillars or very thin structures could be destroyed); secondly, bubbles can occlude channels and not to allow the correct passage of fluids; finally, in bio-tests, bubbles could alter the natural and physiological behavior of cells, leading to incorrect results of measurements.

As we said before, ***diffusion*** is a dominant transport process in microfluidics. Diffusion is the net movement of molecules or atoms from a region of high concentration to a region of low concentration, without a bulk motion. In other words, this is a movement of a substance down a concentration gradient. Since a gradient means the change in the value of a quantity with the change of another variable, the concentration gradient is a change in concentration over a distance.

A phenomenological approach to explain diffusion is regarding *Fick's law of diffusion*:

$$j = -D\frac{\partial N}{\partial x}$$

where j: net flux, D: diffusivity coefficient, N: concentration and x: spacial variable. According to Fick's law, the diffusion flux is proportional to the negative gradient of concentrations. It goes from regions of higher concentration to regions of lower concentration.

Fick asserted a deep analogy between diffusion and conduction of heat or electricity, creating a formalism that is similar to *Fourier's law* for heat conduction (1822) and *Ohm's law* for electric current (1827), as shown in Fig. 2.9.

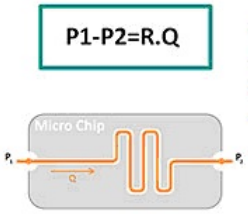

Microfluidics	Electrical	Microfluidic unit
Pressure (Pa)	Potential (V)	*mbar*
Flow-rate ($m^3.s^{-1}$)	Intensity (A)	*$\mu l.min^{-1}$*
Resistance ($Pa.s.m^{-3}$)	Resistance (Ω)	*$mbar.min.\mu l^{-1}$*

FIGURE 2.9: Analogy between microfluidics and electric current

The advantages of the microfluidic usage in technology and especially in Lab-on-Chip (LOC) field are:

- it permits a good portability and lower price due to the reduction of materials for the manufacture and for the very small volumes of the reagents involved;
- for the same reason, a lower energy is required to perform specific experiments if compared to experiments carried on in the macro domain;
- it is possible to analyze smaller samples and, as consequence, there is no waste of reagents and material under analysis.

2.5 State of art

As said before, the study of cells chemotaxis and angiogenesis phenomena plays a significant role in a better understanding of cancer evolution. As a matter of fact, cells are influenced by the physiological environment, which contains all the substances that could influence their regular life. The importance of the study of this influence from nutrients or toxic elements is generally accepted. In order to do this, in the last decade a large number of studies were carried on simple 2D devices.

This type of platform did not allow a well-simulated physiological behavior, and they were overcome by the study of 3D platforms. [49] - [50] - [51] - [52] - [53] - [54] - [55]

In recent years a lot of different procedures were analyzed. For instance, new 3D rapid prototyping techniques are reported [56]. In this work, various 3D printing techniques are analyzed: stereolithography (SL) (Figure 2.10), two photon polymerization (TPP), fused deposition modeling (FDM), 3D inkjet printing and Direct laser writing (used as a process to remove material from a bulk). Unfortunately, these methods do not always guarantee optical transparency, complete polymerization of the resin and even biocompatibility.

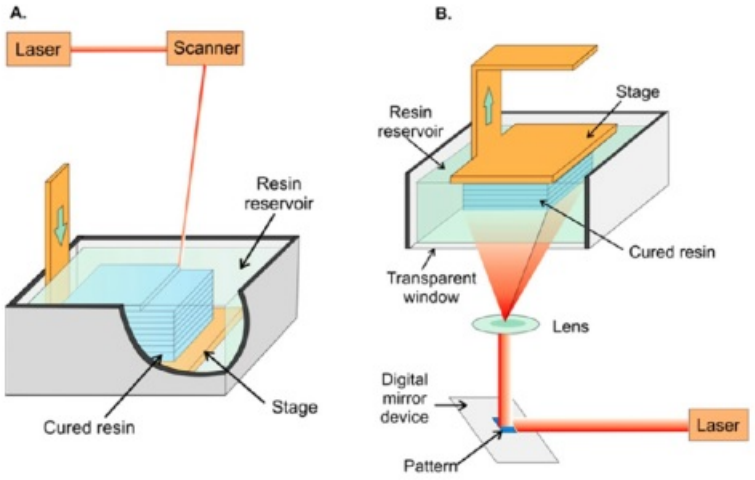

FIGURE 2.10: (a) Schematic of a SL bath configuration with direct laser writing and (b) a SL layer configuration with DMD-based writing.

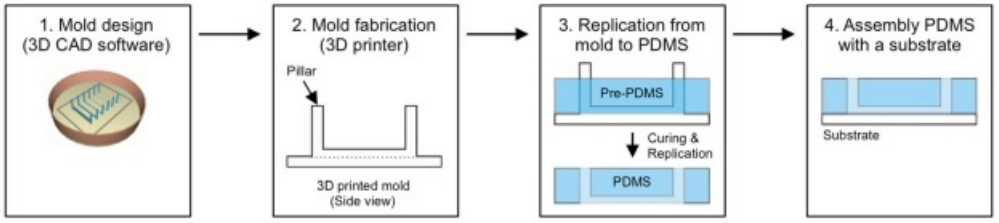

FIGURE 2.11: Fabrication procedure for a PDMS-based microfluidic device with a 3D-printed mold.

Another example is described by Ken-ichiro Kamei et Al. [57]. In this work, a completely photolithographic-free process is described, usign a 3D printing machine to build a master and then using the casting-in-situ technique with PDMS (Figure 2.11). The problem in this case is the low resolution obtained for the construction of a microfluidic device.

For these reasons, the major studies are focused on microfluidic devices that try to establish a chemical gradient of substances under observation.

A lot of works are done in this direction. A very useful review is for instance the one written by Laszlo Hajba et Al. [58]. In this work some devices to capture cells are shown; these devices use different principles in order to block, contain, store, detect and confine cells: for instance, hydrodynamic approach, electrophoretic phenomena, affine-based methods and magnetic trapping are shown (Figure 2.12).

Other studies are focused on behavior of neuron cells, like the work of Hui Huang et Al. [59]. This device uses the mechanical flux of fluids to dilute the fluid in order to obtain

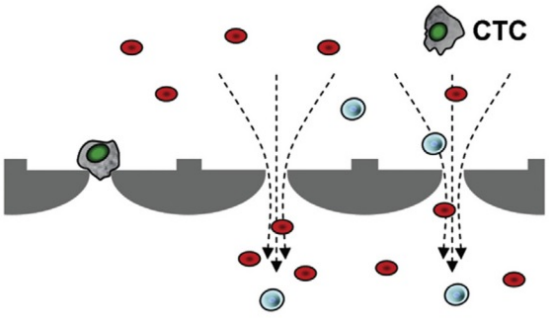

(A) Size-selective cells system (Geislinger et al.)

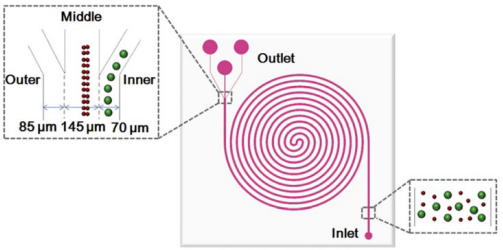

(B) Cell-sorter system (Bhagat et al.)

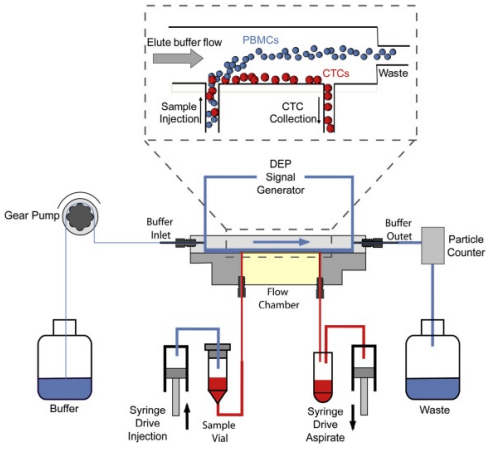

(C) Dielectrophoresi sorter system (V. Gupta et al.)

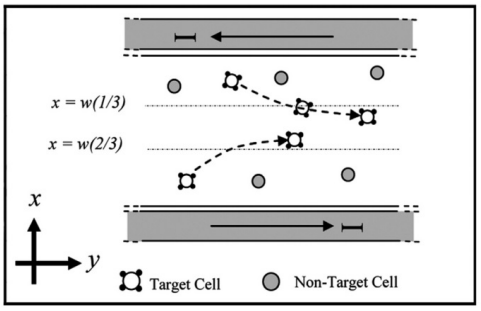

(D) Magnetic separator system (B.D. Plouffe et al.)

FIGURE 2.12: Some examples of devices for cells

a gradient of concentration in a chamber in which neurons can grown up (Figure 2.13).

Another example is a three channel device, led by Shamloo et Al. [60]. In this device a gradient could be led out in order to see how influent is the connection between cells chemotaxis and gradient of substances in fluids (Figure 2.14).

One last example is a static chamber that can allow a gradient exploiting a geometric distance between a central channel and a lateral channel [61]. In this case, a time-lapse phase contrast microscopy analysis is performed, and again the connection between the angiogenesis and chemotaxis phenomena to cells growth is underlined (Figure 2.15).

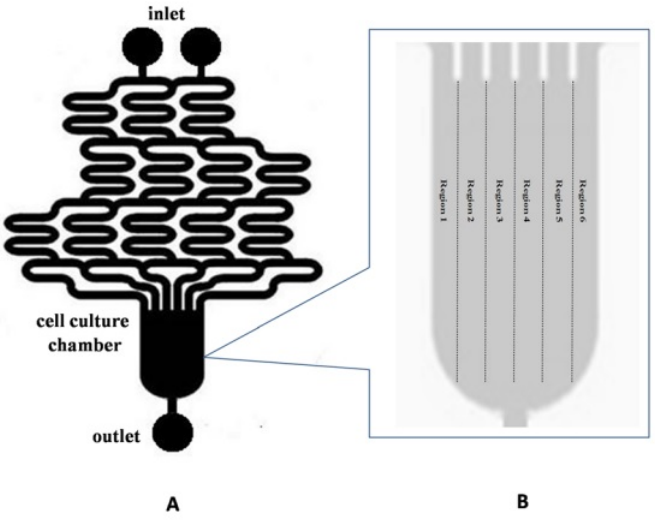

FIGURE 2.13: Device for neuron cells growth

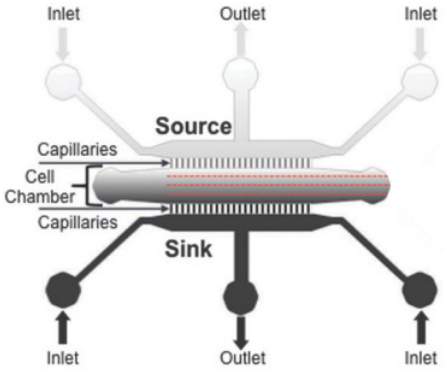

FIGURE 2.14: Device for cells growth

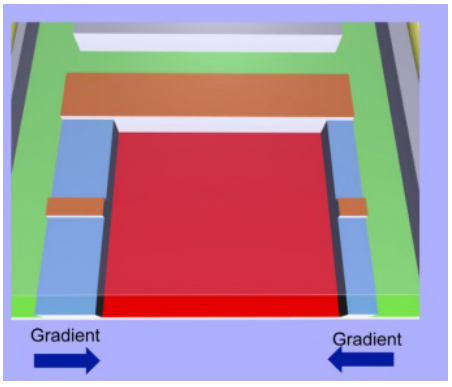

(A) Chamber device - top view

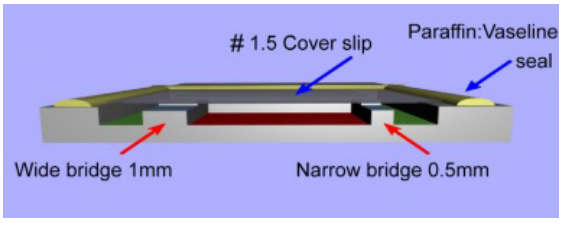

(B) Chamber device - frontal view

FIGURE 2.15: Chamber device for gradient in fluid

Chapter 3

Device realization

In this chapter I will describe all the passages that led to the final chip realization for the study of cells chemotaxis and angiogenesis. All the steps of my work will be analyzed, from the preliminary studies of some materials used in the process, to the final obtained device.

The aim is to obtain a microfluidic device that is considered belonging to the micro-scale thanks to its dimensions but, at the same time, it can allow a 3-Dimensional growth of cells in vivo. This is the very important innovation of this device: it is possible to study, observe, measure and analyze the *real* growth of natural cells, in a 3D environment.

3.1 Introduction

As mentioned before, we can summarize some important points regarding the phenomena studied in this work:

- the cell migration mechanisms play a fundamental role in physiological adult cells processes as well in cancer metastasis as in embryogenesis;
- cells move in a 3D environment where they are subjected to different kinds of stimuli;
- cell culturing is the process by which living cells are grown in similar controlled conditions outside their natural environment;
- traditionally, researchers grow cells in glass or plastic Petri dishes in an attempt to replicate in vivo conditions; these could be considered a 2D in vitro culture;

- cell growth is promoted by periodically replacing the cell culture nutrient media in which the cells reside;
- 3D cell culture systems use growth substrates that more closely simulate those in the body; suspending cells on porous, hydrogel cell culture media is advantageous to facilitate feeding and harvesting the cell cultures.

There are more advantages due to the microscale features of microfluidic LOC systems:

- good portability and lower price are possible due to the reduction of materials for the manufacture and the reagents involved in the analysis;
- a lower energy is required to perform specific experiments due to the miniaturization of the devices as well as volumes needed of reagents or stimuli;
- faster processes are carried on due to increase of Surface/Volume ratio;
- there is the possibility to analyze smaller samples and, consequently, smaller quantities of waste are produced; in the same way, there is no need for higher blood volumes or other substancies to perform some tests;
- some LOC systems have the ability to culture cells under the gradient of a single compound; the ability of the chip to screen for the combinatorial effect of several compounds has great importance because cells receive more than one extracellular signal at once.

Any microfluidic device designed for performing chemotactic processes can be based on two different principles: ***flow-based*** or ***flow-free***. The first one is the most common, in which a laminar flux can introduce stable gradients which can be dynamically varied according to needs. The second one minimizes the stress on cells and structures and the complexity in the control system, but it introduces only static gradients and works only with equilibrium states of the system.

3.2 Newton device

Newton Project is the name given to the microfluidic chip for chemotaxis analysis on Embryonic Stem (ES) cells by the research group operating at the ***Chilab Laboratory*** of the Polytechnic of Turin in collaboration with IRCC (Institute of Research on Cancer of Candiolo) and University of Genoa.

3.2.1 First version

The aim of this project is the fabrication of a microfluidic multi-well platform to analyze chemotaxis mechanisms on ES cells. These cells, which could be induced to differentiate in about 220 adult cells types, represent a well-known model to be studied for a widespread number of applications [62] - [63] - [64] - [65].

The main applied idea is a two parallel micro-channels, in which the solutions flow independently around some chambers in which the biological samples can be positioned and remain fixed; the shape must guarantee that the lateral fluidic flow cannot enter the central (main) chambers, but only lap the cavities to contact the culture field (to be able to diffuse inside) in which spheroids are immersed. This is the key to produce the desired controlled gradient, allowing also to change it dynamically, without direct contamination and physical contact with the cells under study.

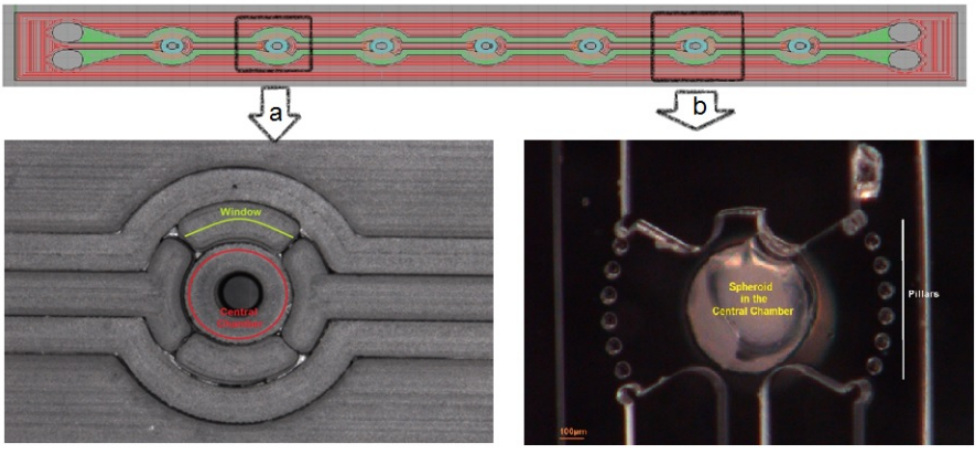

FIGURE 3.1: First version of Newton device with 7 chambers in series. In A) and B) two examples of central chambers and lateral channels are shown.

The first version of Newton device schematic view is shown in Figure 3.1. The chip is provided with an array of 7 chambers in series. A PDMS microfluidic platform was designed and fabricated using standard MEMS technology and connected to an external pumping system as described elsewhere [66] - [67]. The channel depth is about 160 μm, and it is imposed and tuned during the SU-8 spinning. Instead their width is imposed by mask design and it is equal to 800 μm. A parallel micro-channels configuration was chosen to bring stimulating or inhibiting liquids to the micro-chambers. A micro array of pillars allows for the interface with the micro-chamber containing the spheroid (Figure 3.2). The main problem of this configuration is related to the fact that liquids passing into the channels could enter the central chamber, because those windows were not able to really confine them exploiting surface tension only.

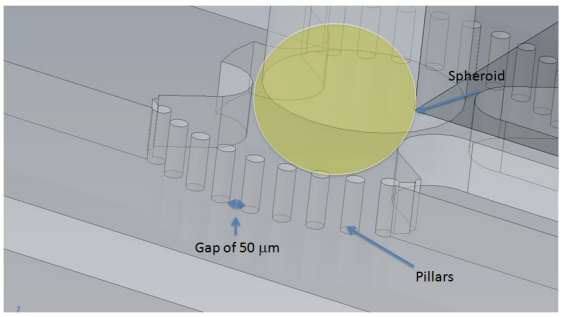

(A) Simulation of chamber with spheroid inside

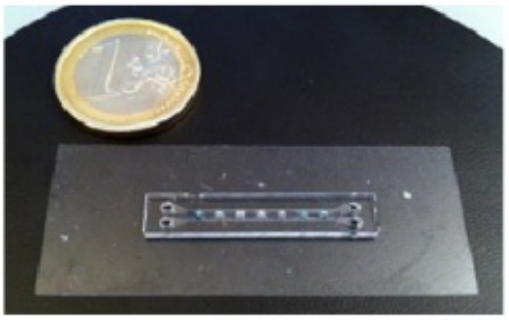

(B) Final PDMS device

FIGURE 3.2: First version of device

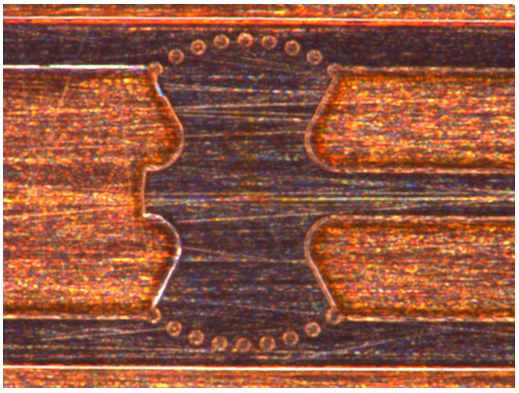

(A) Cu mold of the central channel

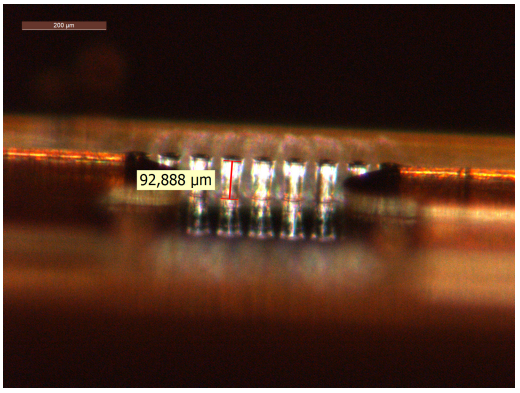

(B) Real height of obtained pillars

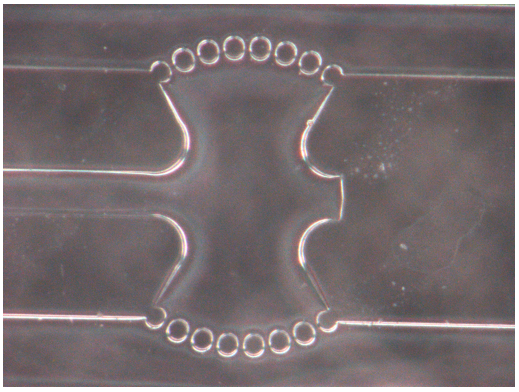

(C) Final chamber obtained in the PMMA chip

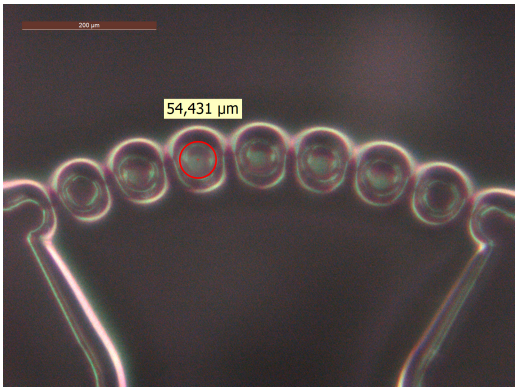

(D) Real final dimensions of pillars in PMMA chip

FIGURE 3.3: Cu mold and PMMA chip obtained by hot embossing process

Pillars are placed along an arch and their diameter is 50 μm, which is also equal to their gap. In the center there is a lodging of dimension comparable to a spheroid of cells so as to keep it in position. The aim of these micro-structural pillars is to act as a barrier that maintains the liquid in contact with the micro-chamber and let the reagents diffuse from the mainstream avoiding any mixing with the reagents in the parallel micro channel. The spheroids (size: 500 μm in diameter), containing the ES cells, were maintained in a hydrogel and inserted in the micro-chamber with a micro-pipette.

Also another process was carried on. The idea was to obtain chip replica using a Cu mold in a hot embossing machine with a PMMA substrate. In the Figure 3.3 we can see the final device obtained. In this case, the results were not optimal, for the same reason described before: liquids couldn't remain in the lateral channels and they were used to pass in the central chamber.

3.2.2 Second version

In order to solve problems that occurred in the first version, a new version has been designed. Moreover, at the same time, some new requirements of chemotactic analysis arised. In particular, instead of working with a single spheroid fixed into a chamber, a high number of cells can be contained in a bigger volume along a one central channel. In this way, it gives the possibility to cells to interact each others, a gradient can be generated and the movement of cells in their 3D culture environment can be observed through microscopy.

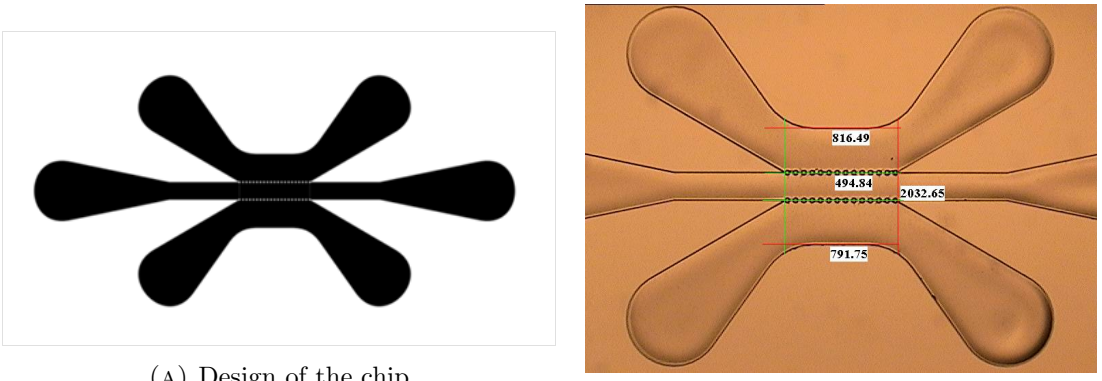

(A) Design of the chip

(B) SU8 result obtained (μm units)

FIGURE 3.4: Overview on second version of Newton device

The design is simpler if compared to the first version. It consists of a central channel 500 μm wide and two lateral channels in which solutions can flow, used as culture field, divided by 75μm-pillars. Every single channel has inlet and outlet in order to load cells and solutions inside the chip. The design is shown in Figure 3.4.

Since the correct idea of surface tension forces is crucial in order to let solutions entry in lateral channels but not in the central one, the correct dimensions of pillars and the distances between them is also very important in order to avoid leaking through the pillars arrays. Simulation of behavior of Matrigel^{TM}, the substance used for the cell culture (as described in Chapter 4), is very complex and not trivial. As a consequence, dimensions and distances were obtained empirically by performing different tests with a variation in pillars diameter and separation.

The diffusion phenomenon is the same in the two different design versions, but in this second one the path is longer and can let a better study of chemotaxis and angiogenesis behavior. Regarding this aspects, some simulations have been performed in order to study the effect of the fluid passage in lateral channels; in particular, the question was if the lateral solution passes or not from the lateral channels to the central one. In the case of study the diameter of the pillars and the distance between them is 75 μm.
The 2D simulation performed using *COMSOL Multiphysics*® involved two important aspects:

- in the calculation only half of the device was considered, since it is symmetric;
- the worst case condition is simulated when water is entering a channel full of air only, since the entrance among pillars is of course easier when there is only atmospheric pressure than when a Matrigel^{TM} is present inside because the Matrigel^{TM} is more viscous than the air.

Below we discuss the simulation results. As shown in Figure 3.5 and in Figure 3.6, even with a high flow rate, the surface tension of water is strong enough to prevent the entrance of flow in the central channel. In the real case we have Matrigel^{TM} instead air, but the counter-pressure would be higher, facilitating the pillar strength.

Since simulations gave encouraging results, the second version was chosen for the following process steps. Here we summarize the most important device features:

- three channels are required: the central one for the cells cultures, 500 μm wide, and two lateral channels for solutions and toxic or nutritional substancies passage;
- every channel must have inlet and outlet holes;
- the volume for cells cultures has to be large enough in order to allow a physiological growth; for the analyzed cells dimensions, this means a channel at least 300 μm high;
- it must allow a constant gradient in order to study cells behavior in time;

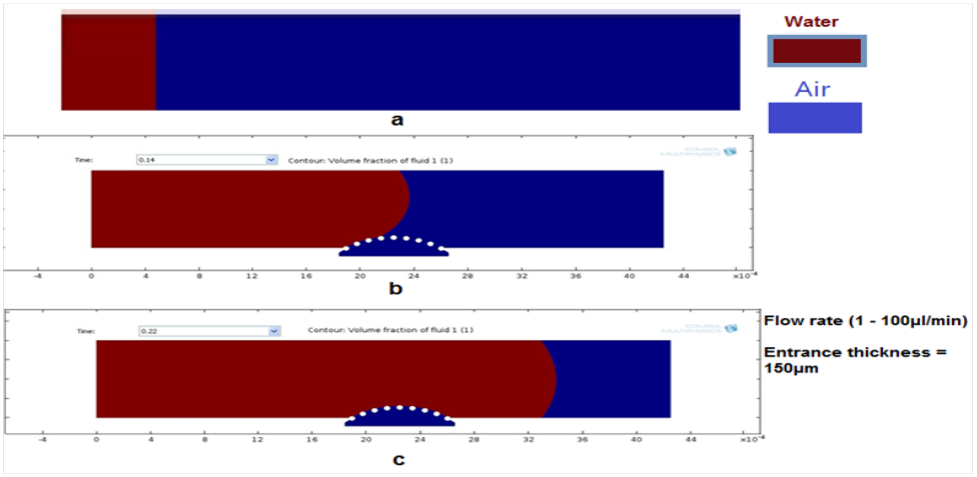

FIGURE 3.5: Simulation of fluid passage using COMSOL Multiphysics®. We can see the initial interface in the model (a) and the result after 0.14 s (b) and 0.22 s (c).

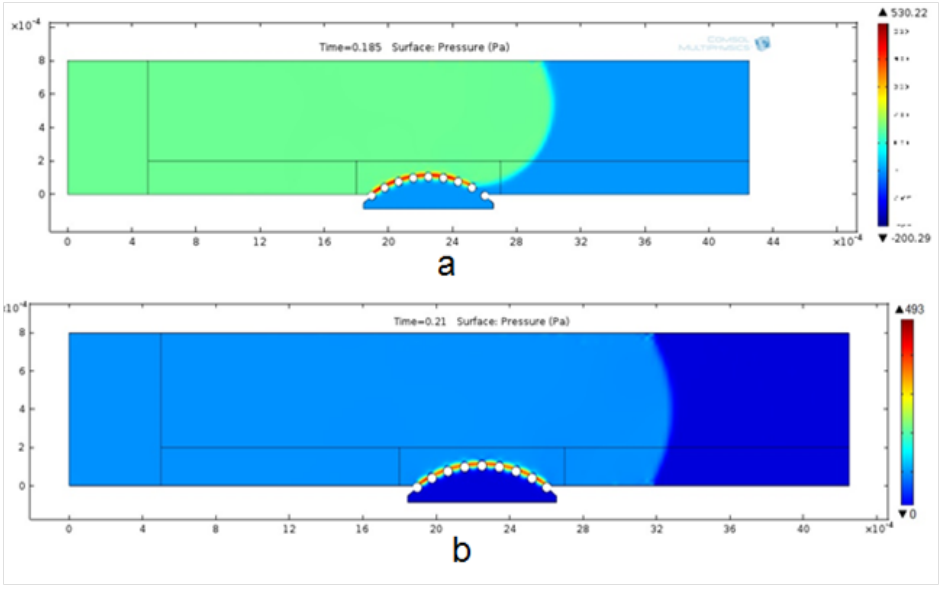

FIGURE 3.6: Pressure values obtained during the fluid passage (a) and after the fluid passage (b) in the COMSOL Multiphysics® simulation.

- the separation between central and lateral channels is obtained through two pillars arrays of 75 μm diameter.

Summarizing, we have said that in the central channel Matrigel^{TM} with cells culture will be inserted, while in lateral channels solutions with toxic substances or nutrients will be included. Figure 3.7 shows the model of this type of tests.

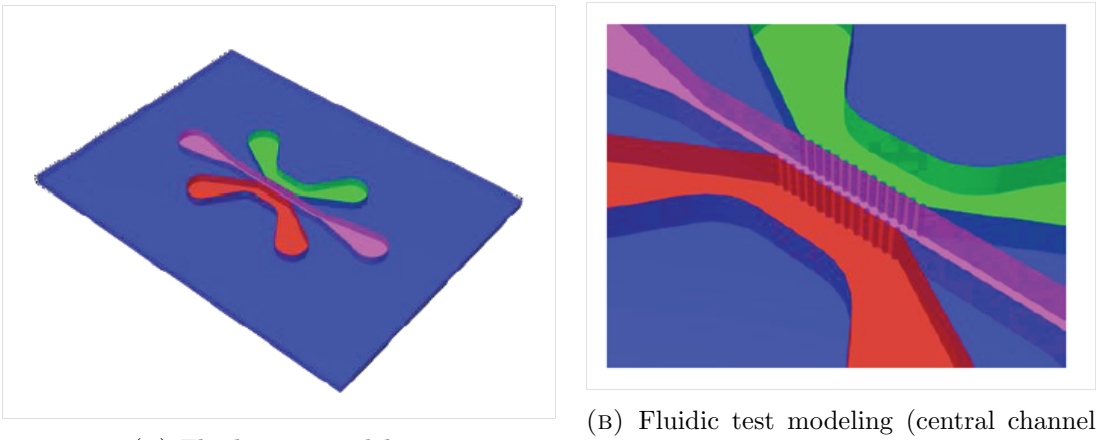

(A) Fluidic test modeling

(B) Fluidic test modeling (central channel zoom)

FIGURE 3.7: In this Figure we can see final fluidic test modeling. In central channel Matrigel^{TM} will be inserted (pink), while in lateral green and red channels stimulating solutions will pass.

3.3 First attempt: milling process

The first idea for producing the device was by milling. This is a traditional process to obtain a mold for devices production by polymeric casting-in-situ.

In this case, following the previously listed requested dimensions, this approach couldn't be followed, for the following reasons:

- since we need the device mold, the milling machine needs to be used to produce the negative geometry of the final device; as a consequence, for instance instead of pillars we have holes of 75 μm of diameter; all the device has to be at least 300 μm high, but these structures have to be positioned in a deeper mold in order to obtain the final chip; since the dimension of the tool has to be smaller than 75 μm, it is not possible to use this type of technique;
- even if this dimensions could be obtained, there should be a too long manufacture time and a too poor final resolution of the process.

For these reasons due to the limitations of this technology, this technique is not suitable for the final device production. The other analyzed techniques are based on the photolithographic process. As a consequence, a mask has to be realized.

3.4 Mask production

After the mask design shown in Figure 3.8a using a CAD program (for example *Rhinoceros*® or *CleWin*®), the first step is to create a lithographic mask for all the following processes. The substrate is a quartz plate (that will be the transparent material), on which a Chromium layer is deposited (that won't allow the UV light passage). This plate is covered by a photoresist layer. The pattern was impressed in this photoresist layer using the *MICROTECH Laser Writer LW405A*^{TM}. After that, the resist has been developed and then the Chromium layer was etched in a Chromium Etching solution, that has the following composition: *Ceric ammonium nitrate* : *perchloric acid* : $H2O$ = 10.9% : 4.25% : 84.85%. After the resist strip, the mask was ready for all the subsequent photolithographic processes. The final result is shown in Figure 3.8. It is possible to notice that, in order to maximize the number of final devices that will be patterned on a single wafer, the design has been repeated in a matrix.

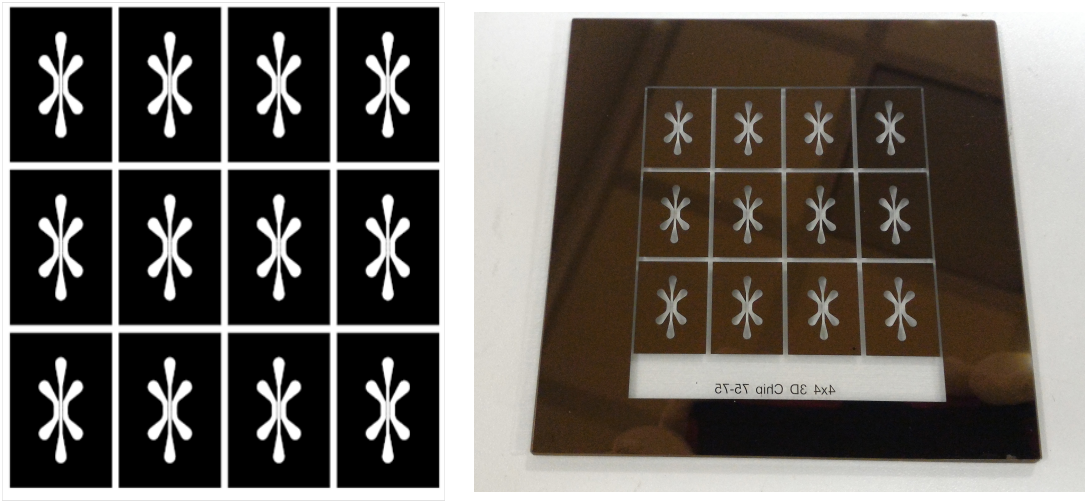

(A) CAD design (B) Final mask

FIGURE 3.8: Photolithographic process mask

3.5 SU8 tests and comparison of process recipes

This paragraph is focused on a particular preliminary work: since all the other processes are based on SU8 lithography, some tests on this particular photoresist were needed, and also a comparison between data sheet recipe and experiments were required.

In Appendix A two SU8 process recipes are reported. The first one shows all the data sheet steps: it is important to notice that, since a wide range of thicknesses can be obtained, all the parameters values belong to a wide range too, since there are a lot

of different conditions that can influence the process results. The second recipe shows instead all the experimental values for the process steps; these values were found after a large number of different tests, considering experimental results.

The aim of this work was to validate experimental recipe for SU8-2150 processing. In order to do this, a lot of different tests were carried on, varying spin coating step velocity, and obtaining subsequently different layer thicknesses. For each of these thickness values, both recipes were carried on in order to see if there were significant differences. In Figure 3.9, some results are shown.

It is possible to notice that, for every velocity value set up in spin coating step, the final layer thickness is comparable in the two different recipes followed. For this reason, it is possible to conclude that the experimental recipe is validated and, therefore, it can be used for all the subsequent work steps explained in this thesis work.

In particular, we can say that in these results also the operator errors measuring operation have to be taken into account; nevertheless, one of the best results is the case of velocity value of 2000 rpm. With this velocity, a 350 μm resist layer is obtained, that suits perfectly one of the requested device prerequisites.

3.6 Second attempt: hot embossing process with Cu mold

The aim of this work was to develop a copper mold that could be used in different ways: to replicate microfluidic PDMS LOC devices, as tool for hot embossing process or as mold for injection molding techniques. Therefore, the first step of this work is the production of a copper mold, in which all the channels are in relief and, moreover, there are micro-wells instead pillars. So that means, we need the dual geometry of the final device.
This mold could be obtained by electroplating techniques, using a SU8 layer as mask in order to confine copper growth only in specific areas.

3.6.1 SU8 photolithographic process on polished and not polished copper plates

As mentioned before, the first step was the realization of SU8 pattern on a Cu plate. Using the design showed in Figure 3.4, the idea of this step is to achieve a SU8 layer in order to have developed channels and resist pillars.

In the first approach I used both polished and not polished copper plates. This because we wanted to compare SU8 performance on these two different types of substrate.

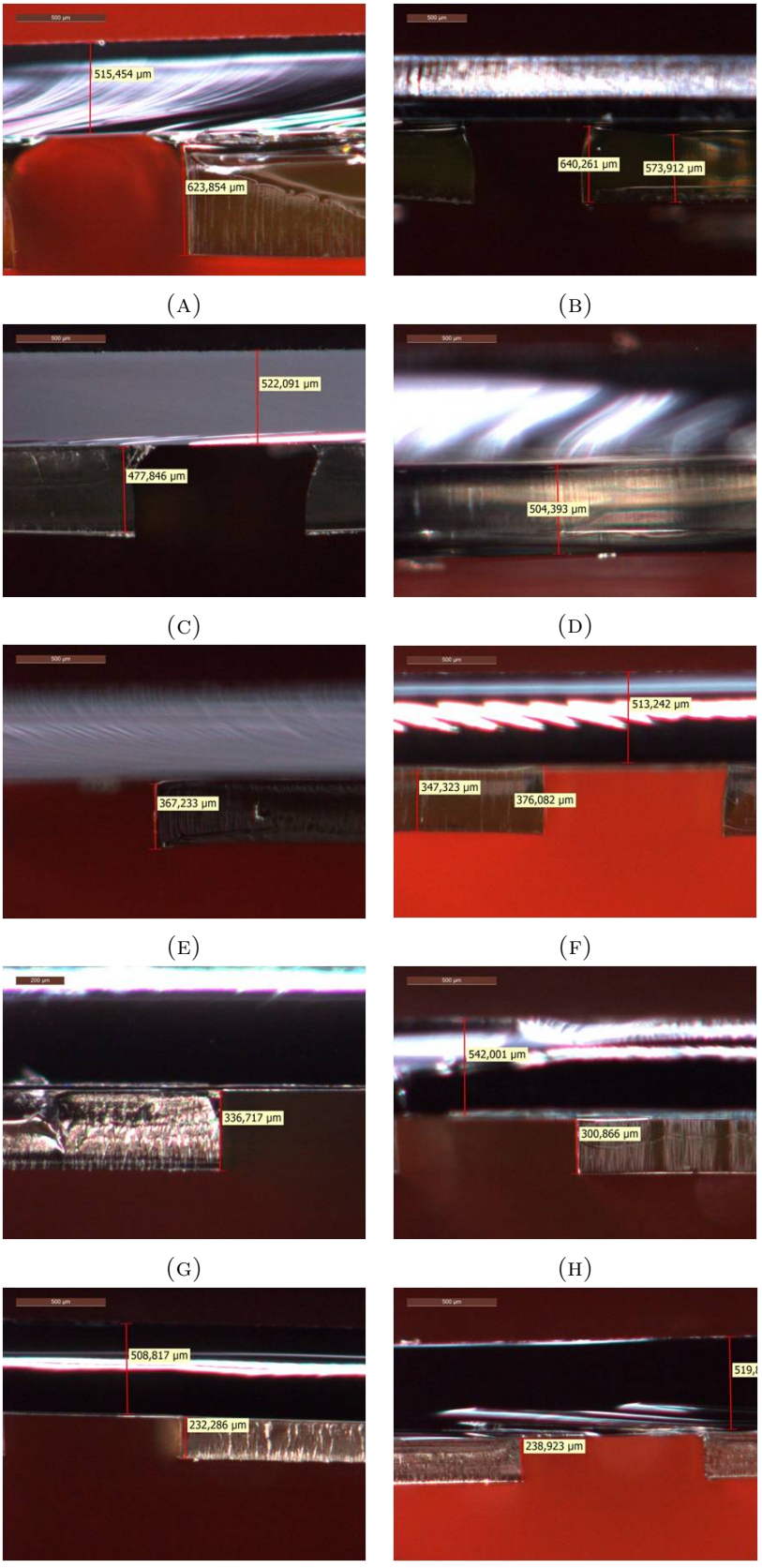

FIGURE 3.9: Comparison between data sheet and experimental recipe. The left column is related to the data sheet recipe, while the right column is reffered to the experimental one, with the following velocity values: (A-B) 1000 rpm, (C-D) 1500 rpm, (E-F) 2000 rpm, (G-H) 2500 rpm, (I-J) 3000 rpm.

Moreover, this was done in order also to see if there are advantages or disadvantages in electroplating process depending on the type of substrate used.

The photolithographic process shown in Appendix A.3 was performed. A lot of samples were prepared in order to better understand the SU8 behavior on copper plates.

Figure 3.10 shows one example of obtained results. We can notice that using a not polished plate all pillars during photolithographic process are removed. The first reason could be that, during exposure, the not polished substrate surface causes a light scattering, reducing the final obtained resolution, and exposing as a consequence also the areas of the resist related to the pillars. In this way, during the development step, also the pillars are soluble in SU8 developer and they are removed. Another reason could be simply a not good mechanical adhesion of the 75 μm diameter pillars with a rough surface.

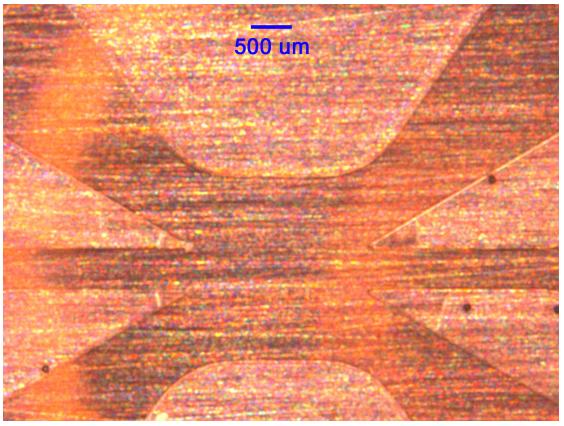

(A) SU8 pattern on a not polished Cu plate

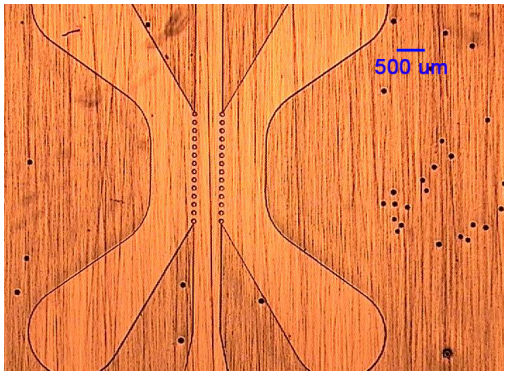

(B) SU8 pattern on a polished Cu plate

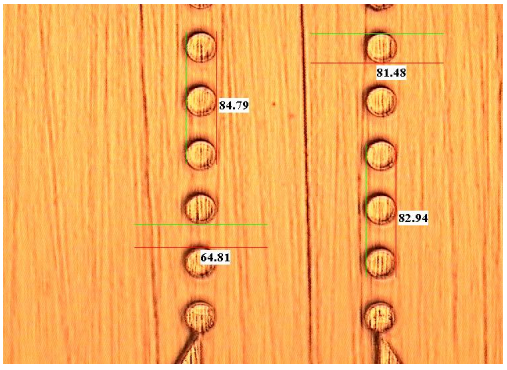

(C) Detail of SU8 pattern on a polished Cu plate

FIGURE 3.10: Comparison of SU8 pattern between not polished and polished Cu substrates. In the first case there are no pillars in the central region of the chip.

Another problem emerged during photolithographic process is the partial oxidation of copper surface during hard bake. This is due to the fact that the areas not covered by resist that was removed during development are exposed to air, combined to the

fact that the high set temperatures promote this phenomenon. Figure 3.11 shows this partial surface oxidation. Consequently, the following electroplating process cannot start because this oxidized layer acts as a mask for the electric conduction requested for this process.

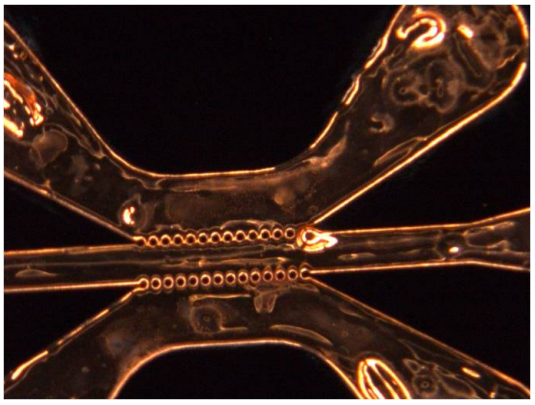

FIGURE 3.11: Partial oxidation of Cu surface

3.6.2 Adhesion problems and tests

As a consequence of results shown in the previous paragraph, we decided to try some tests in order to better understand the SU8 adhesion on copper surfaces, and compare it to the behavior on silicon substrate.

It is known in literature that there is no good SU8 adhesion on copper [68] - [69] - [70].

In the first adhesion tests the procedure was the following:

- substrates with alternate Si/Cu stripes were patterned and etched;
- on these substrates SU8 lithography was performed following the mask shown in Figure 3.12. We can notice that three different geometries were patterned: dotted, checked and striped with different dimensions, in order to cover both silicon and copper surfaces.
- after the complete SU8 development, FESEM and optic observations were performed. Some results are shown in Figures 3.13 and 3.14.

After these types of results we decided to do more tests using our design for Newton chip. The first step was to reproduce on a silicon wafer the chip geometry in a copper seed layer. In order to do this, a lithographic process using a positive thin resist (*OCG Microelectronic Materials HPR504 resist*) and wet etching were carried on. After that, a

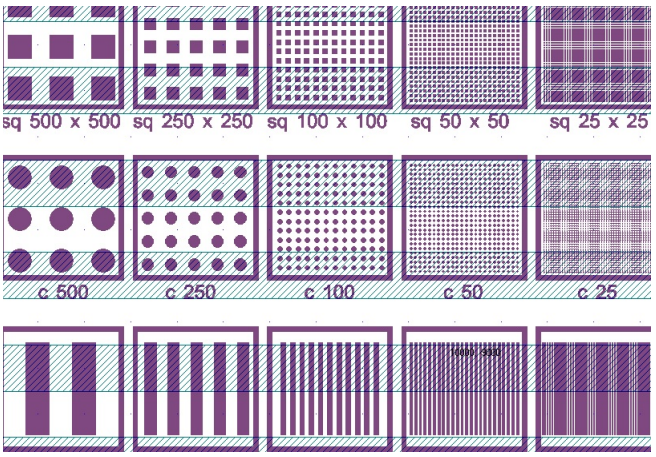

FIGURE 3.12: Mask for SU8 adhesion tests

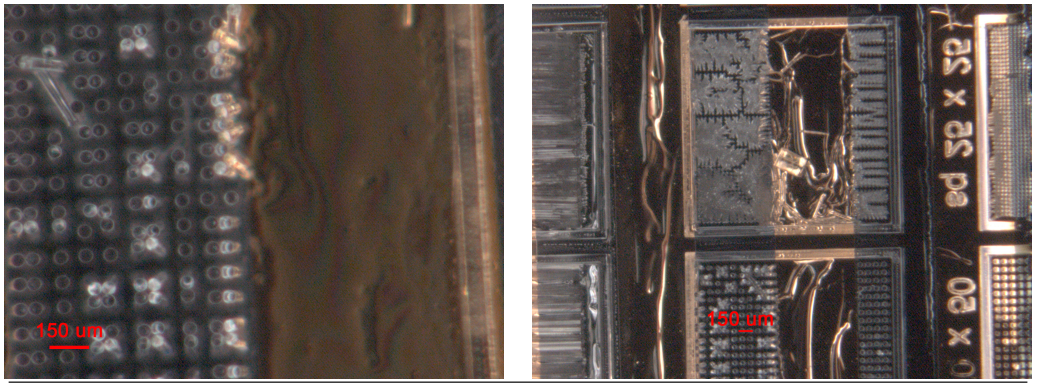

FIGURE 3.13: SU8 adhesion test optical image. On the copper surface SU8 pattern doesn't remain, while on the silicon surface all the geometries are correctly patterned (even if with some imprecisions due to the small dimensions).

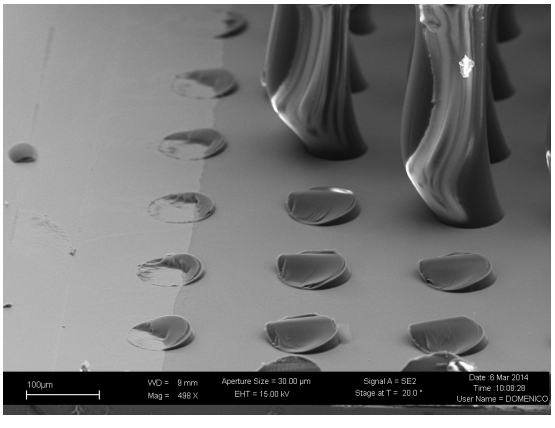

FIGURE 3.14: SU8 adhesion test FESEM image. In the right part of the image, with silicon substrate surface, pillars are present (even if some of them have been destroyed during the sample preparation for FESEM session analysis); on the other hands, in the left part of the image none of the pillars could survive on the copper surface.

SU8 resist layer was patterned: using the process explained in Appendix A.3, lithography was performed so that each pillar is positioned at the same time onto silicon and copper, in order that differences in adhesion can be observed easily and simultaneously between the two materials. To do this, during exposition the mask was deliberately positioned misaligned on the previous copper pattern. Figure 3.15 shows the result and the FESEM image zoom.

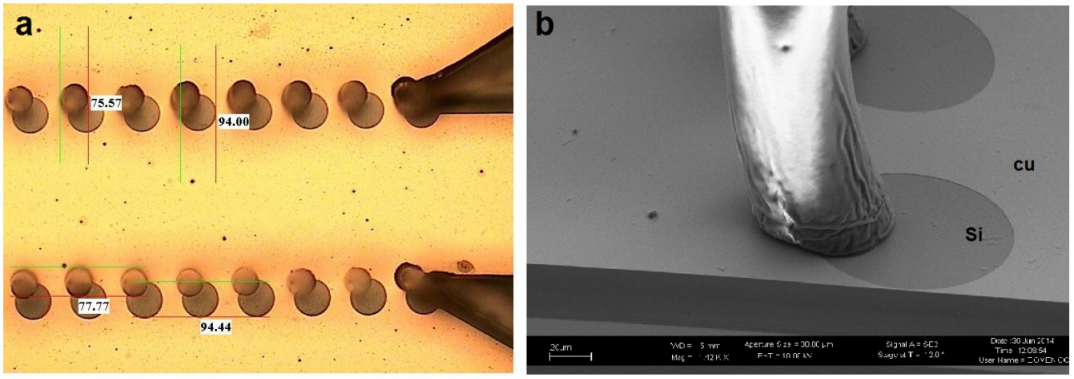

FIGURE 3.15: Pattern for SU8 test adhesion. (a) SU8 misaligned pattern on copper/silicon geometry (measures in μm). (b) Detail of one pillar in FESEM image.

In Figure 3.16 the comparison of the different adhesion areas of the same pillar is shown. We can notice the bad adhesion on copper (left side) and the good adhesion on silicon (right side).

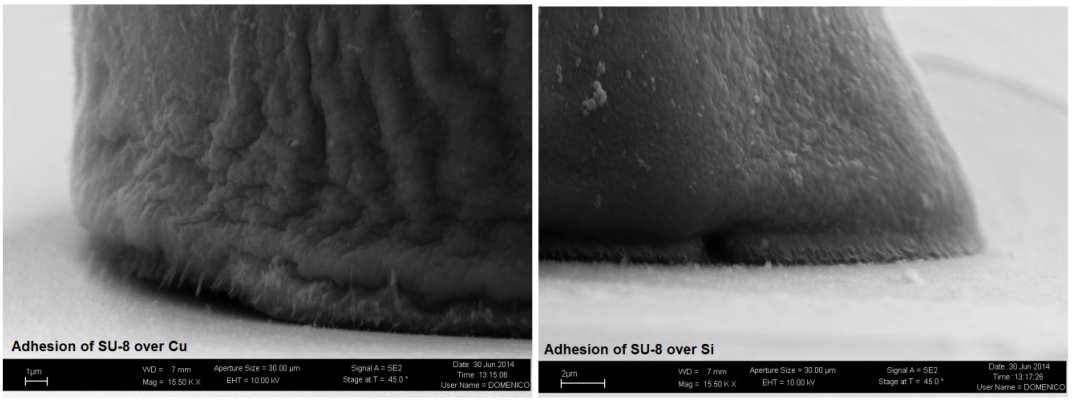

FIGURE 3.16: FESEM images clarifying the difference of weak adhesion of SU-8 on Cu (on the left) and very good adhesion on Si (on the right).

All these results led to the necessity to improve the process, in order to be sure that SU8 pattern was only on silicon surface and not on copper seed layer deposited for the subsequent electroplating step.

3.6.3 Silicon substrate with copper seed layer

After the results shown in previous paragraphs, we decided do create a copper mold by electroplating starting from a silicon substrate on which a copper seed layer is patterned in order to allow the perfect SU8 adhesion on silicon and an assisted electroplating process at the same time.

The complete process is listed below:

- cleaning of silicon substrate;
- deposition of copper seed layer;
- pattern of thin positive resist (*OCG Microelectronic Materials HPR504 resist*);
- etching of copper;
- strip of the HPR 504 resist;
- pattern of aligned SU8 layer following the photolithographic process described in Appendix A.3.

The final result of Cu patterning is shown in Figure 3.17. The final chip with also SU8 pattern on Silicon substrate is shown in Figure 3.18. It is possible to notice that SU8 pattern is aligned to the copper one in order to cover only silicon surface.

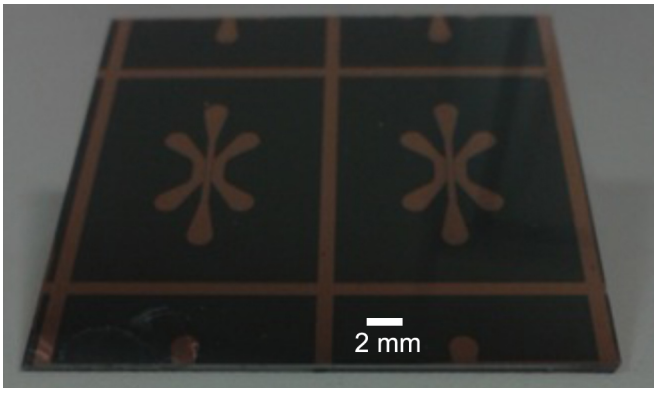

FIGURE 3.17: Cu pattern on silicon substrate

This substrate is then used for an electroplating process described in the following paragraph.

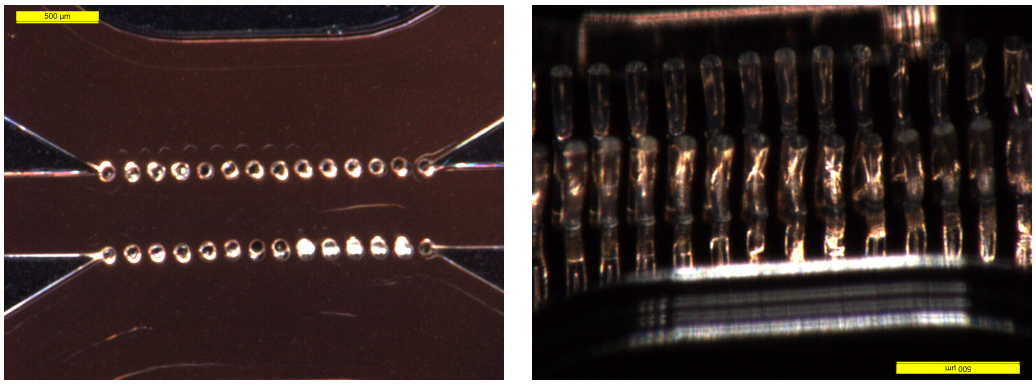

(A) SU8 layer on Cu and Si pattern (B) Detail of central channel and pillars

FIGURE 3.18: Cu and SU8 patterns

3.6.4 Limitations of electroplating process

The electroplating process is carried on in order to grow the copper on substrate, creating the mold in the free areas that are not covered by SU8. The seed layer previously patterned aim is to allow the electric contact for the correct electroplating process, in order to grow a specific copper layer. The SU8 has a mask function, so that means that copper can't grow in the occupied areas.

Electroplating solution data sheet suggests that deposition rate is 30 $\mu m/h$; since copper layer should grow for 350 μm thickness, the current set up for the process was 560 mA*h. All the process, consequently, took more than 11 hours to be completed.

Even if the substrate with copper and SU8 patterns was correctly produced, some problems occur in this particular step. The most important ones are listed as follows:

- holes dimensions don't respect the initial pattern (Figure 3.19); this is probably due to a SU8 pillars collapse

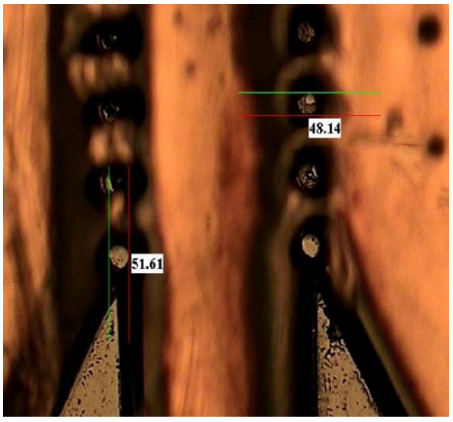

FIGURE 3.19: Holes dimension are smaller than the design specifications

- the surface of the grown copper is not always uniform, but it may have some cracks and holes (Figure 3.20)

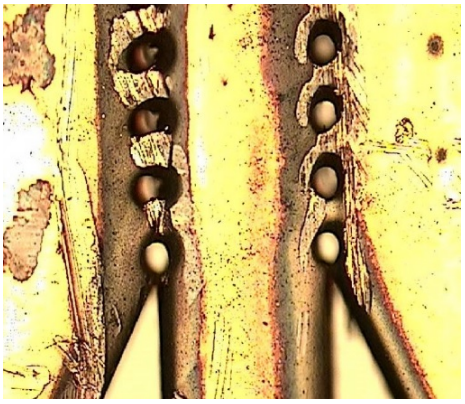

FIGURE 3.20: Surface contains cracks and holes after the electroplating process

- the growth could be too rough and not controlled (Figure 3.21)

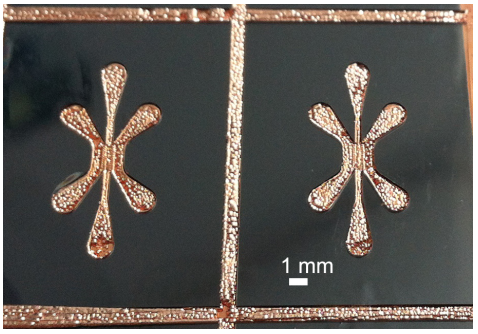

FIGURE 3.21: Surface could be too rough and growth process is not well controlled

- after the electroplating process, SU8 removal process was too hard to be carried on; firstly, all the extended areas stayed covered by SU8 resist even after two days in *SU8 remover*, the official product from the manufacturer that should remove all the SU8 after a complete photolithographic process; moreover, SU8 in micro-wells was impossible to remove, making this mold not usable for further hot embossing or injection molding processes.

All these problems led out to the decision to change process, trying to produce a mold for direct PDMS casting in situ.

3.7 Third attempt: mold for direct PDMS casting in situ

This section will describe the third approach to the problem. In this case, the idea was to produce a mold for the direct PDMS casting in situ. All the steps are explained in detail.

3.7.1 Wafer preparation

The substrate used for the master production is a 4" <100> p-type single side polished silicon wafer. This wafer was cut in four chips of dimensions $3.5cm$x$3.5cm$. These chips were then cleaned by Piranha Solution for 5 minutes and, after five rinses in water, also Acetone and 2-Propanol were used. A dry step with N_2 air is always needed.

3.7.2 SU-8 Lithography and anti-adhesion layer deposition

After the substrates preparation, the photolithographic process described in Appendix A.3 is applied.

It is strictly advised to check the planarity of all the working surfaces and equipment used in the process, since the resist has a relatively good reflow capability moreover helped by the long bake and relaxation steps required, so as to avoid final non-uniform thicknesses of the mold.

Since the final device will be fabricated using PDMS casting in situ, and the mold has a silicon substrate, a passivation layer deposition is required. Indeed, it is known in literature the high affinity between PDMS and silicon and the possibility to eliminate it through a passivation layer (for example C_4F_8) [71] - [72] - [73] - [74]. Since this mold will be used to create more replicas, this passivation layer is crucial for the repeated steps of device casting and peeling-off.

The passivation layer deposition was performed using a Deep Reactive Ion Etching (DRIE) (*STS 320PC Reactive Ion Etching system*), an Inductive Coupled Plasma (ICP) Machine. The equipment has two independent 13.56 MHz radio frequency (RF) power sources. The coil around the etching chamber is used to create plasma, while the platen coil is connected to the wafer electrode to control the RF bias potential of the wafer with respect to the plasma. But instead of using also the etching process, we only deposited a few nano thick film of a *Teflon-Like* material. Backside Helium (He) pressurization was used to provide sufficient heat transfer between the wafers to the electrode to maintain a constant wafer temperature.

When the wafer is placed in the machine, it is clamped by a set of alumina fingers to the electrode. A passivation (deposition) time of 30 s was set. The gas used for deposition was C_4F_8 with a flow rate of 50 sccm, while the He flow rate is 10 sccm. The pressure in the chamber is maintained at 20 mTorr , the pressure is controlled separately by a valve between the chamber and the turbo-pump. The platen power used is 10 W and the coil power (ICP) was 1500 W. The surface of the substrate was kept at 20°C.

An example of the final obtained device is shown in Figure 3.22.

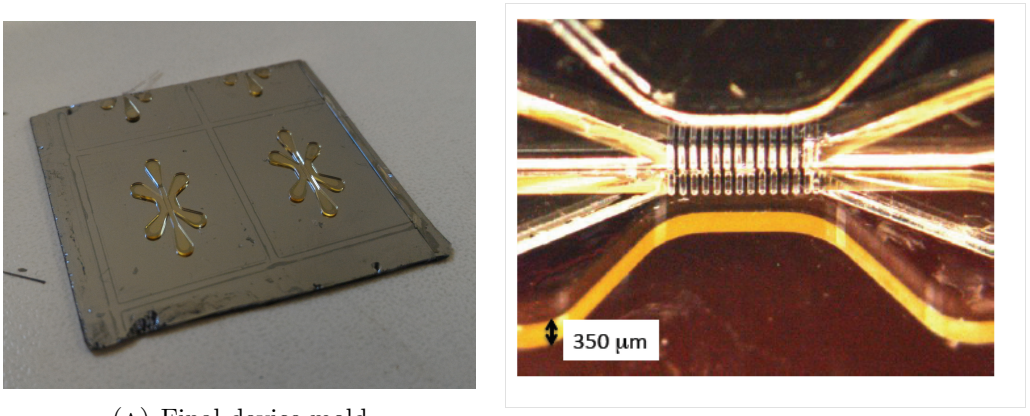

(A) Final device mold

(B) Detail of central channel and pillars

FIGURE 3.22: Final mold

3.7.3 PDMS casting and demolding

The first step was to attach the substrate on a aluminum holder that can facilitate the casting-in-situ and de-molding processes. This can be done using a droplet of wax so that the substrate is fixed and cannot be removed in all the subsequent steps. Figure 3.23 shows the final mold for the PDMS casting.

The PDMS casting is then carried on as explained in Chapter 1.4.1. In the preliminary tests curing agent is added in a 10:1 weight ratio, as the product data sheet shows. But, in our case, the final polymerized PDMS is too soft and during the demolding step all pillars collapse or strain themselves (Figure 3.24). In order to avoid this, the subsequent mixtures were prepared with curing agent in a 10:1,5 weight ratio. Consequently, the final cured PDMS was perfectly reticulated to be demolded.

As explained before, special care must be given to that mixing ratio because it will result to either a very soft PDMS replica device which will be damaged while demolding from the mold, or a very hard replica which can also be damaged while demolding. In order to speed up the polymerization process, the mold was loaded inside a convection oven at 90°C for $25 \div 30$ min.

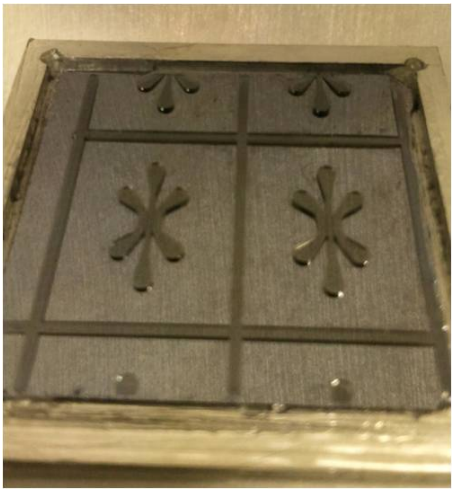

FIGURE 3.23: PDMS final mold

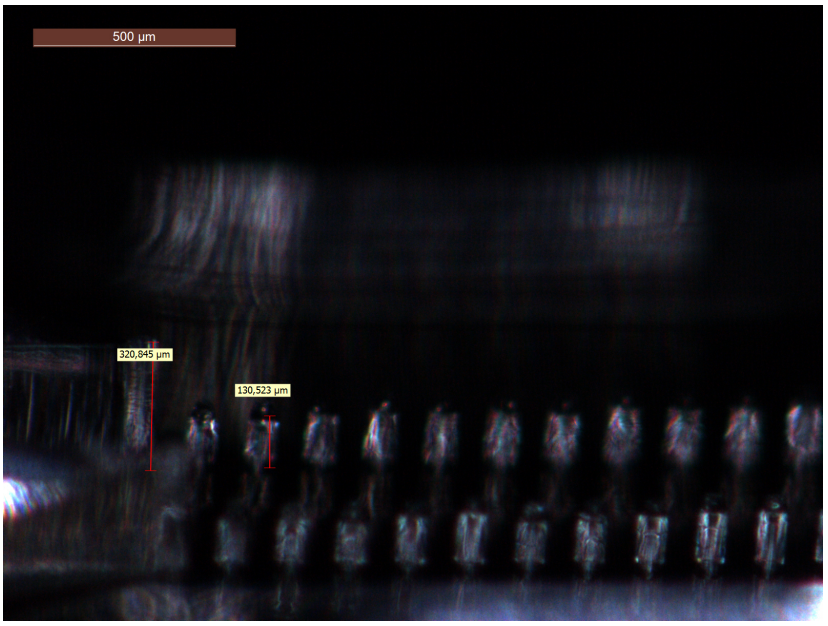

FIGURE 3.24: Strained PDMS pillars

After that the mold is dipped for 5 min inside a becker filled with Ethanol to promote and facilitate peeling-off of the PDMS replica from the mold. Figure 3.25 shows the cured PDMS demolding step and the final chip.

A final check to control the dimensions of pillars and all the structures is required. Figure 3.26 shows the PDMS chip, and we can notice that the pillars length is very good compared to the desired dimensions.

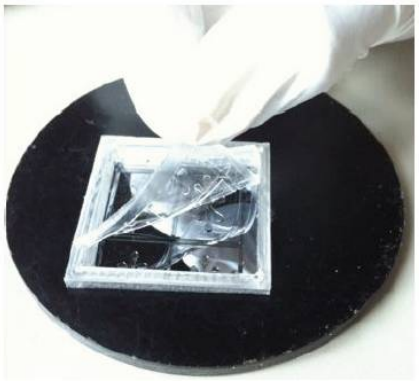

(A) PDMS demolding step

(B) Final PDMS chip

FIGURE 3.25: Final step and obtained chip

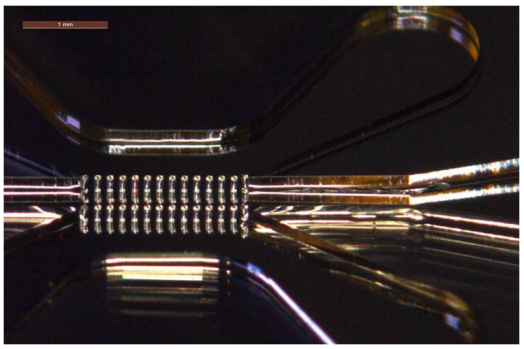

(A) Optic image of final chip

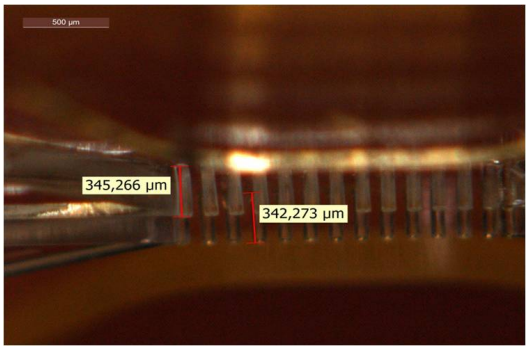

(B) Central pillars optic check

FIGURE 3.26: Pillars dimensions check

3.7.4 Glass bonding

After the chip demolding and cut, holes at the ends of the three channels were achieved in order to create inlet and outlet to allow the final tests (this situation is shown in Figure 3.25b as we have previously seen). This chip is the final device, but it needs to be bonded on a substrate in order to close the channels.

Since following tests will require a transparent surface, *Menzel-Gläser*^{TM} glass substrates are used for the bonding process; in this way, it is possible both to close the channels and to allow optical observations.

In order to perform this bonding, the following process was carried on:

- a little PDMS drop is spin coated on the glass substrate in order to obtain a very thin and uniform layer (10-12 μm); spin coating parameters are:
  - first step → velocity: 500 rpm; time: 5 s; acceleration: 1000 rpm/s;
  - second step → velocity: 4000 rpm; time: 60 s; acceleration: 1000 rpm/s;

- the glass is put on a hot plate at 75°C for 5 minutes in order to pre-reticulate the polymer;
- the chip is then positioned on the glass substrate;
- both glass and device are baked in a convection oven at 90°C for 10 minutes to complete the curing.

The final device is shown in Figure 3.27.

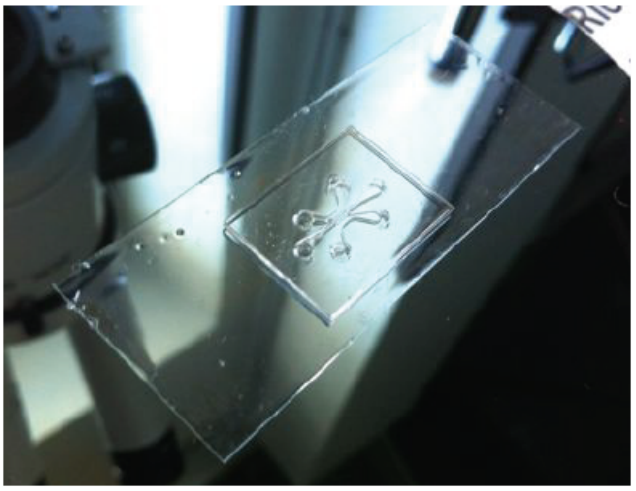

FIGURE 3.27: Final device

Chapter 4

Tests and results

In this chapter all the following fluidic experimental tests will be analyzed:

- simulations of gradient and diffusion phenomena, both in static and dynamic behavior;
- experimental set up for the correct device utilization;
- fluorescence phenomena for the gradient control;
- preliminary biological results.

4.1 Static and dynamic simulations

In order to analyze the subsequent device operational conditions, some fluidic behavior simulations are fundamental. To perform these simulations, the *COMSOL Multiphysics*® program was used. This is a simulation software package for various physics and engineering applications, especially coupled phenomena, or multiphysics.

4.1.1 COMSOL program

In COMSOL a *'function tree'* has to be followed in order to set up all the necessary conditions to carry on the simulation. This is called ***Model Builder***. The general sequence of functions in our case is showed in Figure 4.1.

First of all, the model device insertion is obviously mandatory. A 3D model of our chip is created, with the nominal dimensions that were designed according to the photolithography mask. Figure 4.2 shows the model inserted in COMSOL environment. It is possible

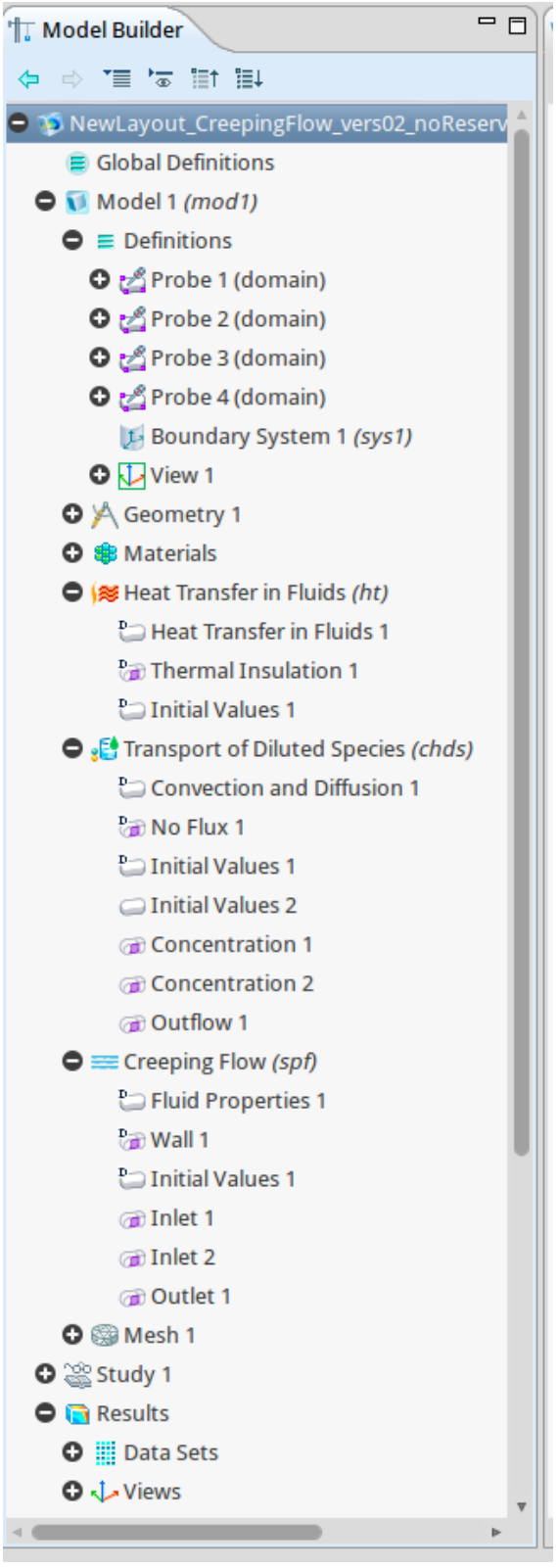

FIGURE 4.1: Device Model Builder in COMSOL

to notice that this model is the negative of the PDMS chip, because the simulation has to be carried on the diffusion or the flux of solutions in channels. In order to do this, we have 'solid' channels, with holes instead of pillars, so that it is possible to observe the fluidic behavior in all the available volume.

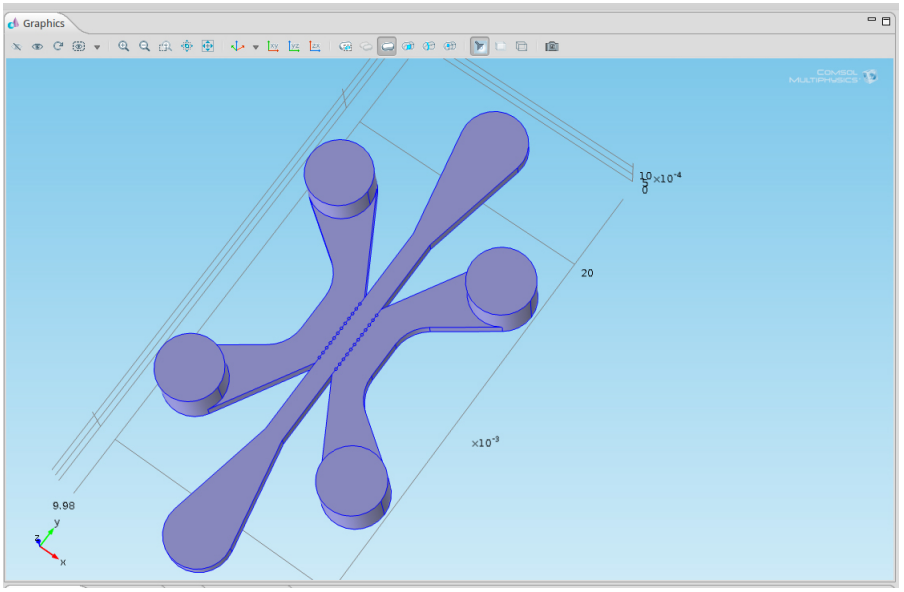

FIGURE 4.2: Device model in COMSOL

After the model, materials have to be imposed. In this case, since Matrigel^{TM} has a very complex composition and behavior, in the central channel water was imposed as the studied material. In lateral channels, water with a solute in a known concentration was used (0.00001 mol/m^3). This approximation of the material in the central channel will not alter the results, for the following reasons:

- in static analysis, the real situation of diffusion of solute in water is at least slower, since Matrigel^{TM} has a higher density than water and a sponge-like structure that allows to slow down these phenomena;
- in dynamic analysis, the attention is focused on the solution capability to maintain a constant gradient between the two lateral channels.

COMSOL allows to study the device behavior depending on which physics or chemical domains are included in the analysis. In order to study the correct fluid behavior in our device, three physics domains have been included (as shown in Figure 4.1):

- ***Heat transfer in fluid*** → With this domain it is possible to set up the temperature of the model and also heat transfer between different areas of the model; in

our case, this environment is used to maintain temperature constant at 37°C, the same that will be imposed in biological tests.

- ***Transport of diluted species*** → With this domain it is possible to set up the concentration of solute in water, inserting diffusion information in the model. In our case, one lateral channel and the central one are set up with no solute (that means only water, that is zero value in concentration), while the other lateral channel is set up with the solute concentration imposed in fluidic and biological tests ($0.00001\ mol/m^3$).
- ***Creeping flow*** → With this domain is possible to set up all the flux and pressure values of lateral solutions, considering this situation in a laminar regime.

It is also important to note that these three physics domains are connected each other: for instance, the velocity of the solutions flux depends on the temperature model but at the same time it influences the diffusion model.

The last part of this setup is related to the mesh of the model. This is one of the most important parts, since the model has to be separated in smaller volumes in order to analyze and calculate the equations solutions. If the model is divided into too big volumes, the simulation could not provide a correct answer and solution; on the other hand, if these volumes are too small, simulations could require one (or more) orders of magnitude greater elaboration time. This could bring to a redundancy of information and solutions. The set up values are shown in Figure 4.3, while the final result of the mesh subdivision is shown in Figure 4.4.

When all the necessary information have been inserted into the program, the analysis can be started. In the following sections the results of static and dynamic simulations are shown.

4.1.2 Static simulations

The first type of simulations are focused on static regime, in order to study the diffusion behavior of solutions.

In these types of simulations, the flux in lateral channels was obviously set to zero. Moreover, in order to be sure that there was a sufficient quantity of solutions for the diffusion phenomenon, two separate reservoirs have been added on the the two lateral channels, linking the inlet and outlet of each channel.

Figure 4.5 shows the simulation results, focusing the attention on the diffusion concentration every 16 hours. The total simulation time was 48 hours, and as said before, the

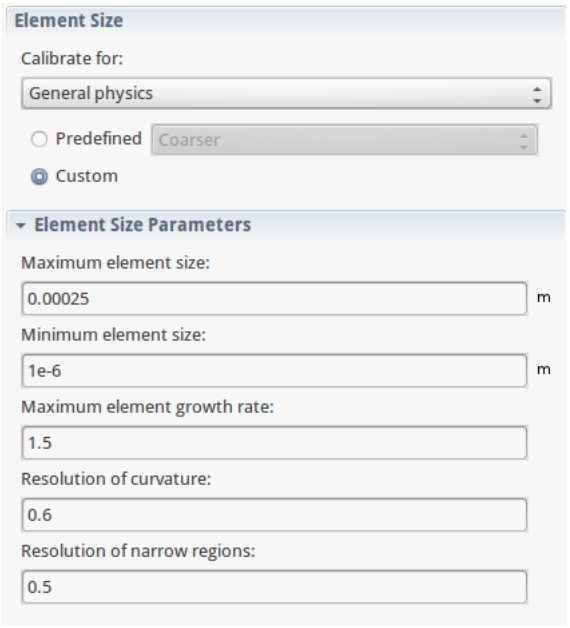

FIGURE 4.3: Mesh parameters

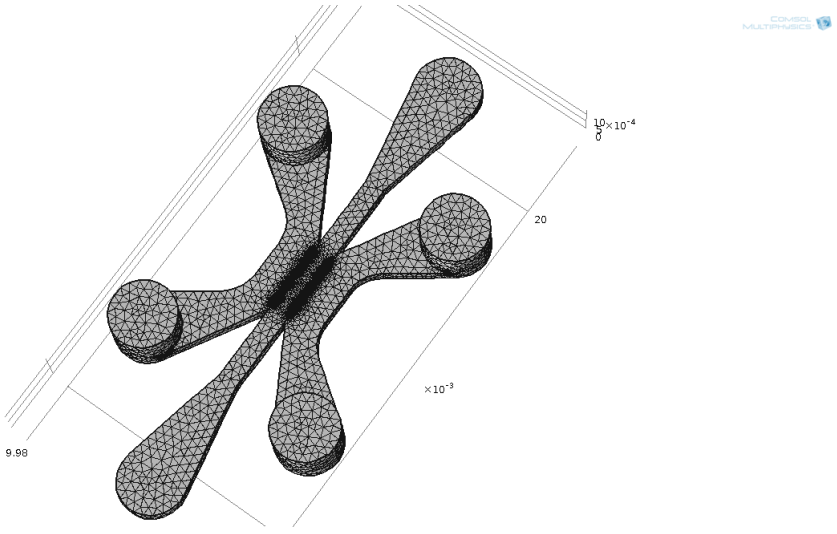

FIGURE 4.4: Model meshing

simulation was set to have no flux in lateral channels and the temperature was fixed at 37°C.

It is possible to see that diffusion phenomenon causes a gradient in concentration that is not constant in time. It is possible to notice this by observing the variation of color in time: the blue is referred to the water, while the red is linked to the solution with solute (that is, the solution with the maximum concentration that is possible to have). In fact, in the central channel it is possible to see how the color varies and changes value in time without reaching a limit value. With a more detailed analysis, shown in Figure

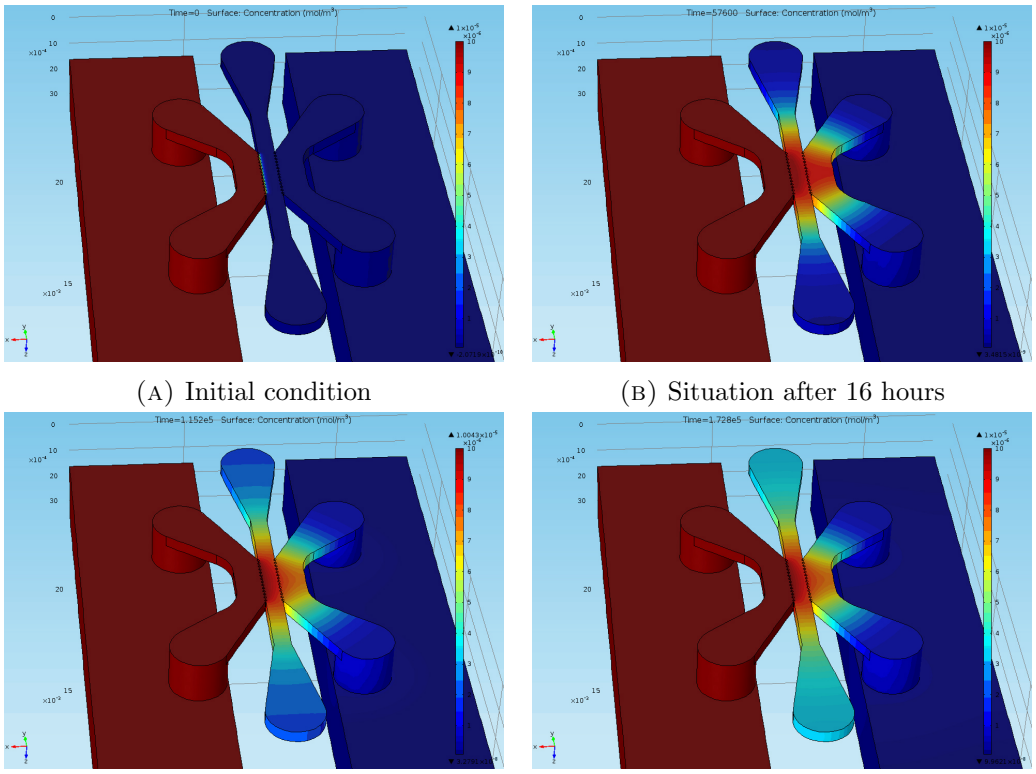

(A) Initial condition (B) Situation after 16 hours

(C) Situation after 32 hours (D) Situation after 48 hours

FIGURE 4.5: Static COMSOL simulation

4.6, it is possible to confirm this behavior. Across the central channel the concentration increases in time, even if there is always a slope that indicate a maximum concentration in one side of the channel and a minimum one on the other side.

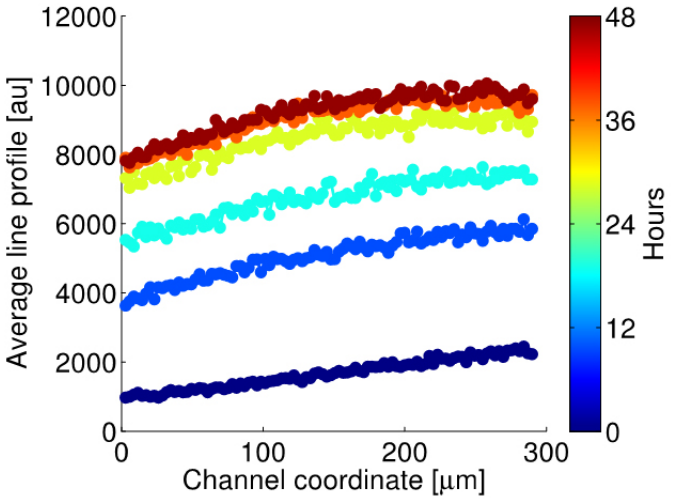

FIGURE 4.6: Static concentration drift

This is not a good behavior for the future biological analysis, since one of the required

features is the constant gradient in time across the central channel, in order to have a constant solutions influence on cells. These factors suggested the development of the study toward a dynamic state.

4.1.3 Dynamic simulations

In the dynamic state the upper reservoirs have been removed, since a solution flow is set up in lateral channels, simulating the pumps actions outside the chip. In Figure 4.7 the starting and final situation of the simulation are shown.

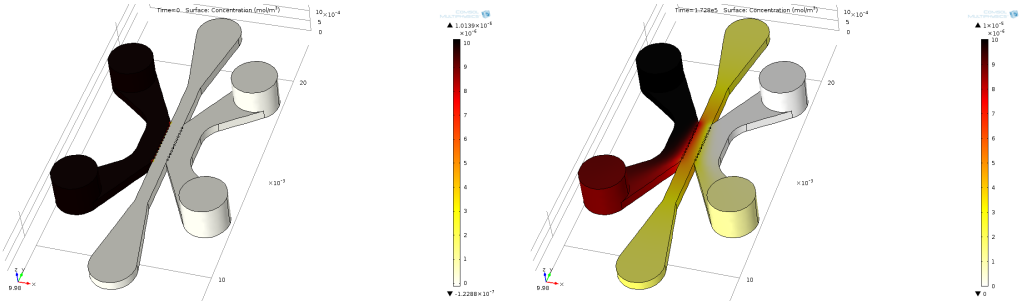

(A) Initial condition (B) Situation after 48 hours

FIGURE 4.7: Dynamic COMSOL simulation

As before, an analysis of the concentration across the central channel has been done. In Figure 4.8 the probes positions in the model are shown. They are positioned in order to divide equally the path across the central channel, in the middle of the total height. In this way, it is possible to calculate the parameters values in those positions, like, for instance, the concentration values.

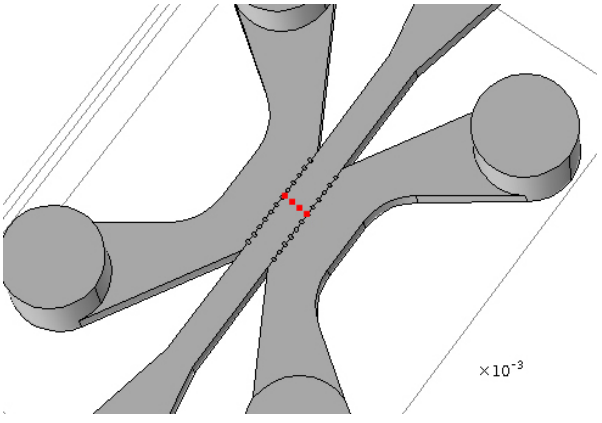

FIGURE 4.8: Probes in the model. The red dots indicate their positions in the channel.

Considering the simulations results, it is possible to draw graphs of the concentration in solutions. The first one is the concentration trend over time of each of the four positions set by the probes (Figure 4.9). It is possible to notice that, after an initial

transitory behavior, all the four values remain constant in time; moreover, the constant value decreases with the increase of the distance from the channel with the maximum concentration (probe 1 is positioned at the border between the central channel and the lateral channel with the maximum concentration solution, while probe 4 is positioned on the opposite side). The second graph shows the concentration trends as a function of the channel coordinates (Figure 4.10). In this case, it is clearly deductible that the values are constant in time, since the various lines are overlapping (again a initial transitory value is shown).

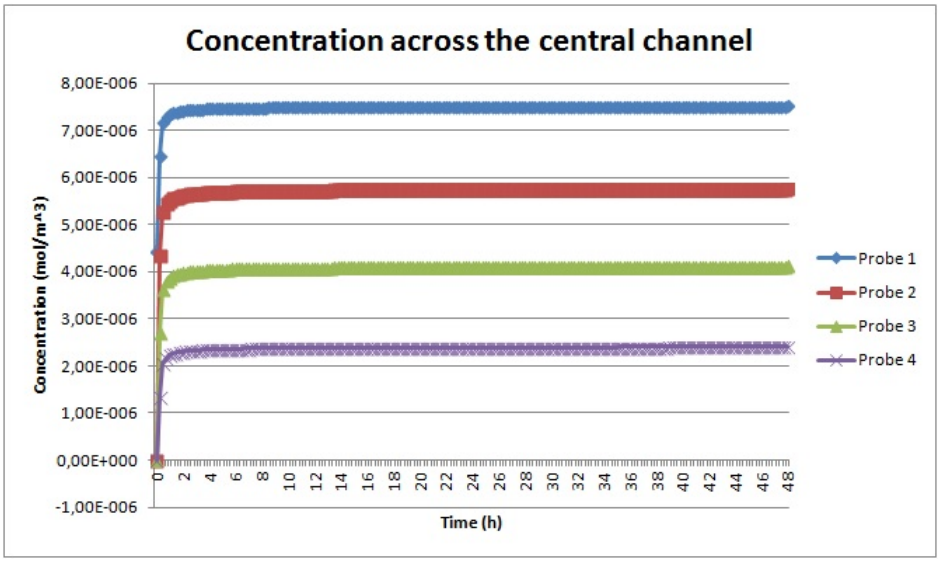

FIGURE 4.9: Concentration gradient over time. After an initial transitory value, all the four concentration values are constant.

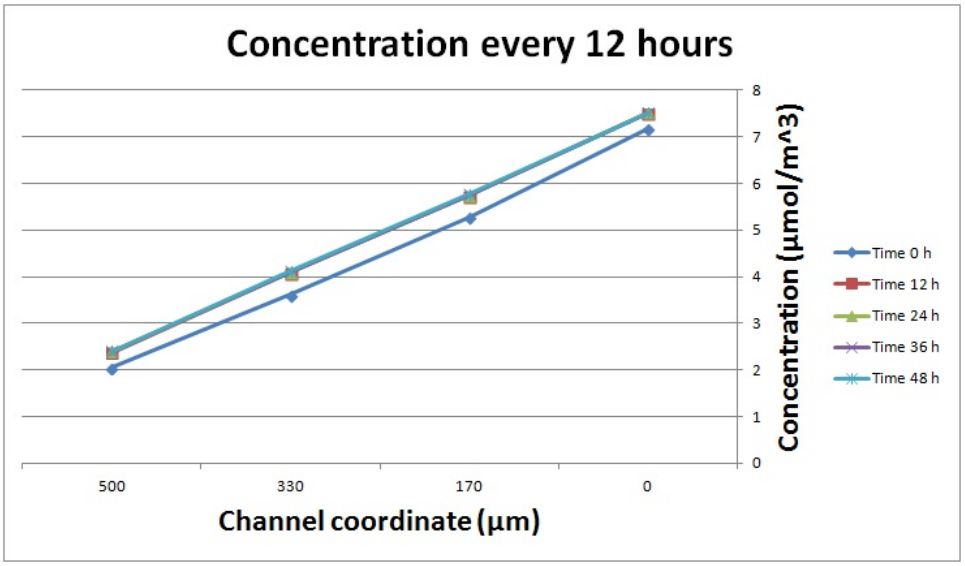

FIGURE 4.10: Concentration gradient over channel coordinate. Also in this case it is possible to notice that values remain constant in time.

These results show that a constant gradient is possible to be established with these devices. In the following paragraphs all the experimental setup and tests are reported.

4.2 Experimental setup for tests

In this paragraph the experimental setup used to conduct the testing part will be explained. It is required to use an automatic pumping system to guarantee a very precise, controllable and repeatable flow; those pumps are connected to a twin syringe pump (*Pump 33* by *Harvard Apparatus*^{TM}) which are able to pump the syringes independently, both infusing or refilling, with a large flow rate range and an accuracy of 0.35% and it is supported by a PC *LabView* by *Texas Instruments*^{TM} interface, thanks to which it is possible to control the laboratory equipment from the computer as can be seen in Figure 4.11.

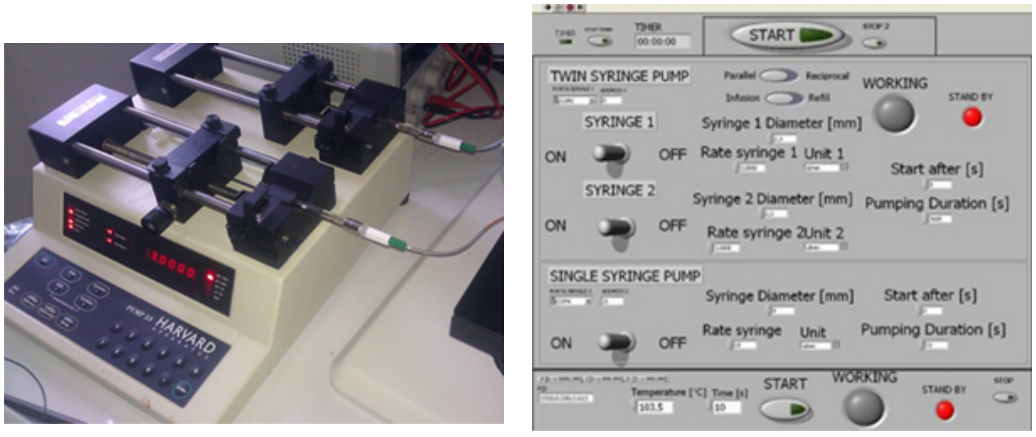

(A) Twin syringe pump

(B) Screen-shot of the LabView program to control syringe system

FIGURE 4.11: Pump system and control interface

As well as the automatic pumps, also syringes used for manual liquid pumping (*Hamilton*) with a volume equal to 250 μl have been used (internal diameter 2.3 mm).

To visualize the fluid flow inside the device, colored liquids are exploited to highlight the visual perception and, in the case of presence of Matrigel^{TM} in the central channel, to see the diffusion within.

The experimental setup is shown in Figure 4.12.

The fluidic circuit is positioned in a PMMA 'box' produced using the milling machine, and both the device and the box are fixed on the cooling and warming surface of a Peltier device that is used to bring Newton chips to a specific temperature. The Peltier device with two fans (that speed up the achievement to the set temperature) is positioned on a

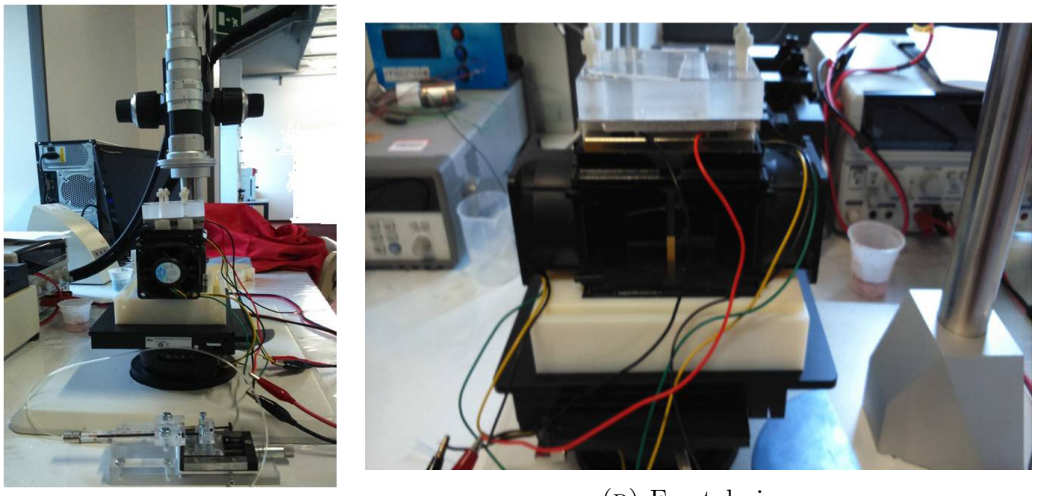

(A) Lateral view

(B) Frontal view

FIGURE 4.12: Peltier system. The cooling device is fixed over a stage made by 3D rapid prototyper; all the system is fixed under the optical microscope. Moreover, the lateral view shows the manual syringe used in fluid injection.

support designed using *Objet30*^{TM}, a 3D rapid prototype equipment. All this assembly is loaded under an optical microscope in order to monitor all the tests and measurements.

The Peltier device has two fans and it is used to cool down (or warm up) the sample, according to the set voltage parameters that are controlled by a voltage supply.

4.3 Fluidic tests

In this section all the fluidic tests for the correct operation of the device are explained. Firstly, the operations to insert Matrigel^{TM} in the central channel are explained; in a following section lateral channels filling procedures and tests are described.

4.3.1 Matrigel^{TM} handling and injection

Matrigel^{TM} (whose main characteristics are described in Appendix B.1) is a very tricky to handle material. First of all, it needs to be stored at -20°C. As soon as it reaches temperatures above 10°C it starts to cure, and this phenomenon is irreversible. That is, above that temperature it cannot be handled anymore. Consequently, all the operations needs to carried out at a maximum of 6°C, and Matrigel^{TM} has to be kept in ice if it is not used. Freeze thaws should be minimized by making aliquots, in order to use the minimum quantity as possible.

The procedure for the correct Matrigel^{TM} handling is described as follows.

1. ***Tools and system preparation***
   First of all it is necessary to keep all the tools that will be used at a cooled temperatures, like for instance pipettes tips, tubes and device. In order to do this, pipettes tips, tubes and device are kept on the PMMA box on the Peltier plate. The voltage supply is set to 1.5 A in order to obtain 5 °C.

2. ***Partial Matrigel^{TM} thaws***
   Matrigel^{TM} needs to be partially thawed in order to be properly handled. A little drop of Matrigel^{TM} (150-200 μl) is put on the Peltier plate using a cooled pipette tip, in order to keep it a constant temperature

3. ***Central channel filling***
   Using the cooled tube and a syringe, the Matrigel^{TM} is then inserted into the central channel of Newton device. This is a very hard operation, because the pressure should not be too high in order not to destroy pillars arrays, and at the same time not too low in order to allow the Matrigel^{TM} insertion. This operation is shown in Figure 4.13.

FIGURE 4.13: Matrigel^{TM} insertion in central channel

4. ***Matrigel^{TM} warming up and results controls***
   Peltier plate wires polarity needs to be reversed, and then the power supply has to be set at 0.61 A. In this way, the device reaches 37°C; keep this temperature for 30 minutes. After this time, the Matrigel^{TM} is ready for the optical controls. Figure 4.14 shows the final result.

As said before, this is a crucial operation, since some problems could occur during the various steps previously described. The most frequent problems are some bubbles formation during the curing at 37°C (see Figure 4.15) and leakage in lateral channels (see Figure 4.16).

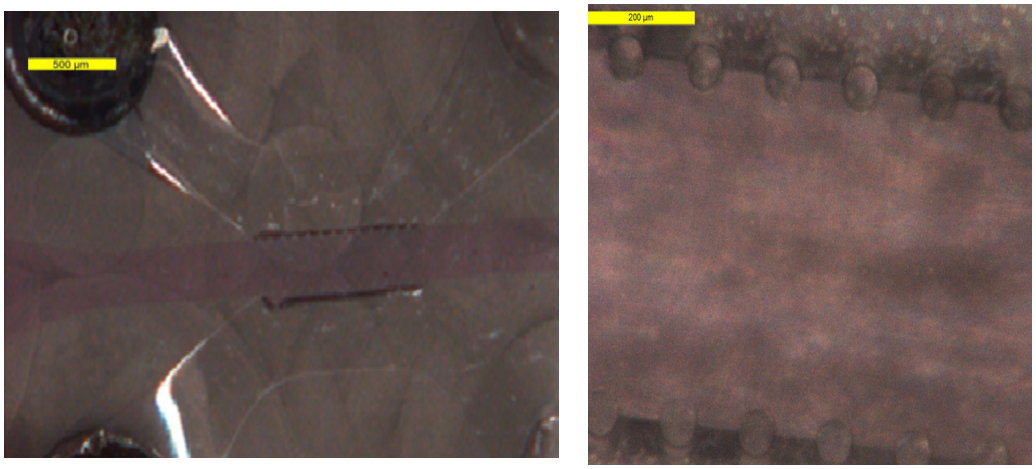

(A) Newton chip with Matrigel™ (B) Central channel zoom

FIGURE 4.14: Final chip with Matrigel™. In the zoom it is possible to notice the meniscus shape of the gel near the pillars indicating no pressure differences between the central channel and lateral one.

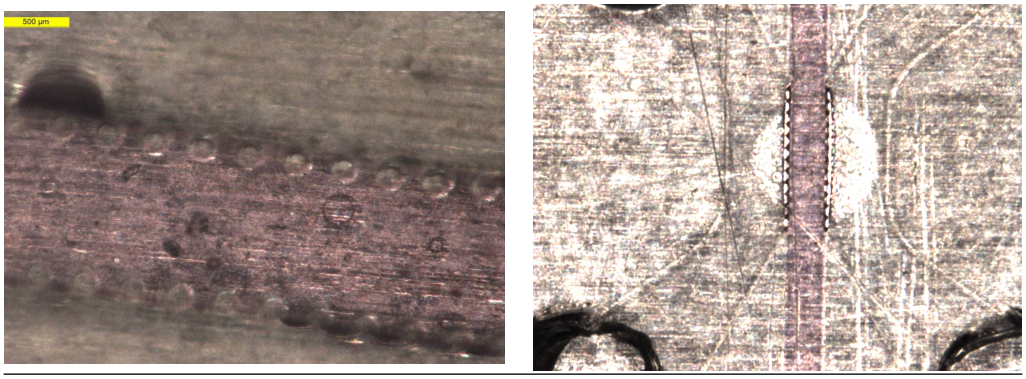

FIGURE 4.15: Bubbles formation problems. Here there are two examples of bubbles formation during curing step at 37°C.

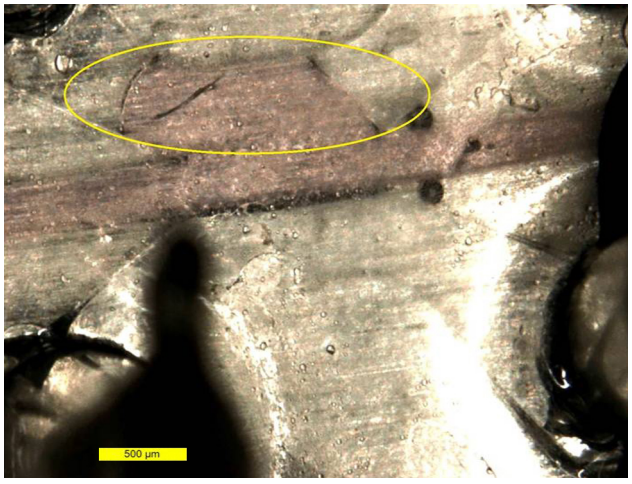

FIGURE 4.16: Matrigel™ leakage in lateral channel

Bubbles formation could be due to the evaporation of liquid inside Matrigel^{TM} that could not escape from the chip; the Matrigel^{TM} leakage could be a consequence of the fact that pillars are not well bound on the glass substrate or that a pressure that was too high was used for the Matrigel^{TM} insertion.

All these examples show that the procedure just explained is very complex and not trivial, and it may imply the failure of the perfect chip produced in the previous steps. So it is strongly advised to provide a special care while filling the channels; a minimum pumping pressure should be used and then it can be increased manually.

4.3.2 Filling lateral channels

After the filling of the central channel with Matrigel^{TM}, colored solutions are pumped into the lateral channels, using the twin syringe pumps; this operation can be manually or automatically performed with the control program. The diffusion results can be seen in Figure 4.17.

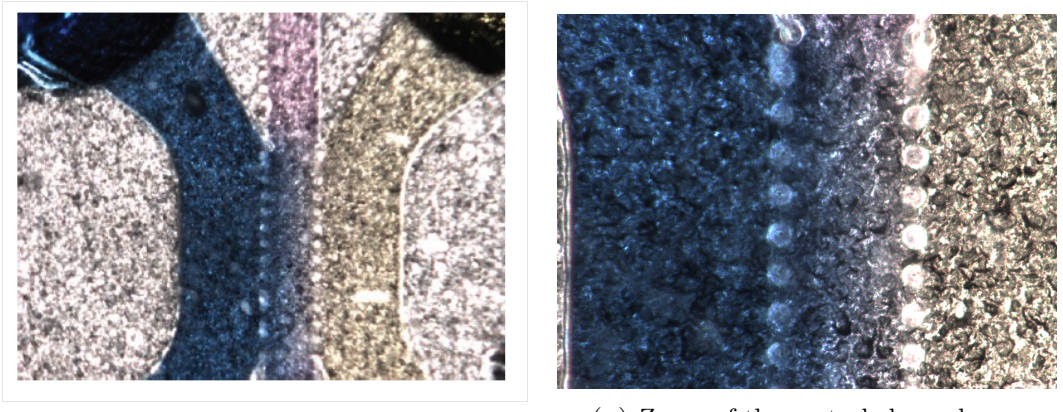

(A) Final result (B) Zoom of the central channel area

FIGURE 4.17: Lateral channels filling. One channel contains a blue solution, the other one is filled by water.

In Figure 4.18 it is possible to see the meniscus of Matrigel^{TM}: there is no pressure difference between lateral channels and the central channel; for this reason, the shape is almost flat in the areas of contact between Matrigel^{TM} and fluids. Moreover, it is also visible that there is a homogeneous longitudinal diffusion flow. This is the expected behavior that should occur during biological tests. This phenomenon is not constant with time, as previous simulations showed, since as time passes, the central area becomes darker and darker, which is visible through a continuous increase of the blue solution.

Also in this step it is important to take care about the operations and methodology. In Figure 4.19 two problems are shown. In this case, two different-colored solutions were used. In particular, Figure 4.19a shows the bubbles formation in lateral channels

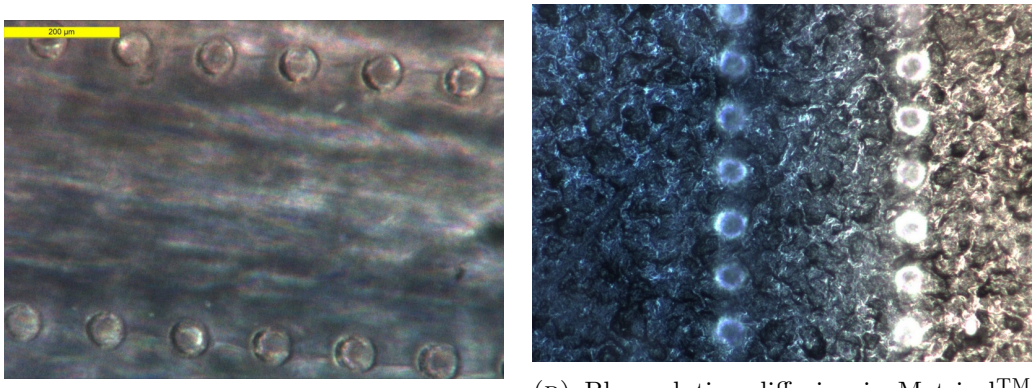

(A) Flat meniscus shape

(B) Blue solution diffusion in Matrigel^{TM} after few minutes.

FIGURE 4.18: Meniscus shape and diffusion.

and Matrigel^{TM} protrusion. The first phenomenon could be due to the fact that the filling manual operation was not precise and some areas of the lateral channels were not correctly filled. The second phenomenon could be due to the fact that there is no pressure balance between the two lateral channels. Moreover, in Figure 4.19b we can see that there could be a net flow of colored solution through the central channel. This could be caused by the fact that Matrigel^{TM} was not correctly cured during previous steps, leaving some areas in the central channel that are not occupied by this gel substance. As a consequence, a net flux is added to the diffusion phenomenon and tests cannot be applied.

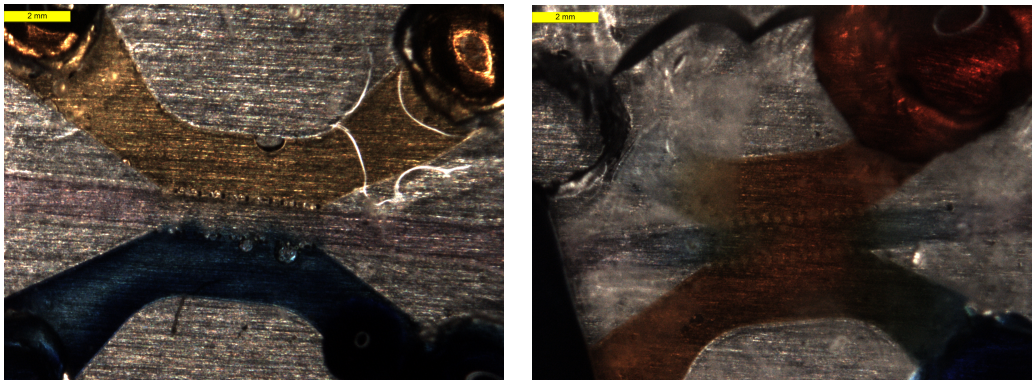

(A) Bubbles formation and Matrigel^{TM} protrusion

(B) Not diffusive passage of one colored solution through the central channel

FIGURE 4.19: Filling lateral channels problems

We have demonstrated that, with opportune care handling, these devices can be used for the fluidic tests with Matrigel^{TM}. In the following sections, the aim is to prove that it is possible to obtain a constant gradient with time through lateral channels.

4.4 New reservoirs

In order to perform the fluidic tests, an improvement in layout is needed. Some reservoirs have to be designed in order to allow future tests. This is because the pumps will be set in a refilling mode. As a consequence, reservoirs are crucial in order to have always new solution volumes flowing into the lateral channels.

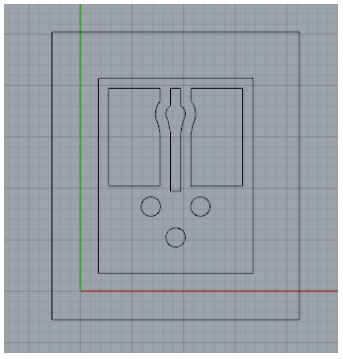

(A) CAD design for reservoirs

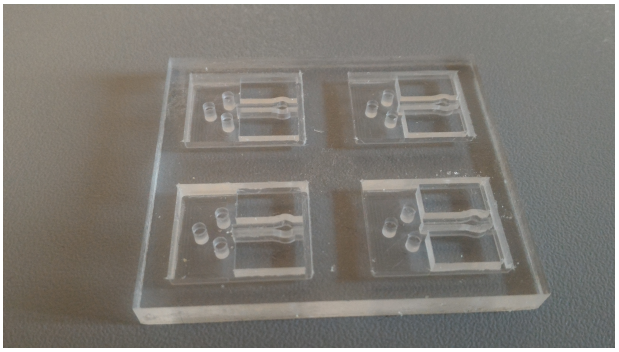

(B) PMMA mold for PDMS casting

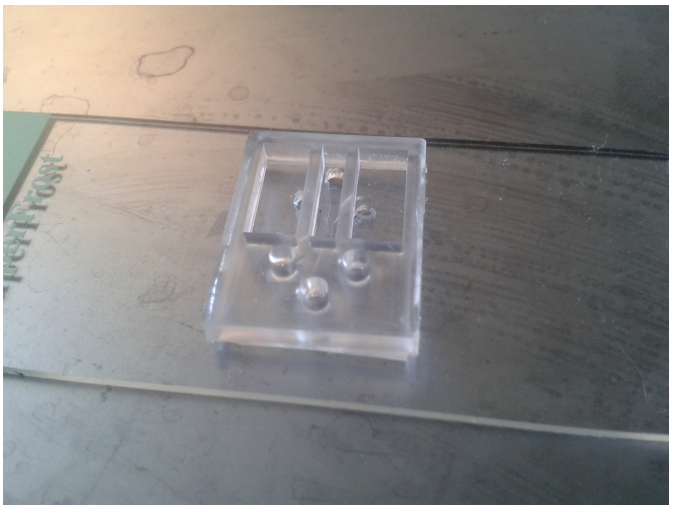

(C) Final device with bonded reservoirs

FIGURE 4.20: Reservoirs production process

The process is described in detail in the following points.

1. *CAD design* → This design was conceived following the previous chip design. There are two square reservoirs that are positioned on the two lateral channel inlets, a central space that allows optical observation and three holes for the channel outlets (Figure 4.20a); the single reservoir volume is 116.7 mm^3.

2. *Milling process* → Following the CAD design, the milling process is carried out in order to obtain the PMMA mold (Figure 4.20b). It is possible to notice that the CAD design was repeated four times in order to maximize reservoirs production.

3. *PDMS casting in situ* → Following the casting in situ process procedure explained in 1.4.1, PDMS reservoirs were produced.

4. *Reservoirs bonding* → After the complete curing of PDMS, reservoirs are bonded with the use of not cured PDMS that allows a perfect bonding without leakage between reservoirs and the Newton chip. The final result is shown in Figure 4.20c.

In this way it is possible to proceed with the fluorescence tests in order to verify the correct bonding and the constant gradient.

4.5 Fluorescence control

In this section the fluorescence tests are explained. The aim of this work is to demonstrate that with this device it is possible to obtain a constant gradient with time.

4.5.1 Experimental setup

The setup requires a fluorescent/optical microscope and the twin syringe pump. In Figure 4.21 we can see how the device is positioned under the microscope; moreover, we can also see the fluidic circuit that connects the Newton device to the pump system.

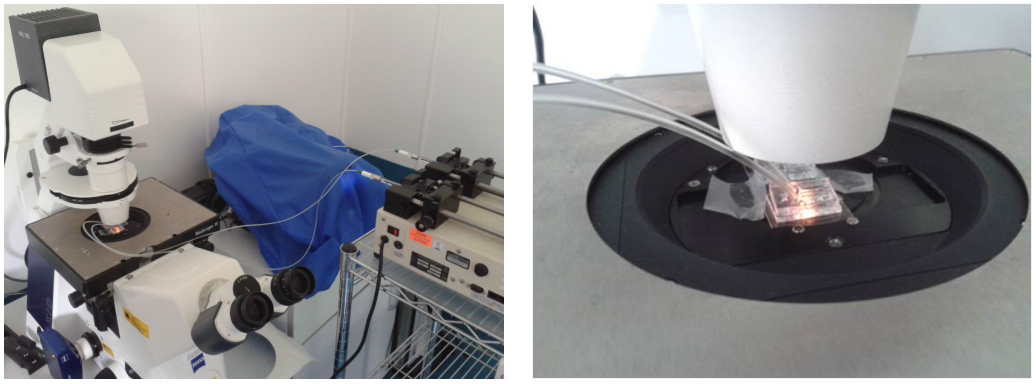

(A) Complete system (B) Detail on the Newton device

FIGURE 4.21: Fluorescence test setup

The first step is the reservoirs filling: one is filled with a fluorescent solution, the other one with only water. The pumps will work in a refilling regime, so this means that solutions are sucked up from the reservoirs to the pumps. Figure 4.22 shows the filled reservoirs.

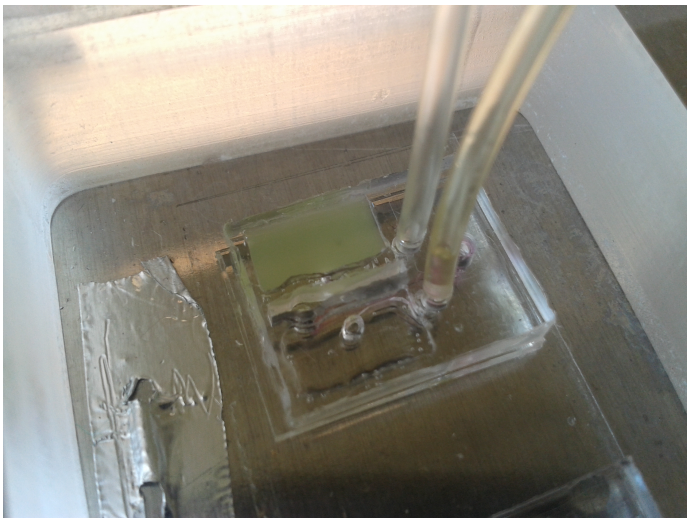

FIGURE 4.22: Filled reservoirs with fluorescent solution and water

4.5.2 First type of measurements

In the first type of experiments, a solution with fluorescent spheres was used. This means that in water there are micro-spheres that are covered by a fluorescent substance. These experiments had the aim to prove the correct filling process of Newton device. The imposed flux was 2.4 $\mu l/h$; this value was calculated from the single reservoirs volume, divided by 48 hours (the minimum requested duration for a measurement). Figure 4.23 shows the fact that the device works quite as expected; it is important to notice that, since in solution there are spheres bigger than the pillars distance, it is obvious that no spheres will pass through the central channel with Matrigel^{TM}. Moreover, it is possible to see that a part of the central channel is occupied by the fluorescent solution: this means that some pillars have been destroyed by the big spheres present in the solution.

4.5.3 Second type of measurements

The second, and more important, type of experiments was the analysis of the gradient studying the profiles of fluorescence intensity. For these measurements, a Fluorescein IsoThioCyanate (FITC) solution was used (for details see Appendix B.2). Our solution is 100 μM, in a dilution of 1:10.

Since these molecules can pass through the pillars, it is possible to obtain fluorescent images from which it is possible to derive information about the fluorescent profile and, as a consequence, about the concentration of the fluorescent solute. In these experiments, one shot was captured every 15 minutes. Finally, using the *ImageJ* image processing program, a mean of all the images in the 15^{th} and in the 35^{th} hour were calculated. In

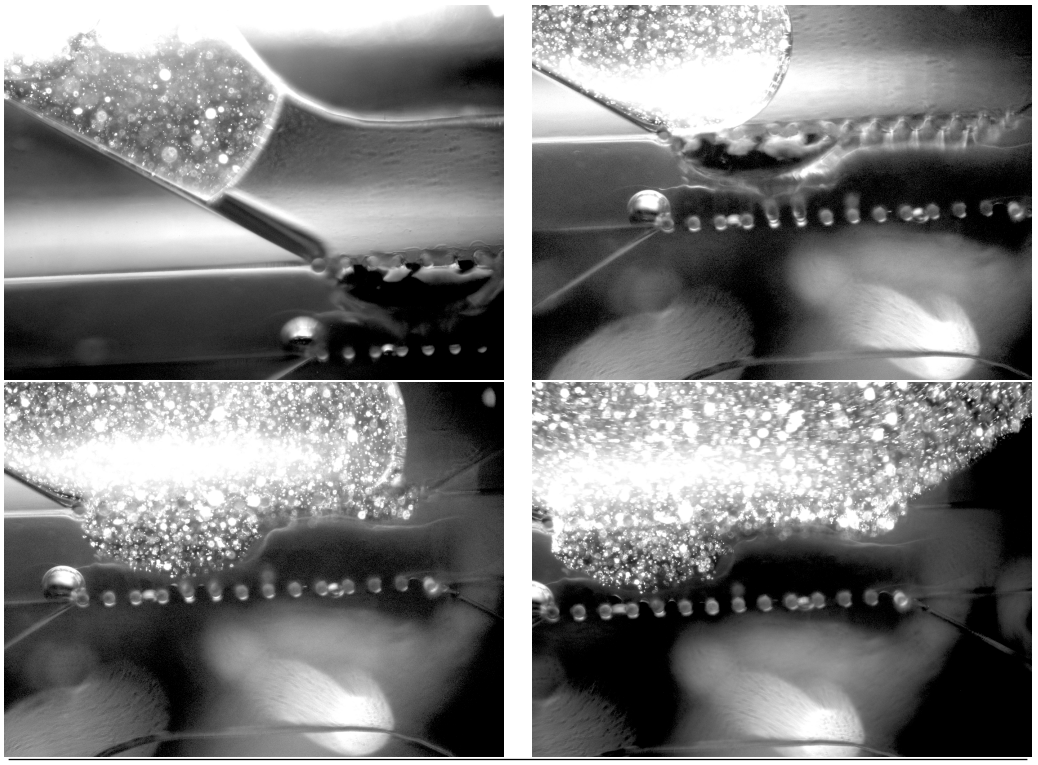

FIGURE 4.23: Tests with fluorescence microspheres. The four images show subsequent moments of lateral channel filling.

this way, the average of all the information in those specific hours is calculated. Always using *ImageJ*, three profiles in each of the two mean images are calculated in the same positions along the central channel. Figure 4.24 shows this situation.

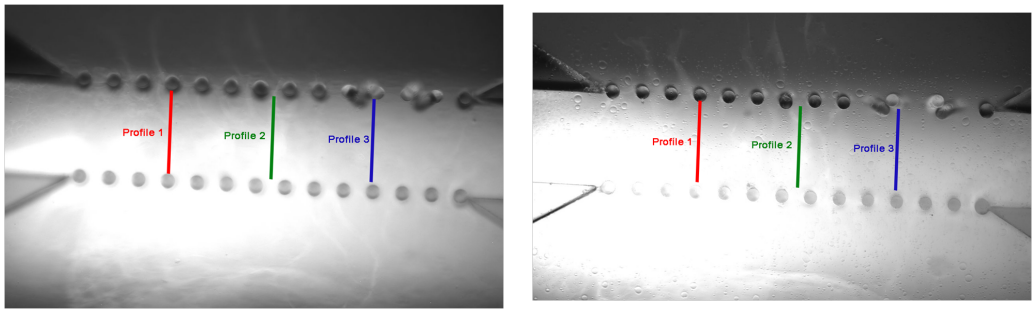

(A) Averaged image calculated from the 15^{th} hour of measurements

(B) Averaged image calculated from the 35^{th} hour of measurements

FIGURE 4.24: Fluorescence profiles

In this way, every profile contains information about one hour of measurement that can be plotted. In Figure 4.25 all the fluorescence intensity profiles are collected in one single graph. It is easy to notice that for each profile the two lines (one for the 15^{th} and one for the 35^{th} hour) are almost overlapped. Moreover, only the two lines related to the third profile are separated from the others (that indicates probably an error due to light contamination depending on the light reflection of the PDMS).

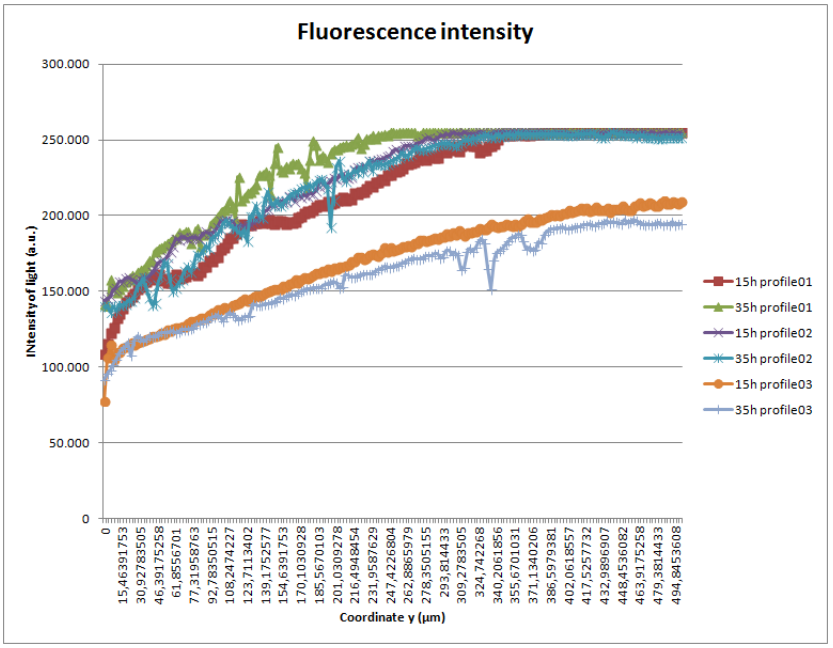

FIGURE 4.25: Total profiles diffusion intensity

All these information can be separately plotted (Figure 4.26) in order to see exactly that the curve trend not only is similar in all the examined cases, but also it follows the simulation results previously reported. In particular, the first line is referred to the 15^{th} hour, while the second line is referred to the 35^{th} hour. The three columns are referred to the first, second and third profile respectively.

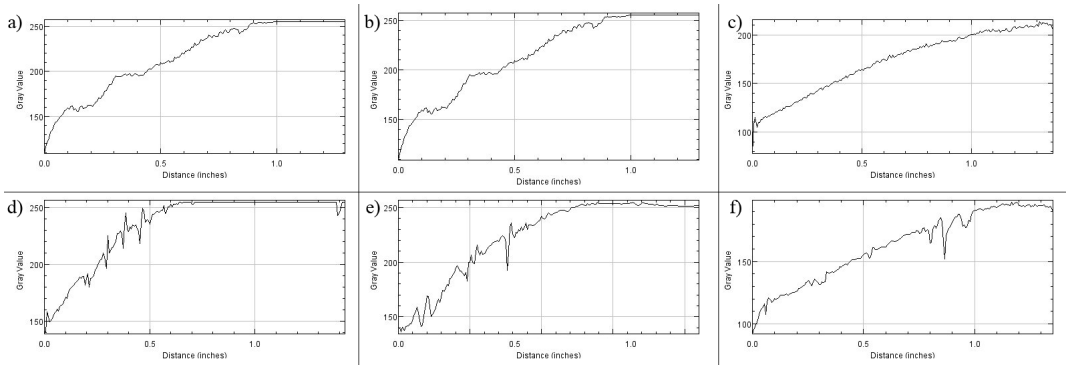

FIGURE 4.26: Separated profiles diffusion intensity. (a-d) First profile, (b-e) Second profile, (c-f) Third Profile; (a-b-c) 15^{th} hour, (d-e-f) 35^{th} hour.

From all these results we can conclude that this device can allow a spatially and temporally constant gradient. This is an encouraging result for all the future biological tests and measurements.

4.6 Preliminary biological results

In this section some results referred to biological tests are reported. These measurements are carried out by the IRCC Institute of Candiolo team. The procedure is described in Appendix B.3.

In Figure 4.27 an example of cells growth in Newton device is shown. In particular, we have in (a) the bright field images that are high magnification images of cell clusters growing in the chip; on the right a cell with filopodial-like protrusion indicating cell adhesion to the matrigel. In (b) bright field and dark field of the image of the chip are shown. In this way, in dark field it is possible to see more precisely cells growth. Finally, in (c) spheroids ranging from 50 to 80 microns in diameter can be observed after 5 days of culture in regular media supplemented with Fetal Bovine Serum (FBS).

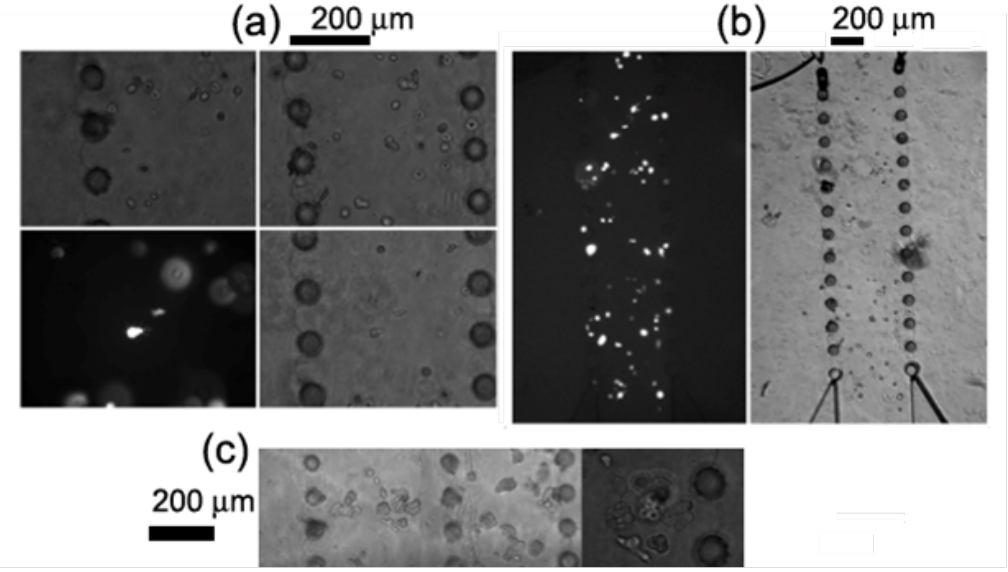

FIGURE 4.27: Cells cultures in Newton device

In Figure 4.28 a fluorescence image of cells growth is shown. In particular, from the stacks it is possible to verify that clusters were indeed positioned in three dimensions. The color legend is green stains for actin, while blue for cell nuclei.

In Figure 4.29 another result is shown. In this case, it is possible to notice cells protrusion that are used for the movement inside Matrigel^{TM} during tests.

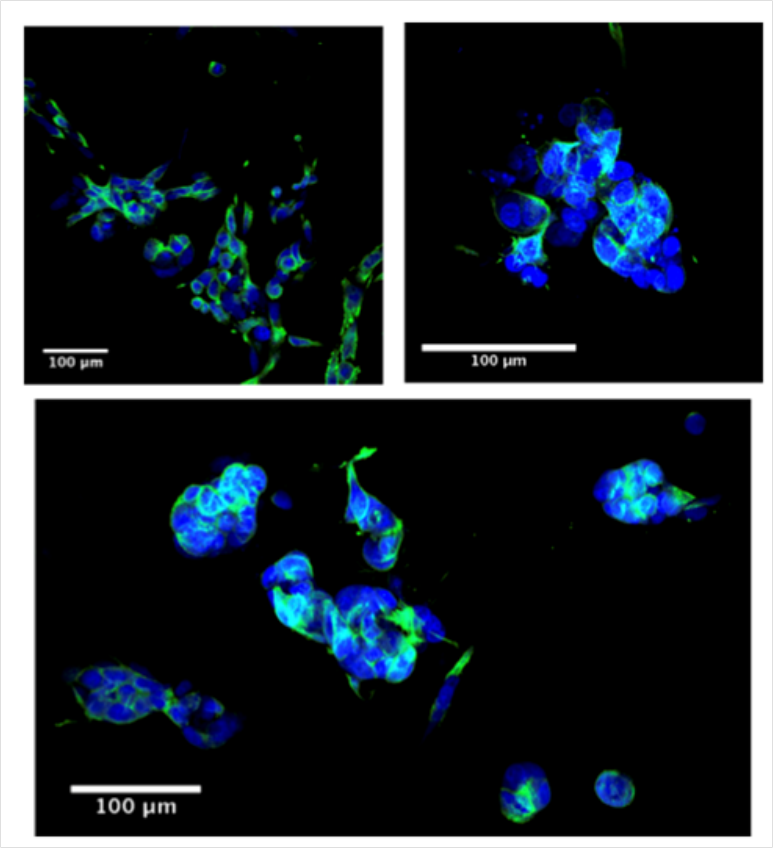

FIGURE 4.28: Fluorescence image of cells cultures in Newton device

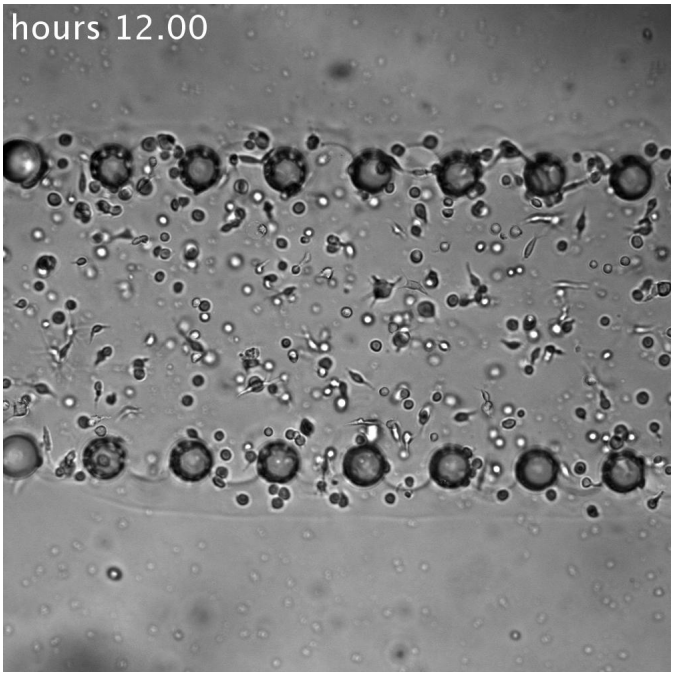

FIGURE 4.29: Cells with protrusion for the movement inside Matrigel^{TM}

Chapter 5

Conclusive Remarks

In the first part of this work we analyzed the possibilities for the manufacturing of a device for the study of cells chemotactic and angiogenesis phenomena. Our approach has been process-oriented in order to provide a feasibility report with low-cost fabrication. Our consideration started from the basic step of these devices fabrication until the final realization. The main challenge has been to provide the right fabrication procedure and processes to be followed. All the problems related to the various steps have been overcome. Various process alternatives have been analyzed, and in particular device production with casting in situ in a PMMA mold realized with milling machine, chips production by electroplating process using a copper mold and PDMS casting with SU8 mold are reported; for each of these alternatives advantages and disadvantages are reported. Finally, the device was successfully realized, with the possibility to produce several replica in order to allow a lot of tests and future analyses. Possible future implementation could be a method to improve the speed of production and the possibility to reduce the probability of failure in pillars reproduction and bonding success.

In the second part, simulations and experimental tests for the device validation were carried out, both for fluidic working regime and biological and fluorescence tests. Preliminary works were simulations of static and dynamic regimes of the device. After that, all the procedure for the utilization is presented and described, in order to verify the correct device behavior. Since the device aim is to maintain a constant gradient with solutions, the following work was the control of this phenomenon, using fluorescence behavoir of particular solutions. Finally, some preliminary biological tests are reported. To sum up, we discussed all the validation and utilization processes in order to have the final insurance of the correct behavior of this device. Future implementations may involve more analyses in a biological context, continuing the verification of the correct device behavior.

This work has been oriented towards the technological processes and technology for the production of a device for biological analysis. In particular, the angiogenesis and chemotactic phenomena are the focus of this work.

The main advantages are:

- possibility to grow spheroids and cells agglomerates of hundreds of micrometers in vitro, with the ability to control and observe the complete process; this 3D environment for experimental analysis of this type of cells is a quite new field of research and allows a lot of future implementations;
- capability of imposing a spatially and temporally constant gradient of solutions and nutritive or toxic substances, in order to be able to check the behavior for at least 48 hours.

The main disadvantages are:

- difficulty of handling this type of devices, since there is not a specific protocol yet;
- difficulty of carrying on the whole procedure in sterile conditions; this is a crucial aspect for any type of biological analysis.

Finally, an important goal has been obtained through the work of this project; however, future approaches could be oriented towards the improvement of the above negative aspects.

Appendix A

SU8 photolithographic processes

A.1 SU8 characteristics

SU-8 is a negative photoresist produced by *MICROCHEM*®. SU-8 is a high contrast, epoxy based photoresist designed for micromachining and other microelectronic applications, where a thick, chemically and thermally stable image is desired. SU-8 is available in twelve standard viscosities. Film thicknesses of 0.5 to >200 microns can be achieved with a single coat process. The exposed and subsequently thermally cross-linked portions of the film are rendered insoluble to liquid developers. SU-8 has excellent imaging characteristics and is capable of producing very high aspect ratio structures. SU-8 has very high optical transmission above 360 nm, which makes it ideally suited for imaging near vertical sidewalls in very thick films. SU-8 is best suited for permanent applications where it is imaged, cured and left on the device.

Here we can summarize SU8 main characteristics:

- High aspect ratio imaging
- 0.5 to > 200 μm film thickness in a single coat
- Improved coating properties
- Faster drying for increased throughput
- Near UV (350-400 nm) processing
- Vertical sidewalls

Figure A.1 shows the main physical properties of *MicroChem*^{TM} SU8.

Adhesion Strength (mPa) Silicon/Glass/Glass & HMDS	38/35/35
Glass Transition Temperature (Tg °C), tan δ peak	210
Thermal Stability (°C @ 5% wt. loss)	315
Thermal Conductivity (W/mK)	0.3
Coeff. of Thermal Expansion (CTE ppm)	52
Tensile Strength (Mpa)	60
Elongation at break (εb %)	6.5
Young's Modulus (Gpa)	2.0
Dielectric Constant @ 10MHz	3.2
Water Absorption (% 85/85 RH)	0.65

FIGURE A.1: Physical Properties

A.2 Data sheet recipe

In this paragraph all the SU-8 data sheet photolithographic process is explained. Since it is possible to obtain different layer thicknesses, all the parameters belong to a range of different values.

1. ***Resist spin coating***

   It is possible to obtain different thickness values setting different velocities in spin coater. Figure A.2 provides the information required to select the appropriate SU-8 resist and spin conditions to achieve the desired film thickness.

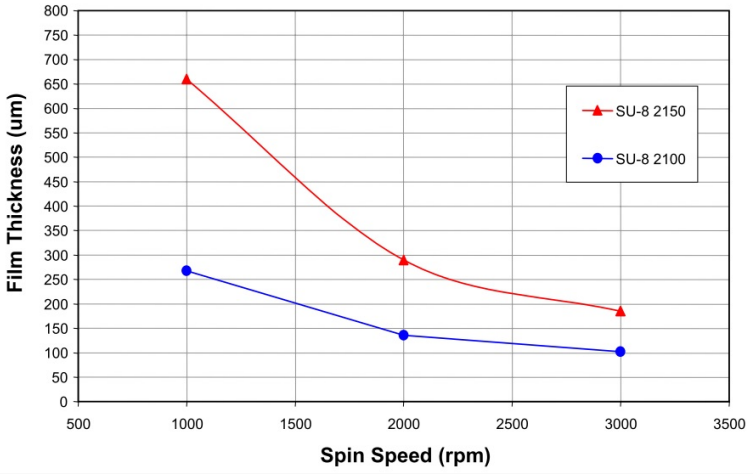

FIGURE A.2: SU-8 Spin Speed versus Thickness

2. ***Soft bake***

   Figure A.3 shows the recommended Soft Bake temperatures and times for the various SU-8 products at selected film thicknesses.

THICKNESS microns	SOFT BAKE TIMES (65°C)* minutes	(95°C) minutes
100 - 150	5	20 - 30
160 - 225	5 - 7	30 - 45
230 - 270	7	45 - 60
280 - 550	7 - 10	60 - 120

FIGURE A.3: Soft bake times

3. ***Exposure***

   Figure A.4 shows different exposure dose values. It will be necessary to calculate the right time of exposition starting from the exposure dose and considering the power of the mask aligner utilized.

THICKNESS microns	EXPOSURE ENERGY mJ/cm^2
100 - 150	240 - 260
160 - 225	260 - 350
230 - 270	350 - 370
280 - 550	370 - 600

FIGURE A.4: Exposure dose

4. ***Post exposure bake (PEB)***

   PEB should take place directly after exposure. Figure A.5 shows the recommended times and temperatures.

THICKNESS microns	PEB TIME (65°C)* minutes	PEB TIME (95°C) minutes
100 - 150	5	10 - 12
160 - 225	5	12 - 15
230 - 270	5	15 - 20
280 - 550	5	20 - 30

FIGURE A.5: Post Exposure Bake Times. Note: *Optional step for stress reduction

5. ***Development***
   The recommended development times for immersion processes are given in Figure A.6. These development times are approximate, since actual dissolution rates can vary widely as a function of solution agitation.

THICKNESS microns	DEVELOPMENT TIME minutes
100 - 150	10 - 15
160 - 225	15 - 17
230 - 270	17 - 20
280 - 550	20 - 30

FIGURE A.6: Development Times for SU-8 Developer

A.3 Experimental recipe

In this paragraph I will describe the experimental lithographic process followed during all this thesis work. This process was validated after a long series of tests, so that final obtained results were comparable to the results explained in data sheet. The aim of the calibration of SU8 resist is to find the most suitable parameters values for the final device to be obtained.

The steps and all the parameters values are listed as follows.

1. ***Sample cleaning***
   This step is crucial in every photolithographic process:
   - first cleaning procedure in *Piranha solution*: dip the sample in this solution for 10 minutes;
   - carry out at least five rinses in water under chemical hood;
   - rinse with acetone and ethanol;
   - drying step with nitrogen.
2. ***MCC Primer 80/20 deposition***
   The deposition of this material allows a better adhesion of SU8 resist on substrate. After the application of Primer on the substrate positioned on the chuck in the spin coater, it is necessary to wait at least 10 seconds in order to allow the perfect

contact between Primer and substrate.
Spin coater settings are the following:

- velocity: 4000 rpm
- time: 30 s
- acceleration: 1000 rpm/s

Then a bake step on a hot plate is required: 2 minutes at 110° C are enough to ensure the perfect adhesion.

Note: MicroChem Primer 80/20 is based on a combination of 20% HMDS and 80% PM Acetate. HMDS is known as a chemical pretreatments for increasing photoresist adhesion to Oxides, Nitrides, PolySilicon, Glass, Quartz and other difficult surfaces. PM acetate acts as an active pre-wetting agent. Some advantages are the improved wet etching performance, a compatibility with most of positive photoresists and an improved critical dimension control.

3. ***SU8-2150 deposition***
   A drop of SU8-2150 is deposited on the substrate. Wait 15-30 seconds to allow the best possible adhesion between the drop and the surface. Parameters for the spin coating steps are the following:

   - First step: velocity = 500 rpm, time = 5 s, acceleration = 100 rpm/s
   - Second step: velocity = 2000 rpm, time = 30 s, acceleration = 100 rpm/s

4. ***Soft bake***
   The steps of soft bake are the following:

   - Load the sample on hot plate at 65°C for 8 minutes
   - After this period of time, set the temperature at 95 °C and bake for 1 hour and 15 minutes
   - Remove the sample from the hot plate and let it to cool down for at least 30 minutes. This time is crucial in order to avoid sticking in following lithographic process.

5. ***UV exposition***
   Set up the following time exposition values (for the mask aligner located in our lab):

   - 36.3 s for Si substrates;
   - 72.6 s for Cu substrates.

6. ***Post exposure bake***

   It is important to follow steps here reported:

   - Load substrate on hot plate at room temperature
   - Set up temperature at 65 °C
   - Bake for 5 minutes
   - Set up temperature at 95 °C
   - Bake for 20 minutes
   - Cool down the sample on the hot plate to room temperature

7. ***Development***

   Put the sample in a becker containing SU8 developer and follow the puddle development method, putting samples in vertical position. After every 5 minutes check the result, rinsing the sample with ethanol or isopropilic alcohol. If there is some SU8 not developed yet, a white film appears. In this case, it is necessary to keep on the development process.

   At the end of this step, a final rinse with some new SU8 developer is required; finally, dip the sample in water.

8. ***Hard bake***

   Hard bake is not necessary, since it doesn't introduce any improvement in final results.

All this process has been validated and was performed in every photolithographic procedure explained in this thesis. A particular aspect of this process is that one day of work is requested to prepare one sample. This can provide an idea how long it takes to perform only one measure or test with only one sample.

Appendix B

Materials and procedures

B.1 Matrigel^{TM}

Matrigel^{TM} Basement Membrane Matrix is a solubilized basement membrane preparation extracted from the Engelbreth-Holm-Swarm (EHS) mouse sarcoma, a tumor rich in extracellular matrix proteins. Its major component is laminin, followed by collagen IV, heparan sulfate proteoglycans, entactin/nidogen [75] - [76]. Matrigel^{TM} also contains TGF-beta, epidermal growth factor, insulin-like growth factor, fibroblast growth factor, tissue plasminogen activator and other growth factors which occur naturally in the EHS tumor. It is effective for the attachment and differentiation of both normal and transformed anchorage dependent epithelioid and other cell types (including neurons, hepatocytes, Sertoli cells, chick lens, and vascular endothelial cells). Matrigel^{TM} will influence gene expression in adult rat hepatocytes, vascular endothelial cells, as well as three dimensional culture in mouse ([77] - [78]) and human mammary epithelial cells. It is the basis for several types of tumor cell invasion assays, will support in-vivo peripheral nerve regeneration, and provides the substrate necessary for the study of angiogenesis both in vitro and in vivo [79]. Matrigel^{TM} also supports in-vivo propagation of human tumors in immunosupressed mice. It can be used for the transplantation of unsorted mammary cells, as well as sorted epithelial subpopulation embedded in Matrigel^{TM}. This matrix has also been used as a cancer stem cell model and shown to enhance tumor growth rates in vivo [80]. It is compatible with all culture media. This mixture resembles the complex extracellular environment found in many tissues.

Matrigel^{TM} is more dense with respect to collagen and at room temperature crystallizes rapidly, forming a porous net exploited as substrate for cell culture.The storage of the Matrigel^{TM} must be stable when stored at -20°C. Freeze thaws should be minimized using aliquots; they have to be stored in the -20°C freezer until they are ready for use.

Some precautions must be taken when dealing with Matrigel^{TM}([81]), as summarized as follows:

- *Storage* → It is extremely important that Matrigel and all culture-ware or media coming in contact with it should be prechilled/ ice-cold since Matrigel will start to gel above 10°C. Keep Matrigel on ice at all times even while operating it;
- *Reconstitution and use* → Color variations may occur in frozen or thawed vials of BD Matrigel, ranging from straw yellow to dark red due to the interaction of carbon dioxide with the bicarbonate buffer and phenol red. Variation in color is normal, it does not affect the Matrigel efficacy, and will disappear upon equilibration with 5% CO_2;
- *Handling* → Matrigel must be handled gently using a pre-cooled pipette to ensure homogeneity. Gelled Matrigel may be reliquified if placed at 4°C in ice for 24-48 hours;
- *Advice* → Matrigel may be used as a thin gel layer (0.5 mm), with cells plated on top. Cells may also be cultured inside the Matrigel, using a 1 mm layer. Extensive dilution will result in a thin, non-gelled protein layer. This may be useful for cell attachment, but may not be as effective in differentiation studies

In conclusion, Matrigel^{TM} is a very hard-handling material, from its preparation to its usage in biological devices. Its curing process makes it a very difficult material to be used, since a temperature higher than 8°C allows a gel reticulation, which solidifies the material and renders it unmanageable.

B.2 Fluorescein IsoThioCyanate (FITC)

Fluorescein isothiocyanate (FITC) is a derivative of fluorescein used in wide-ranging applications including flow cytometry. FITC is the original fluorescein molecule functionalized with an isothiocyanate reactive group (-N=C=S), replacing a hydrogen atom on the bottom ring of the structure. This derivative is reactive towards nucleophiles including amine and sulfhydryl groups on proteins.

A succinimidyl-ester functional group attached to the fluorescein core, creating "NHS-fluorescein", forms another common amine reactive derivative that has much greater specificity toward primary amines in the presence of other nucleophiles.

FITC has excitation and emission spectrum peak wavelengths of approximately 495 nm/519 nm. Like most fluorochromes, it is prone to photobleaching. Because of the

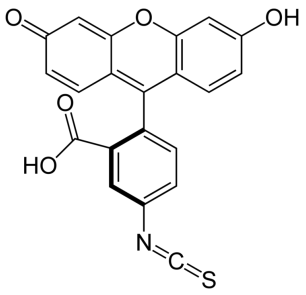

FIGURE B.1: FITC molecule

problem with photobleaching, derivatives of fluorescein such as Alexa 488 and DyLight 488 have been tailored for various chemical and biological applications where greater photostability, higher fluorescence intensity, or different attachment groups are needed.

B.3 Biological procedure

In this section the complete procedure followed in IRCC Institute of Candiolo is reported. One of the main characteristics of this procedure is that a sterile environment is required, since biological cells are manipulated. In the following all the main steps are summarized.

1. ***Tools and device preparation***
   We cooled the setup by placing chips, tubes and reagents on ice or on metal block on ice (Figure B.2).

FIGURE B.2: Tools and devices cooling

2. ***Chemical and sterile hood preparation***
   All the setup, devices and tools are positioned in the sterile chemical hood (Figure B.3).

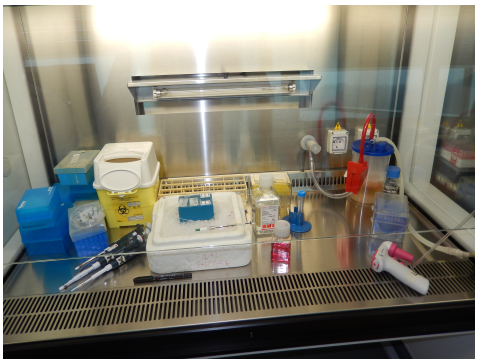

FIGURE B.3: Chemical sterile hood

3. ***Cells preparation***

   The cells preparation is crucial for the following steps. So, a particular care is needed in order not to destroy biological cells behavior and responses.

   - We detached cells in culture by trypsinizing them (Figure B.4)

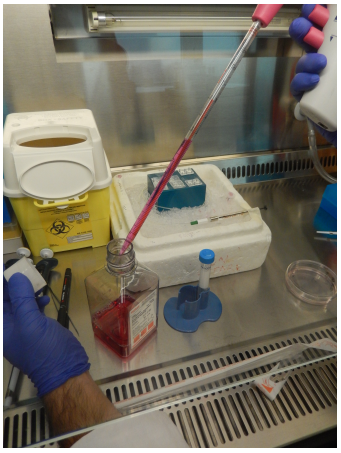

(A) Trypsin solution for detaching cells

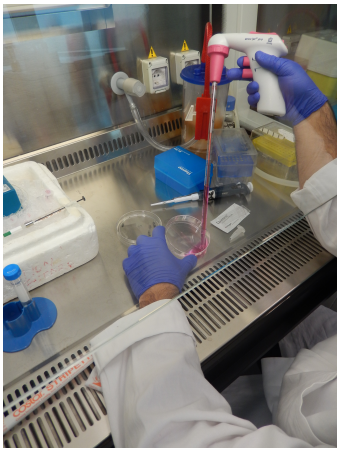

(B) Cells detaching process in Petri dish

FIGURE B.4: Detaching cells process

   - We counted them by means of an automated cell counter (Figure B.5); this device counts cells when they are colored using a black ink solution.
   - We resuspended cells (Figure B.6) at the desired concentration (10^6 cells/ml)

4. ***Devices filling***

   The chip was filled by means of a precision syringe (Hamilton 250 μl) connected by silicone tubings. Tubes, syringe and Matrigel^{TM} were kept on ice to prevent polymerization and subsequent viscosity increase (Figure B.7).

5. ***Cells incubation***

   Poymerization was achieved by incubating the filled chips in a standard cell culture

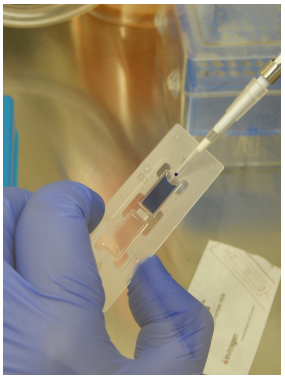

(A) Cells and ink solution

(B) Cells counter equipment

FIGURE B.5: Counting cells process

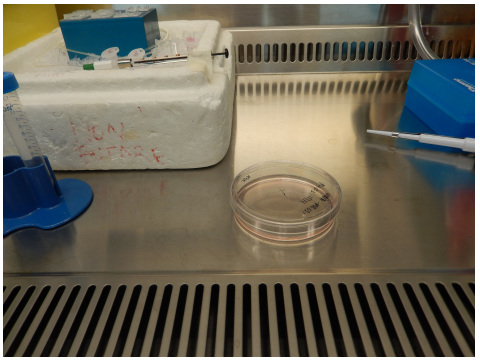

FIGURE B.6: Cells resuspension in Petri dish

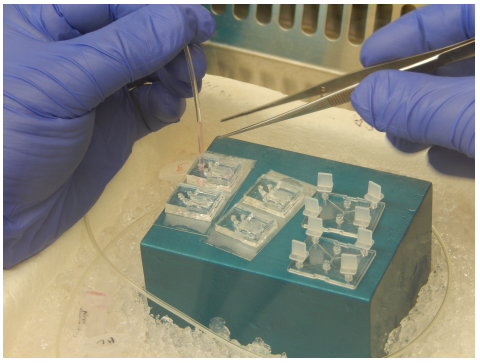

FIGURE B.7: Device filling

incubator for 20 minutes. Humidity was further guaranteed by adding wet tissue in the Petri dish side by side with the chip.

6. ***Serum free media insertion***
   Side channels were filled with serum free media (Figure B.8).

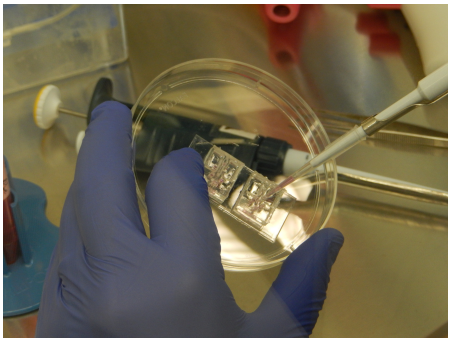

(A) Side channel filling with serum free media

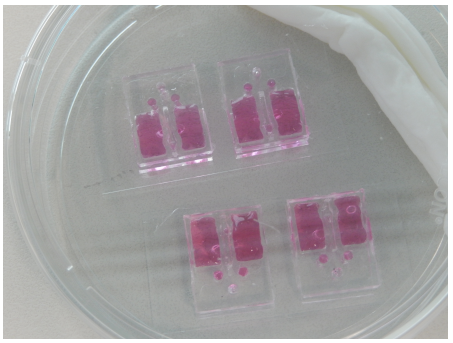

(B) Final result

FIGURE B.8: Lateral channels and reservoirs filling

7. ***Microscope setup***
   The chip was connected properly to the tubings and to the syringe pumps and the microscope incubator was prepared in order to avoid thermal drift (Figure B.9).

(A) Optical and fluorescence microscope

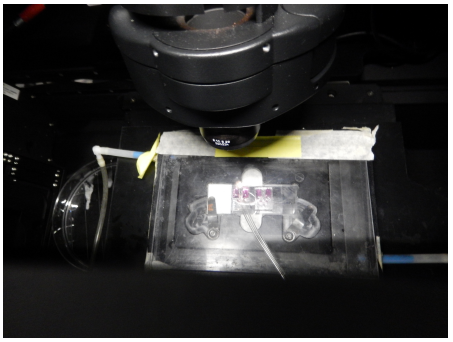

(B) Setup inside the microscope

FIGURE B.9: Microscope setup

8. ***Serum replacement***
   Once the chip was set up on the microscope stage, we replaced the serum free media in one of the channels with 10% fetal bovine serum, used as the chemoattractant.

9. ***Measuring step***
   The last step is the measurement start, in order to analyze cells behavior with time. The lateral flux in side channels is imposed by twin pumps, setted at 2.4 $\mu l/h$

Bibliography

[1] Camilla Coletti, MJ Jaroszeski, Alessia Pallaoro, AM Hoff, Salvatore Iannotta, and SE Saddow. Biocompatibility and wettability of crystalline sic and si surfaces. In *Engineering in Medicine and Biology Society, 2007. EMBS 2007. 29th Annual International Conference of the IEEE*, pages 5849–5852. IEEE, 2007.

[2] Debashis Maji, SK Lahiri, and Soumen Das. Study of hydrophilicity and stability of chemically modified pdms surface using piranha and koh solution. *Surface and Interface Analysis*, 44(1):62–69, 2012.

[3] Hiroshi Miyajima and Mehran Mehregany. High-aspect-ratio photolithography for mems applications. *Microelectromechanical Systems, Journal of*, 4(4):220–229, 1995.

[4] J Zhang, KL Tan, and HQ Gong. Characterization of the polymerization of su-8 photoresist and its applications in micro-electro-mechanical systems (mems). *Polymer testing*, 20(6):693–701, 2001.

[5] Yoshikazu Hirai, Yoshiteru Inamoto, Koji Sugano, Toshiyuki Tsuchiya, and Osamu Tabata. Moving mask uv lithography for three-dimensional structuring. *Journal of Micromechanics and Microengineering*, 17(2):199, 2007.

[6] Dirk W Schubert and Thomas Dunkel. Spin coating from a molecular point of view: its concentration regimes, influence of molar mass and distribution. *Materials research innovations*, 7(5):314–321, 2003.

[7] Konstantin Vorotilov, Vladimir Petrovsky, and Vladimir Vasiljev. Spin coating process of sol-gel silicate films deposition: effect of spin speed and processing temperature. *Journal of Sol-Gel Science and Technology*, 5(3):173–183, 1995.

[8] Patrick J Paniez, Gilles Festes, and Jean-Paul E Chollet. Physical description of lithographic processes: correlation between bake conditions and photoresist contrast. In *Micro-DL Tentative*, pages 623–637. International Society for Optics and Photonics, 1992.

[9] GI Parisi, SE Haszko, and GA Rozgonyi. Tapered windows in sio2: The effect of nh 4 f: Hf dilution and etching temperature. *Journal of the Electrochemical Society*, 124(6):917–921, 1977.

[10] MJM Vugts, GLJ Verschueren, MFA Eurlings, LJF Hermans, and HCW Beijerinck. Si/xef2 etching: temperature dependence. *Journal of Vacuum Science & Technology A*, 14(5):2766–2774, 1996.

[11] MJM Vugts, LJF Hermans, and HCW Beijerinck. Ion-assisted si/xef2 etching: Temperature dependence in the range 100–1000 k. *Journal of Vacuum Science & Technology A*, 14(5):2820–2826, 1996.

[12] DJ Blackwood and Y Zhang. The effect of etching temperature on the photoluminescence emitted from, and the morphology of, p-type porous silicon. *Electrochimica acta*, 48(6):623–630, 2003.

[13] Arturo A Ayón, R Braff, Chuang-Chia Lin, Herb H Sawin, and Martin A Schmidt. Characterization of a time multiplexed inductively coupled plasma etcher. *Journal of the Electrochemical Society*, 146(1):339–349, 1999.

[14] Brian Matthews and Jack W Judy. Design and fabrication of a micromachined planar patch-clamp substrate with integrated microfluidics for single-cell measurements. *Microelectromechanical Systems, Journal of*, 15(1):214–222, 2006.

[15] Meint J De Boer, JGEH Gardeniers, Henri V Jansen, Edwin Smulders, Melis-Jan Gilde, Gerard Roelofs, Jay N Sasserath, and Miko Elwenspoek. Guidelines for etching silicon mems structures using fluorine high-density plasmas at cryogenic temperatures. *Microelectromechanical Systems, Journal of*, 11(4):385–401, 2002.

[16] HV Jansen, MJ De Boer, S Unnikrishnan, MC Louwerse, and MC Elwenspoek. Black silicon method x: a review on high speed and selective plasma etching of silicon with profile control: an in-depth comparison between bosch and cryostat drie processes as a roadmap to next generation equipment. *Journal of Micromechanics and Microengineering*, 19(3):033001, 2009.

[17] C Flagg Brayton. Dimethyl sulfoxide (dmso): a review. *The Cornell Veterinarian*, 76(1):61–90, 1986.

[18] Leonid Gitlin, Philipp Schulze, and Detlev Belder. Rapid replication of master structures by double casting with pdms. *Lab on a Chip*, 9(20):3000–3002, 2009.

[19] H Schift, C David, M Gabriel, J Gobrecht, LJ Heyderman, W Kaiser, S Köppel, and L Scandella. Nanoreplication in polymers using hot embossing and injection molding. *Microelectronic Engineering*, 53(1):171–174, 2000.

[20] Werner Risau and Ingo Flamme. Vasculogenesis. *Annual review of cell and developmental biology*, 11(1):73–91, 1995.

[21] Ingo Flamme, Thomas Frölich, and Werner Risau. Molecular mechanisms of vasculogenesis and embryonic angiogenesis. *Journal of cellular physiology*, 173(2):206–210, 1997.

[22] John S Penn. *Retinal and choroidal angiogenesis*. Springer Science & Business Media, 2008.

[23] Douglas Hanahan and Robert A Weinberg. Hallmarks of cancer: the next generation. *cell*, 144(5):646–674, 2011.

[24] Gabriele Bergers and Laura E Benjamin. Tumorigenesis and the angiogenic switch. *Nature reviews cancer*, 3(6):401–410, 2003.

[25] Daniel J Hicklin and Lee M Ellis. Role of the vascular endothelial growth factor pathway in tumor growth and angiogenesis. *Journal of clinical oncology*, 23(5): 1011–1027, 2005.

[26] Diane R Bielenberg and Bruce R Zetter. The contribution of angiogenesis to the process of metastasis. *The Cancer Journal*, 21(4):267–273, 2015.

[27] Michael Simons, Kari Alitalo, Brian H Annex, Hellmut G Augustin, Craig Beam, Bradford C Berk, Tatiana Byzova, Peter Carmeliet, William Chilian, John P Cooke, et al. State-of-the-art methods for evaluation of angiogenesis and tissue vascularization a scientific statement from the american heart association. *Circulation research*, 116(11):e99–e132, 2015.

[28] Dipak K Banerjee, Aditi Banerjee, Krishna Baksi, Usha Katiyar, Jesus Santiago, and Neysharie Sanchez. Therapeutic er stress induced by tunicamycin is anti-angiogenic/anti-tumorigenic and signals through unfolded protein response. *Cancer Research*, 75(15 Supplement):1243–1243, 2015.

[29] Zongwei Wang, Charlotta Dabrosin, Xin Yin, Mark M Fuster, Alexandra Arreola, W Kimryn Rathmell, Daniele Generali, Ganji P Nagaraju, Bassel El-Rayes, Domenico Ribatti, et al. Broad targeting of angiogenesis for cancer prevention and therapy. In *Seminars in cancer biology*. Elsevier, 2015.

[30] Katherine Margulis, Evgenios A Neofytou, Ramin E Beygui, and Richard N Zare. Celecoxib nanoparticles for therapeutic angiogenesis. *ACS nano*, 9(9):9416–9426, 2015.

[31] Ofrat Beyar Katz and Yuval Shaked. Host effects contributing to cancer therapy resistance. *Drug Resistance Updates*, 19:33–42, 2015.

[32] Savalan Babapoor-Farrokhran, Kathleen Jee, Brooks Puchner, Syed Junaid Hassan, Xiaoban Xin, Murilo Rodrigues, Fabiana Kashiwabuchi, Tao Ma, Ke Hu, Monika Deshpande, et al. Angiopoietin-like 4 is a potent angiogenic factor and a novel therapeutic target for patients with proliferative diabetic retinopathy. *Proceedings of the National Academy of Sciences*, page 201423765, 2015.

[33] Takanori Kitamura, Bin-Zhi Qian, and Jeffrey W Pollard. Immune cell promotion of metastasis. *Nature Reviews Immunology*, 15(2):73–86, 2015.

[34] Sara I Cunha, Matteo Bocci, John Lövrot, Nikolas Eleftheriou, Pernilla Roswall, Eugenia Cordero, Linda Lindström, Michael Bartoschek, B Kristian Haller, R Scott Pearsall, et al. Endothelial alk1 is a therapeutic target to block metastatic dissemination of breast cancer. *Cancer research*, 75(12):2445–2456, 2015.

[35] Maria C Marin and Margarita M Marques. Novel role of p73 as a regulator of developmental angiogenesis: implication for cancer therapy. *Molecular & Cellular Oncology*, (just-accepted):00–00, 2015.

[36] Valeria Tarallo and Sandro De Falco. The vascular endothelial growth factors and receptors family: Up to now the only target for anti-angiogenesis therapy. *The international journal of biochemistry & cell biology*, 64:185–189, 2015.

[37] Pranesh M Gunjal, Gabriela Schneider, Ahmed Abdelbaset Ismail, Sham S Kakar, Magda Kucia, and Mariusz Z Ratajczak. Evidence for induction of a tumor metastasis-receptive microenvironment for ovarian cancer cells in bone marrow and other organs as an unwanted and underestimated side effect of chemotherapy/radiotherapy. *Journal of ovarian research*, 8(1):20, 2015.

[38] Mark Tyler Nelson. *Biomimetic Electrospun Fibers for Cancer Cell Migration, Chemotaxis, and Anti-Metastatic Drug Testing*. PhD thesis, The Ohio State University, 2015.

[39] Katherine M Broadway, Elizabeth AP Denson, Roderick V Jensen, and Birgit E Scharf. Rescuing chemotaxis of the anticancer agent salmonella enterica serovar typhimurium vnp20009. *Journal of biotechnology*, 211:117–120, 2015.

[40] Akvilė Jarmalavičiūtė, Virginijus Tunaitis, Ugnė Pivoraitė, Algirdas Venalis, and Augustas Pivoriūnas. Exosomes from dental pulp stem cells rescue human dopaminergic neurons from 6-hydroxy-dopamine–induced apoptosis. *Cytotherapy*, 2015.

[41] Bradley A Justice, Nadia A Badr, and Robin A Felder. 3d cell culture opens new dimensions in cell-based assays. *Drug discovery today*, 14(1):102–107, 2009.

[42] Ching-Yu Lin, Chi-Hui Huang, Yuan-Kun Wu, Nai-Chen Cheng, and Jiashing Yu. Maintenance of human adipose derived stem cell (hasc) differentiation capabilities using a 3d culture. *Biotechnology letters*, 36(7):1529–1537, 2014.

[43] Alois Knoll, Torsten Scherer, Iris Poggendorf, Dirk Lütkemeyer, and Jürgen Lehmann. Flexible automation of cell culture and tissue engineering tasks. *Biotechnology progress*, 20(6):1825–1835, 2004.

[44] Rita Barallon, Steven R Bauer, John Butler, Amanda Capes-Davis, Wilhelm G Dirks, Eugene Elmore, Manohar Furtado, Margaret C Kline, Arihiro Kohara, Georgyi V Los, et al. Recommendation of short tandem repeat profiling for authenticating human cell lines, stem cells, and tissues. *In Vitro Cellular & Developmental Biology-Animal*, 46(9):727–732, 2010.

[45] Maria E Kempner and Robin A Felder. A review of cell culture automation. *Journal of the Association for Laboratory Automation*, 7(2):56–62, 2002.

[46] Brian J Kirby. *Micro-and nanoscale fluid mechanics: transport in microfluidic devices*. Cambridge University Press, 2010.

[47] George Karniadakis, Ali Beskok, and Narayan Aluru. *Microflows and nanoflows: fundamentals and simulation*, volume 29. Springer Science & Business Media, 2006.

[48] Patrick Tabeling. *Introduction to microfluidics*. Oxford University Press, 2010.

[49] Beum Jun Kim and Mingming Wu. Microfluidics for mammalian cell chemotaxis. *Annals of biomedical engineering*, 40(6):1316–1327, 2012.

[50] Vernella Vickerman, Choong Kim, and Roger D Kamm. Microfluidic devices for angiogenesis. In *Mechanical and Chemical Signaling in Angiogenesis*, pages 93–120. Springer, 2013.

[51] Gi Seok Jeong, Sewoon Han, Yoojin Shin, Gu Han Kwon, Roger D Kamm, Sang-Hoon Lee, and Seok Chung. Sprouting angiogenesis under a chemical gradient regulated by interactions with an endothelial monolayer in a microfluidic platform. *Analytical chemistry*, 83(22):8454–8459, 2011.

[52] Anthony P Napolitano, Peter Chai, Dylan M Dean, and Jeffrey R Morgan. Dynamics of the self-assembly of complex cellular aggregates on micromolded nonadhesive hydrogels. *Tissue engineering*, 13(8):2087–2094, 2007.

[53] Cristina Del Amo, Carlos Borau, Raquel Gutiérrez, Jesús Asín, and José Manuel García-Aznar. Quantification of angiogenic sprouting under different growth factors in a microfluidic platform. *Journal of Biomechanics*, 2015.

[54] G Pagano, M Ventre, M Iannone, F Greco, PL Maffettone, and PA Netti. Optimizing design and fabrication of microfluidic devices for cell cultures: An effective approach to control cell microenvironment in three dimensions. *Biomicrofluidics*, 8 (4):046503, 2014.

[55] Jose M Ayuso, Haneen A Basheer, Rosa Monge, Pablo Sánchez-Álvarez, Manuel Doblaré, Steven D Shnyder, Victoria Vinader, Kamyar Afarinkia, Luis J Fernández, and Ignacio Ochoa. Study of the chemotactic response of multicellular spheroids in a microfluidic device. *PloS one*, 10(10):e0139515, 2015.

[56] PF O'Neill, A Ben Azouz, Mercedes Vazquez, Jinghang Liu, Steven Marczak, Zdenek Slouka, Hsueh Chia Chang, Dermot Diamond, and Dermot Brabazon. Advances in three-dimensional rapid prototyping of microfluidic devices for biological applications. *Biomicrofluidics*, 8(5):052112, 2014.

[57] Ken-ichiro Kamei, Yasumasa Mashimo, Yoshie Koyama, Christopher Fockenberg, Miyuki Nakashima, Minako Nakajima, Junjun Li, and Yong Chen. 3d printing of soft lithography mold for rapid production of polydimethylsiloxane-based microfluidic devices for cell stimulation with concentration gradients. *Biomedical microdevices*, 17(2):1–8, 2015.

[58] Laszlo Hajba and Andras Guttman. Circulating tumor-cell detection and capture using microfluidic devices. *TrAC Trends in Analytical Chemistry*, 59:9–16, 2014.

[59] Hui Huang, Lili Jiang, Shu Li, Jun Deng, Yan Li, Jie Yao, Biyuan Li, and Junsong Zheng. Using microfluidic chip to form brain-derived neurotrophic factor concentration gradient for studying neuron axon guidance. *Biomicrofluidics*, 8(1):014108, 2014.

[60] Amir Shamloo, Milan Manchandia, Meghaan Ferreira, Maheswaran Mani, Christopher Nguyen, Thomas Jahn, Kenneth Weinberg, and Sarah Heilshorn. Complex chemoattractive and chemorepellent kit signals revealed by direct imaging of murine mast cells in microfluidic gradient chambers. *Integrative Biology*, 5(8):1076–1085, 2013.

[61] Andrew J Muinonen-Martin, Douwe M Veltman, Gabriela Kalna, and Robert H Insall. An improved chamber for direct visualisation of chemotaxis. *PLoS One*, 5 (12):e15309–e15309, 2010.

[62] Erkki S Hujanen and Victor P Terranova. Migration of tumor cells to organ-derived chemoattractants. *Cancer research*, 45(8):3517–3521, 1985.

[63] Victor P Terranova, Erkki S Hujanen, David M Loeb, George R Martin, Lora Thornburg, and Victor Glushko. Use of a reconstituted basement membrane to

measure cell invasiveness and select for highly invasive tumor cells. *Proceedings of the National Academy of Sciences*, 83(2):465–469, 1986.

[64] Robert S Bresalier, Steven E Raper, Erkki S Hujanen, and Young S Kim. A new animal model for human colon cancer metastasis. *International journal of cancer*, 39(5):625–630, 1987.

[65] Suzanne L Tomchuck, Kevin J Zwezdaryk, Seth B Coffelt, Ruth S Waterman, Elizabeth S Danka, and Aline B Scandurro. Toll-like receptors on human mesenchymal stem cells drive their migration and immunomodulating responses. *Stem cells*, 26 (1):99–107, 2008.

[66] Simone Luigi Marasso, Eros Giuri, Giancarlo Canavese, Riccardo Castagna, Marzia Quaglio, Ivan Ferrante, Denis Perrone, and Matteo Cocuzza. A multilevel lab on chip platform for dna analysis. *Biomedical Microdevices*, 13(1):19–27, 2011.

[67] Marzia Quaglio, Giancarlo Canavese, E Giuri, Simone Luigi Marasso, Denis Perrone, M Cocuzza, and CF Pirri. Evaluation of different pdms interconnection solutions for silicon, pyrex and coc microfluidic chips. *Journal of Micromechanics and Microengineering*, 18(5):055012, 2008.

[68] Wen Dai, Kun Lian, and Wanjun Wang. A quantitative study on the adhesion property of cured su-8 on various metallic surfaces. *Microsystem technologies*, 11 (7):526–534, 2005.

[69] V Seidemann, J Rabe, M Feldmann, and S Büttgenbach. Su8-micromechanical structures with in situ fabricated movable parts. *Microsystem technologies*, 8(4-5): 348–350, 2002.

[70] Aránzazu del Campo and Christian Greiner. Su-8: a photoresist for high-aspect-ratio and 3d submicron lithography. *Journal of Micromechanics and Microengineering*, 17(6):R81, 2007.

[71] Xiao-Sheng Zhang, Shi-Gan Chu, Nicolas Peter, and Hai-Xia Zhang. Fabrication of tunable wetting pdms membrane by nanostructuring and plasma treatment. In *Nano/Micro Engineered and Molecular Systems (NEMS), 2013 8th IEEE International Conference on*, pages 159–162. IEEE, 2013.

[72] Xiao-Sheng Zhang, Bai-Hong Jin, Shi-Gan Chu, Nicolas Peter, Fu-Yun Zhu, and Hai-Xia Zhang. Single-step fabrication of superhydrophobic micro/nano dual-scale pdms film replicated from ultra-low-surface-energy mold. In *Micro Electro Mechanical Systems (MEMS), 2013 IEEE 26th International Conference on*, pages 331–334. IEEE, 2013.

[73] Sozaraj Rasappa, Lars Schulte, Dipu Borah, Michael A Morris, and Sokol Ndoni. Sub-15nm silicon lines fabrication via ps-b-pdms block copolymer lithography. *Journal of Nanomaterials*, 2013:14, 2013.

[74] Jinsheng Gao, Dongzhi Guo, Suresh Santhanam, and Gary K Fedder. Material characterization and transfer of large-area ultra-thin polydimethylsiloxane membranes. *Microelectromechanical Systems, Journal of*, 24(6):2170–2177, 2015.

[75] Hynda K Kleinman, Mary L McGarvey, Lance A Liotta, Pamela Gehron Robey, Karl Tryggvason, and George R Martin. Isolation and characterization of type iv procollagen, laminin, and heparan sulfate proteoglycan from the ehs sarcoma. *Biochemistry*, 21(24):6188–6193, 1982.

[76] A Albini, Y Iwamoto, HK Kleinman, GR Martin, SA Aaronson, JM Kozlowski, and RN McEwan. A rapid in vitro assay for quantitating the invasive potential of tumor cells. *Cancer research*, 47(12):3239–3245, 1987.

[77] Charles H Streuli, Nina Bailey, and Mina J Bissell. Control of mammary epithelial differentiation: basement membrane induces tissue-specific gene expression in the absence of cell-cell interaction and morphological polarity. *The Journal of cell biology*, 115(5):1383–1395, 1991.

[78] Ren Xu, Celeste M Nelson, John L Muschler, Mandana Veiseh, Barbara K Vonderhaar, and Mina J Bissell. Sustained activation of stat5 is essential for chromatin remodeling and maintenance of mammary-specific function. *The Journal of cell biology*, 184(1):57–66, 2009.

[79] Tatiana Lopatina, Natalia Kalinina, Maxim Karagyaur, Dmitry Stambolsky, Kseniya Rubina, Alexander Revischin, Galina Pavlova, Yelena Parfyonova, and Vsevolod Tkachuk. Adipose-derived stem cells stimulate regeneration of peripheral nerves: Bdnf secreted by these cells promotes nerve healing and axon growth de novo. *PloS one*, 6(3):e17899, 2011.

[80] Elsa Quintana, Mark Shackleton, Michael S Sabel, Douglas R Fullen, Timothy M Johnson, and Sean J Morrison. Efficient tumour formation by single human melanoma cells. *Nature*, 456(7222):593–598, 2008.

[81] Matrigel^{TM} basement membrane matrix, 2008. URL https://www.bd.com/resource.aspx?idx=17841.